INDIAN - ATLANTIC INTEROCEAN EXCHANGE: VARIABILITY AND CONTROLS.

UITWISSELING TUSSEN DE INDISCHE EN ATLANTISCHE OCEAAN: VARIABILITEIT EN FORCERING.

(met een samenvatting in het Nederlands)

PROEFSCHRIFT

ter verkrijging van de graad van doctor aan de Universiteit Utrecht op gezag van de Rector Magnificus, prof. dr. W.H. Gispen, ingevolge het besluit van het College voor Promoties in het openbaar te verdedigen op woensdag 15 mei 2002, om kwart voor één 's middags.

DOOR

MATHIJS WILHELMUS SCHOUTEN

geboren op 3 juli 1975 te 's Gravenhage

Promotor: Prof. dr. W.P.M. de Ruijter
Co-promotor: Dr. P.J. van Leeuwen
Faculteit Natuur- en Sterrenkunde, Universiteit Utrecht

Dit proefschrift werd mede mogelijk gemaakt door financiële steun van de Nederlandse organisatie voor Wetenschappelijk Onderzoek (NWO), in het kader van het tweede nationaal Onderzoeks Programma (NOP II, contract 013001237-10.

ISBN 90-393-3028-X

Contents

Chapter 1

Introduction

The incoming part of the radiation budget of the earth is characterized by strong solar input of heat at low latitudes. The outgoing radiation is more evenly distributed over the earth, implying that there must be considerable transport from low to higher latitudes. This transport is accomplished both by the atmosphere and the oceans, in about equal parts (Peixoto and Oort, 1992). The ocean-component is achieved mainly by the wind-driven ocean circulation, but in some basins the thermohaline circulation has a considerable impact too, for instance in the climatic conditions of Northern Europe.

Large scale wind driven circulation

The global ocean circulation is driven by winds and fluxes of heat and fresh water. To first order, the location and shape of the large scale surface currents are determined by the shape of the wind field driving it: the curl of the wind stress is the primary source of vorticity for the gyre circulation, by the so-called Sverdrup balance (Sverdrup, 1947). The average winds over the years 1990-2001 are plotted in Fig. 1.1 for the Atlantic and Indian Ocean basins. The meridional extent of the gyres is confined to the regions between two (more or less zonal) lines of zero wind stress curl, where the vorticity input changes sign. Between those lines (the grey lines in Fig. 1.1), large and more or less closed current systems are formed: the wind-driven gyres. The gyres are far from symmetric: the rotation of the earth results in a strong intensification along the western boundaries. The equatorward transport takes place over almost the entire gyre, whereas the poleward flow is established in very narrow bands along the western boundaries. The mean surface velocities of the Atlantic and Indian Ocean basins, determined from satellite tracked surface drifters (Hansen and Poulain, 1996), are plotted in Fig. 1. The western boundary currents that form the western limbs of the gyres are the strongest permanent currents of the World Oceans. Among them are the Gulf Stream and Kuroshio currents on the northern hemisphere, and the Agulhas and Brazil currents in the southern hemisphere. These western boundary currents all carry large amounts of heat from low latitudes into the midlatitudes, thus having strong impact on local and global climatological conditions. Also, they show strong variability on the shorter timescales: meandering and eddy formation are characteristic to all of them.

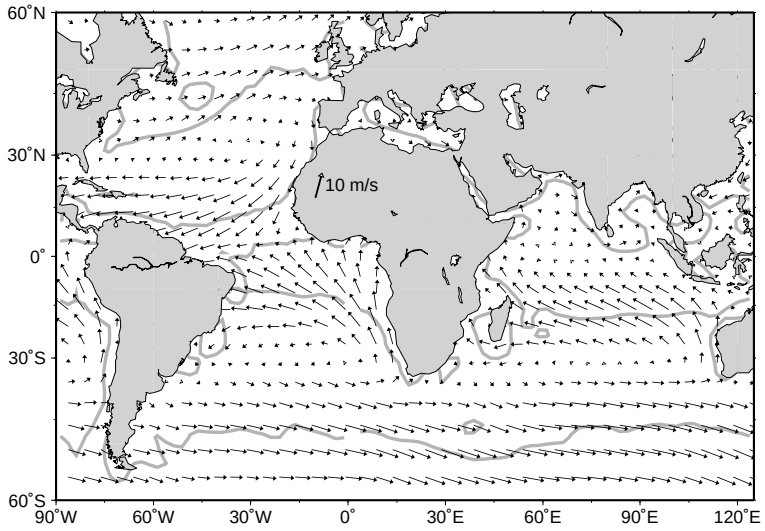

Figure 1.1: *Mean winds in the American National Centers for Environmental Prediction and Atmospheric Research (NCEP/NCAR) reanalysis for 1990-2000 (Kalnay et al., 1996). The lines of zero wind stress curl have been added in grey.*

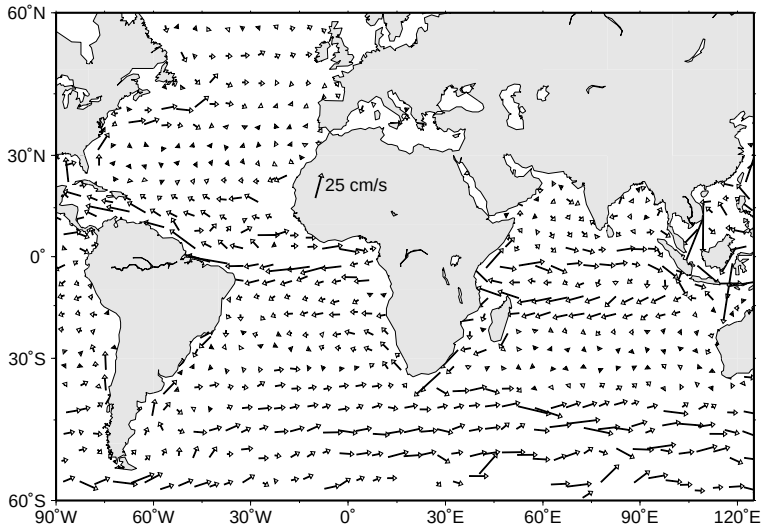

Figure 1.2: *Mean surface velocities as measured by satellite tracked surface drifters (Hansen and Poulain, 1996)* .

The region around South Africa is a region of unusual current characteristics. The line of zero wind stress curl is located roughly at 45°S (Fig. 1.1), the African continental shelf ends at 37°S. Therefore, a gap of about 1000 km exists between the southern tip of the continent

and the 'natural' southern extremum of the subtropical gyres of the South Atlantic and South Indian Oceans. Application of Sverdrup theory alone would result in the formation of an Atlantic-Indian Ocean 'Supergyre' with the western boundary current of the South Indian Ocean turning westward at the end of the African continent, only to return its Indian Ocean waters via a loop across the south Atlantic (De Ruijter, 1982). This is not what is observed. Most of the Agulhas current retroflects back into the Indian Oceanalmost immediately after leaving the African continent. About 10% of its waters are leaking into the South Atlantic Ocean, but this still provides a crucial connection in the global overturning circulation of the ocean (Gordon, 1985).

The retroflection of the Agulhas current has been noticed and described long ago (Rennell, 1832) (see Lutjeharms et al. (1992) for a historical overview), but we are only recently coming towards a dynamical understanding. The 'gap' between the continent and the region of zero wind stress curl is bridged by a delicate interplay of inertial overshoot, advection of planetary vorticity (β-effect) (De Ruijter and Boudra, 1985; Boudra and de Ruijter, 1986), bottom topography (Matano, 1996) and continental geometry (Ou and de Ruijter, 1986). Recent numerical studies (Dijkstra and de Ruijter, 2001b) indicate that the seemingly realistic retroflections obtained by several large scale general circulation models (GCM's) are due to their unrealistically high eddy viscosities. Viscous boundary layers in these models may artificially enlarge the African continent beyond its true size.

Thermohaline circulation

The wind is not the only driving force of the ocean currents. Part of the motion is forced by fluxes of heat and fresh water. These buoyancy fluxes can be provided through the ocean surface by the nett effect of incoming and outgoing radiation for heat, and by the nett effect of precipitation and evaporation for fresh water. They can also be established by direct input of water from other ocean basins, with different temperature and salinity characteristics. The Atlantic ocean circulation is thus forced by differential heating, a nett surface loss of freshwater, by inflow of relatively warm and saline water from the Mediterranean, and by interocean exchanges at its northern and southern extrema. The Bering Strait throughflow provides the Northern Atlantic with cold but relatively fresh water; water entering the Atlantic via Drake Passage south of South America is also relatively cold and fresh, whereas the inflow of Indian Ocean water around South Africa provides the South Atlantic with warm and saline waters.

At deeper levels, the inflow into the Atlantic ocean is balanced by an outflow of North Atlantic Deep Water (NADW). Another important link between two oceans is the Indonesian throughflow, where warm but relatively fresh Pacific water enters the Indian ocean.

Together these surface and inter-ocean fluxes constitute the overturning circulation of the ocean. A salient feature of this circulation is the nett equatorward transport of heat in the South Atlantic Ocean. In the northern part of the Atlantic NADW is formed by convection when the saline water is cooled at high latitudes. It flows southward along the western boundary of the Atlantic, into the Antarctic Circumpolar current (ACC) region where it is spread throughout the oceans. A qualitative picture of this component of the ocean circulation is summarized in Fig. 1.3.

The replacement of NADW in the Atlantic is still a topic of active research. The original

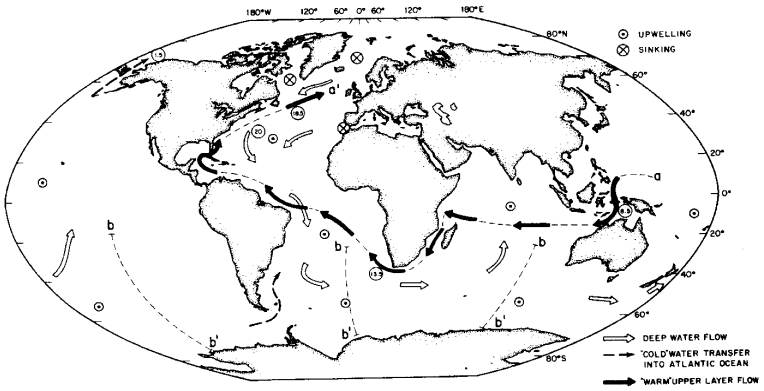

Figure 1.3: *Global overturning circulation. The warm water route, transporting warm and saline water into the Atlantic via the route south of Africa, partially provides the replacement for NADW exported from the Atlantic (Gordon, 1986).*

picture of Gordon (1986) (Fig. 1.3) which shows the NADW upwelling through the thermoclines of the Indian and Pacific oceans, and re-entering the Atlantic almost completely via the pathway south of Africa has been challenged by a scheme whereby most of the NADW is replaced by colder waters entering the Atlantic via Drake Passage around South America. This so-called 'cold water route' has been favoured by many studies based on the inversion of hydrographic data (Rintoul, 1991; Weijer, 2000). A combined circulation scheme was then proposed by Gordon et al. (1992), based on a detailed analysis of hydrographic data obtained around South Africa. These data suggest a combination of the warm and cold water route, by which the cold water that enters the Atlantic via Drake passage first loops through the western Indian Ocean before spreading northward into the Atlantic (Fig. 1.4).

This scheme is supported by recent modeling results. By Lagrangian analysis of output from a state-of-the-art OGCM Speich et al. (2001) find a total contribution of 13.9 Sv (1 Sv equals 10^6 m^3s-1) flowing from the Indian Ocean northward through 20°N in the Atlantic Ocean. This value, surprisingly close to the 13.5 Sv Indian-Atlantic exchange estimated by Gordon (1986), is composed of waters entering the Indian Ocean as Indonesian Throughflow water (ITF), following the route described by Gordon et al. (1992) from Drake Passage looping through the Indian subtropical gyre, and an additional input from south of Australia.

The impact of the interocean exchange south of Africa has been studied by Weijer et al. (1999, 2001). Their modeling results show a considerable sensitivity of the meridional overturning strength of the Atlantic, to a thermohaline source such as the Agulhas leakage (Weijer et al., 1999). In a modelling study, Weijer et al. (2001) show that the present day thermohaline circulation is stabilized by the inflow of warm saline waters from the Indian Ocean. In the absence of this inflow of Agulhas water, the fresh inflow from the Bering Strait may destabilize the Atlantic meridional overturning circulation, which is of vital importance to the mild climatic conditions of the North Atlantic region. GCM simulations by Weijer (2000)

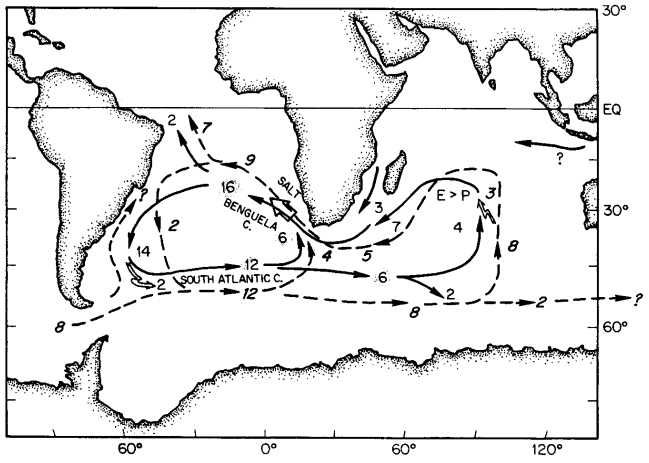

Figure 1.4: *The hybrid scenario proposed by Gordon et al. (1992). The cold water route loops through the Indian Ocean Subtropical Gyre before re-entering the Atlantic as Agulhas leakage.*

show that a strengthening (weakening) of the Indian-Atlantic exchange results in enhanced (reduced) meridional overturning within decades.

A wide range of paleoclimatic observations exists, providing evidence for a strong coupling of North Atlantic Climate to that over the Indian Ocean, on timescales of centuries (Verschuren et al., 2000), to millennia (Zonneveld et al., 1997; Van Campo et al., 1987) and Milankovitch timescales (Beaufort et al., 1997; Cayre et al., 1999). Three mechanisms are generally mentioned to explain these connections. All three (changes in the global thermohaline circulation, in the atmospheric circulation patterns over the northern hemisphere, and in ice/snow coverage of Central Asia and Tibet) are used to describe how the glacial/interglacial periods over the North Atlantic sector may have modified the climatic boundary conditions of the Indian Ocean. More specifically, most observations seem to find weaker monsoon activity over the equatorial Indian Ocean region (Zonneveld et al., 1997; Marcantonio et al., 2001) during glacial periods, and strong intensification of (southwest) monsoon activity during deglaciation and interglacial periods. On the other hand, Cayre et al. (1999) find enhanced primary production in the central equatorial Indian Ocean during glacial periods, which is attributed to stronger equatorial winds, inducing upwelling near the Maldives. Also, Verschuren et al. (2000) show how colder episodes in more recent history (the past 2000 years) were accompanied by periods of enhanced precipitation over equatorial Eastern Africa.

A link to the thermohaline circulation has been made by Berger and Wefer (1996), with observations of tropical foraminifera (*Globorotalia menardii*). This species was not found in the Atlantic Ocean during the last glacial maximum, but was reintroduced during the deglaciation, probably from the Indian ocean, where the species is observed in records from the glacial period. This suggests a temporary breakdown of the interocean exchange south of Africa during the last glacial maximum, and a restart of Agulhas leakage during deglaciation. A northward translation of the wind systems of the southern hemisphere during the glacial

period may have been responsible for this effect. As described above, the line of zero wind stress curl, defining the southern boundary of the subtropical gyre, lies south of Africa in our present day climate (Fig. 1.1), thus allowing for interocean exchange between the Indian and Atlantic Oceans. A northward translation of this subtropical convergence zone might close this route forexchange between the oceans.

Indian-Atlantic interocean exchange

The exchange of waters from the Indian to the Atlantic Ocean south of Africa is largely achieved by the shedding of Agulhas Rings (see De Ruijter et al. (1999) for a review). The rings shed from the Agulhas current consist of relatively warm and salty Indian Ocean water (Olson and Evans, 1986; Gordon et al., 1987) compared to the ambient South Atlantic waters. Together with direct Agulhas leakage (Gordon, 1985), they constitute a distinctive source of heat and salt for the Atlantic.

Assuming complete compensation by NADW for a total volume flux of 14 Sv, Gordon (1985) has obtained a heat flux estimate from the Indian to the Atlantic Ocean of 0.5 PW. Based on six rings shed per year (see also below) they contribute about one third to the total estimated fluxes. These numbers are of comparable magnitude to estimates of the equatorward heat flux from observations across 30°S (Fu, 1981; Schlitzer, 1996).

Agulhas Rings have been measured hydrographically (eg. (Gordon et al., 1987), see Fig. 1.5) and by remote sensing techniques. Until recently, the latter were confined to sea-surface temperature measurements (eg. Harris et al. (1978)). Because of strong air-sea interaction, the positive sea surface temperature anomalies of Agulhas rings disappear quickly (Olson et al., 1992). Rings can therefore be identified from thermal infrared images only for a very limited part of their lifetime. Moreover, clouds are dominant over the region south of Africa. The signature of Agulhas rings in sea surface height (SSH) stays visible far longer, making satellite altimeter measurements very useful for monitoring the behavior of Agulhas rings (Wakker et al., 1990; Gordon and Haxby, 1990).

Observations of Agulhas Rings

The first altimeter satellite that provided the oceanographic community with a considerably long period of high quality data, thus enabling the monitoring of Agulhas Rings over several years, was the GEOSAT satellite in its Exact Repeat Mission (ERM) between 1986 and 1989. Using the GEOSAT data, a number of studies were made, and the first reliable estimates of the number of Agulhas rings shed per year could be made. Gordon and Haxby (1990) showed that between November 1986 and 1987 five rings were shed into the Atlantic. Feron et al. (1992) extended these measurement over two more years, and counted between four and eight rings per year. This number was confirmed by the results of Byrne et al. (1995), who used the same GEOSAT ERM data. Goñi et al. (1997) studied the first years of the TOPEX/Poseidon altimeter data (1992-1995) and counted between four and six rings per year over that period.

Not only the number of rings is important in estimating the possible contribution of the Agulhas Rings to the global overturning circulation. Also the amount of Indian Ocean water carried by each ring, the paths followed by the rings, and their decay rate are important quantities in this estimate. The volume transports associated with an average Agulhas Ring

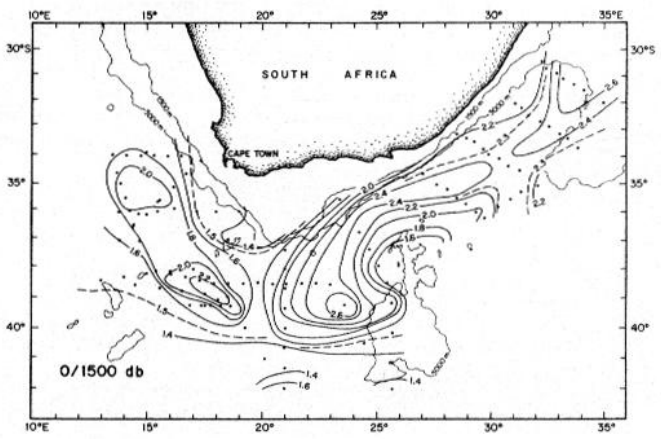

Figure 1.5: *Dynamic sea-surface heights relative to the 1500 dbar surface (m) (Gordon et al., 1987). The hydrographic measurements were made in October-December 1983.*

are estimated between 0.5 and 1.5 Sv, yielding comparably large ranges for the heat and salt anomaly estimates (see De Ruijter et al. (1999) for a review of the various estimates). Decay of the rings was estimated to be roughly exponential with the distance from the Agulhas Retroflection region (van Ballegooyen et al., 1994; Byrne et al., 1995). The decay estimated by Byrne et al. (1995) was based on a small number of rings (10). As more recent observations have shown that the propagation of the rings may be very irregular (sometimes showing hardly any movement at all for several months (Arhan et al., 1999)) the age of the ring may be a better predictor for its decay than its location with respect to the Agulhas retroflection. With the large amount of new high quality altimeter data provided by the TOPEX/Poseidon satellite, it may be possible to give a more detailed description of the rate of decay of the Agulhas Rings. This decay may be particularly important: deposition of Indian Ocean water in the Benguela region provides the South Atlantic with temperature and salt anomalies that may be available for the meridional overturning circulation.

In this thesis, research is presented on the characteristics of the Agulhas leakage by Agulhas Rings that can be observed in several years of TOPEX/Poseidon altimeter data. Emphasis is on the number of rings, the decay rate, and on some processes that may play a role in the decay of the rings, such as the interaction with bottom topography and the splitting of large rings into smaller ones.

Upstream Control and Agulhas Ring shedding

The monitoring of the Agulhas system over several years that has been enabled by the altimeter data, also strongly improved our ability to investigate the ring shedding mechanism itself. Lutjeharms and Van Ballegooyen (1988) were the first to do so from infrared SST measurements, and found that the Agulhas Retroflection slowly progrades westward with a constant speed of about 13 km/day. This process is ended by an eastern shortcutting of the current which results in a sudden return to an eastern position of the retroflection, and the

shedding of a large anticyclonic ring of Agulhas water to the west. Their observations were severely hampered by the cloudiness over the Agulhas region, and their number of Agulhas rings shed per year (9 per year between 1978 and 1983) seems to be unrealistically high.

The Agulhas ring statistics obtained by the less problematic SSH measurements (Feron et al., 1992; Goñi et al., 1997) have shown long periods (up to six months) during which no Agulhas rings are shed into the Atlantic at all. This observation, and the rather stable ring shedding frequency of 4-6 during the 80's and 90's raises the question what controls the timing and frequency of Agulhas Ring shedding. An interesting feature of the Agulhas current system that has been related to the control of the ring shedding is the Natal pulse (Lutjeharms and Roberts, 1988). Growing cyclonic meanders in the upstream Agulhas (originating near the Natal Bight) have been found to precede the shedding of Agulhas Rings by almost half a year (van Leeuwen, 1999). A theoretical analysis of the local current characteristics and continental shelf configuration along the path of the upstream Agulhas has shown that the slope of the shelf is steep enough to prevent barotropic instability of the Agulhas along most of its trajectory. The exception to this is the Natal Bight near Durban (30°S) where the slope relaxes and the Agulhas becomes marginally stable: small perturbations to the strength or shape of the current may lead to instabilities and start a Natal Pulse (De Ruijter et al., 1999). These perturbations of the flow may be caused by fluctuations of the strong local recirculation gyre in the southwest Indian Ocean (Stramma and Lutjeharms, 1997; Feron et al., 1998), by eddies interacting with the Agulhas current (Gründlingh, 1995; Biastoch and Krauss, 1999), or by nonlinear interaction between the flow and initial perturbations (van der Vaart and de Ruijter, 2001).

Eddies interacting with the Agulhas current have been observed in altimeter data and ocean circulation models (Gründlingh, 1995; Biastoch and Krauss, 1999). Gründlingh (1995) showed that (cyclonic) eddies may become attached to the offshore side of the Agulhas. These cyclonic eddies are not likely to provide the perturbation to the current that may cause instability, but absorption into the current proper may lead to the (cyclonic) Natal Pulses. Biastoch and Krauss (1999) showed that anticyclonic eddies may also be found on the offshore edge of the Agulhas. Their high resolution local model of the Agulhas system produced strongly surface-intensified eddies in the Mozambique Channel propagating southward into the Agulhas Retroflection region, where they modulate the inter-oceanic exchange. The existence of these eddies was confirmed by altimetric observations. Recent hydrographic observation in the Mozambique Channel have confirmed the dominance of anticyclonic eddies in the channel, and have shown that the eddies have a strong barotropic component (De Ruijter et al., 2002).

In this thesis, the upstream control of Agulhas Ring shedding is investigated further, using altimetric data from the TOPEX/Poseidon and ERS satellites. These data enable a detailed study of the eddies in the Mozambique channel and from south of Madagascar, and their influence on the Agulhas Retroflection. Also, their relation to the Natal Pulse is investigated. From the local processes in the upstream Agulhas regions, we investigate more remote forcing of the Indian-Atlantic exchange variability. A four per year cycle present throughout most of the Indian Ocean has been discovered, and found to form a link between wind variability over the equatorial Indian Ocean, and the interbasin exchange south of Africa. This may help to explain the paleo-oceanographic links found between the glacial-interglacial periods over the North Atlantic basin and the equatorial Indian Ocean.

Outline of the thesis

Although considerable progress has been made within the last two decades in the understanding of the complex interplay of local and large scale current systems coming together in the Agulhas Retroflection region, there are numerous outstanding questions considering the interbasin exchange south of Africa. In this thesis, a few of these questions are treated, some questions are answered, and new questions are raised. The two leading questions of this thesis are:

- Can we characterize the interbasin exchange south of Africa by means of altimetric measurements of the sea-surface elevation?
- What dynamical processes control the shedding of Agulhas rings, and thereby the interbasin exchange around South Africa?

After a short chapter (chapter 2) on the tools and techniques used in this thesis, we investigate in chapter three the interocean exchange south of Africa by analysis of satellite altimetric measurements of the sea-surface height anomalies. The specific questions dealt with in chapter three, are: How many rings are shed into the Atlantic? What is the decay rate of the rings? Where does the decay take place? Can processes be identified which play a role in this decay?

In chapter four, it is shown that there seems to be far more regularity in the ring shedding process itself, than was expected from previous studies (Feron et al., 1992; Goñi et al., 1997; Schouten et al., 2000). It turns out that the irregularity observed in those studies does not originate in the Agulhas Retroflection region, but rather in the Atlantic itself. Ring splitting, irregular paths, ring-ring and ring-topography interactions in the Cape Basin may cause the intrusion into the Atlantic to appear irregular. In this chapter, we investigate how the regularity in the shedding of Agulhas Rings is related to upstream (i.e. Indian Ocean) processes. Specific questions answered here are: What processes control the timing and frequency of Agulhas Ring shedding? How crucial are these processes for the interocean exchange?

Next, in chapter five we investigate a mechanism that may be responsible for the frequency of the regular ring shedding process described in chapter four. Statistical analyses of the SSH measurements in the Indian Ocean are applied to investigate the following questions: Where does the observed frequency (of about four per year) originate? How does this signal propagate towards the upstream Agulhas Regions? To what extent may large scale interannual variability (e.g. the El Niño/Southern Oscillation cycle) disturb this signal?

The four per year signal seems to originate in the equatorial band of the Indian Ocean, and propagate into midlatitude regions by means of a coastal Kelvin wave along the Indonesian coast. The signal then crosses the Indian Ocean at midlatitudes by means of baroclinic Rossby waves. Around Madagascar, the signal amplifies and eddies are formed in the Mozambique Channel and south of Madagascar. These drift southward into the Agulhas Retroflection region. The chain of information propagation thus proposed might form an alternative connection between climate variability over the Indian and Atlantic Oceans: changes in the atmospheric or oceanic circulation over the Indian Ocean may disrupt the pin-ball mechanism, and reduce the Indian-Atlantic leakage. This may make the Atlantic vulnerable to regime switches whereby the complete thermohaline circulation is altered (Weijer et al., 2001) with all the climatic implications, such as glacial periods over the regions surrounding the North

Atlantic. However, several difficulties with the pin-ball mechanism still remain. Some of these difficulties are dealt with in chapters six and seven. The main question treated there is: How is the (relatively small amplitude) Rossby wave signal in the south Indian Subtropical gyre transformed into the highly energetic eddies observed in the Mozambique Channel?

Chapter 2

Tools and techniques

2.1 Satellite altimetry and oceanic variability

Since 1975, successful efforts have been made to measure the geometrical shape of the global sea surface. Since the GEOSAT satellite was launched in 1985, oceanographers have been able to study the variability of the ocean surface. Altimeter measurements have greatly improved the accuracy by which the marine geoid is known. The GEOSAT and ERS-1 altimeters have been measuring the sea surface at very high spatial resolution in so-called 'geodetic missions'. For these missions the orbital parameters were such, that the spatial resolution was very high, but with no repeat measurements. Combined with surface gravity data, and data from the repeat period missions of T/P, ERS-1/2 and GEOSAT this has led to the new Earth Gravity Model 1996 (EGM96) (Lemoine, 1998). By now, we have over a decade of reliable measurements of which especially the TOPEX/Poseidon data have greatly improved our knowledge of the oceans and its time-varying component in particular. In table 2.1 all altimeter missions and their period of operation are listed. In this thesis, data from the TOPEX/Poseidon (T/P) and ERS-1 and 2 altimeters are used.

Satellite	From	Period
GEOS-3	NASA	1975 - 1978
SEASAT	NASA	1978
GEOSAT	US Navy	1985 - 1990
ERS-1	ESA	1991 - 1996
TOPEX/Poseidon	NASA/CNES	1992 - ?
ERS-2	ESA	1995 - ?
GEOSAT Follow On	US Navy	1998 - ?
JASON	NASA/CNES	2002 - ?
ENVISAT	ESA	2002- ?

Table 2.1: *Overview of past, present and near future satellite altimeter missions. By February 2002, six altimeters may be working simultaneously.*

Here only a short summary of the altimetric technique is given. The interested reader is referred to other literature for more details. Much of the information has been obtained from (Chelton, 1988) and (Schrama, 1996).

The first step, quite far from the oceanographic application of altimetry, in the altimetric process is the geometrical determination of the sea-surface height. This is achieved by combining very accurate information on the location of the satellite and high precision measurements of the distance between the satellite and the sea surface topography from space. The exact orbit determination of the satellites is one of the crucial steps in which great improvements have been made over the last decade. One of the main improvements between the GEOSAT altimeter and the next generation (TOPEX/Poseidon (T/P) and the European Remote Sensing Satellite (ERS)-1) was in the improvement of the orbit estimation. The radial orbit errors were typically 1.5 m, mainly due to the limited knowledge of the gravity field. These poorly defined orbits did not make altimetry useless for the study of the oceans, as intelligent processing could reduce the impact of the individual orbit errors (Schrama, 1989). The higher orbit of the T/P satellite (1330 km) with respect to the older altimeters, but also ERS (800 km) and the improved gravity models made the gravity model a less crucial part of the total accuracy assessment. Also the modern tracking systems such as DORIS, and the application of GPS on the satellite have brought the orbit errors of T/P down to less than 2.5 cm.

The determination of the distance between the satellite and the ocean surface is the other main component in the determination of the geometrical ocean surface. Microwaves transmitted by the altimeter travel through the atmosphere, interact with the ocean surface, and travel back to the altimeter. Underway, the atmospheric conditions modify the speed of the signal, and the conditions of the ocean surface determine the amount of signal that is reflected to the satellite, and the shape in which this occurs. Also the characteristics of the ocean surface modify the received signal. The small scale roughness of the ocean,closely related to the surface wind speed, largely influences the amount of radar signal that is reflected towards the satellite. This does not modify the travel time of the signal. However, the large scale roughness of the ocean, the waves, do. The shape of the pulse that is received back is determined by the wave height: large waves cause a large time difference between the part of the signal that returns from the troughs of the waves, and the part that is reflected by the crests. Algorithms have been developed to determine the significant wave height from the shape of the returned signal (Chelton, 1988). A correction is also made for the fact that troughs reflect more of the signal than the wave crests do (due to geometrical conditions), causing the sea level to be estimated lower than it is, depending on the wave height. This correction is called the electromagnetic bias.

Once all corrections are applied, we are now able to define the geometrical shape of the sea surface to an accuracy of about 2 cm. With this quantity defined, different approaches are possible, depending on peoples interests. The signal of one person is usually the noise of another. For oceanographic applications, the main quantity to be derived is the dynamic sea surface topography: the deviation from an ocean at rest, unforced by tidal forces. However, for other disciplines this hypothetical 'ocean at rest', which is also called the marine geoid, is of crucial importance. We will here look from the oceanographic point of view.

contributor	range
Marine geoid	-100 to +100 m
Ocean tides	1-2 m
Earth tides	10-20 cm
Atmospheric pressure loading	10-20 cm
Large scale ocean circulation	$<$ 1 m
Mesoscale eddies	$<$ 1 m
Rossby waves	$<$ 10 cm

Table 2.2: *The main contributions to the geometrical shape of the sea surface as determined by satellite altimetry.*

The shape of the sea surface is made up of several components. We will mention most of these shortly, and tabulate their order of magnitude in table 2.1. The marine geoid ranges roughly between -100 and +100 m relative to a reference ellipsoid we take as the basis of our geometrical description. Its large scale features, i.e. at length scales of 1000 km and up, have been fairly well resolved, but for oceanographic applications the errors at the shorter scales are still unacceptably large. Ocean tides are usually corrected for, but may also be the scope of study. In fact, altimetry has greatly improved tidal models over the last decade. Also, the dissipation of tidal energy in the oceans, for long an outstanding question in oceanography, is being estimated using satellite altimetry (Egbert and Ray, 2000). Tidal forces are not just affecting the oceans: also the earth itself is subject to deformation. These effects are not measured by land based tide gauges, but do show up in the altimeter data.

Another important correction to be applied is that for the effect of atmospheric pressure loading on the oceans. Pressure differences will cause the ocean surface to be depressed by about 1 cm per mbar difference, but the exact effect of atmospheric pressure is subject to change depending on the scales in time and space on which pressure differences are imposed.

The remaining signal may be attributed to the ocean circulation. The part of the dynamic height of the sea surface not caused by the tidal currents is the signal that is of use in this thesis. More specifically, it is the time-varying part of this signal that is used throughout this thesis, as the mean oceanic circulation is not yet completely determined. The mean ocean circulation contribution cannot yet be discriminated from the geoidal signal, as for that we need independent measurements of either the gravitational field of the earth, or the time mean oceanic circulation. Mesoscale eddies and Rossby waves have been added to table 2.1 with their respective maximum ocean surface expressions, as they are the main observed phenomena in this thesis.

The total variability of the SSH due to the transient processes (the deviations from the mean sea-surface height) is plotted in Fig. 2.1. From this figure, the regions showing strong variability in oceanic flow can be determined. Regions of high variability are primarily associated with the western boundary currents and their extensions into the basins. These currents show variability in their paths, but are also known for various types of eddy shedding processes. Regions of enhanced variability are also observed in the Antarctic Circumpolar current (ACC) and at several other locations.

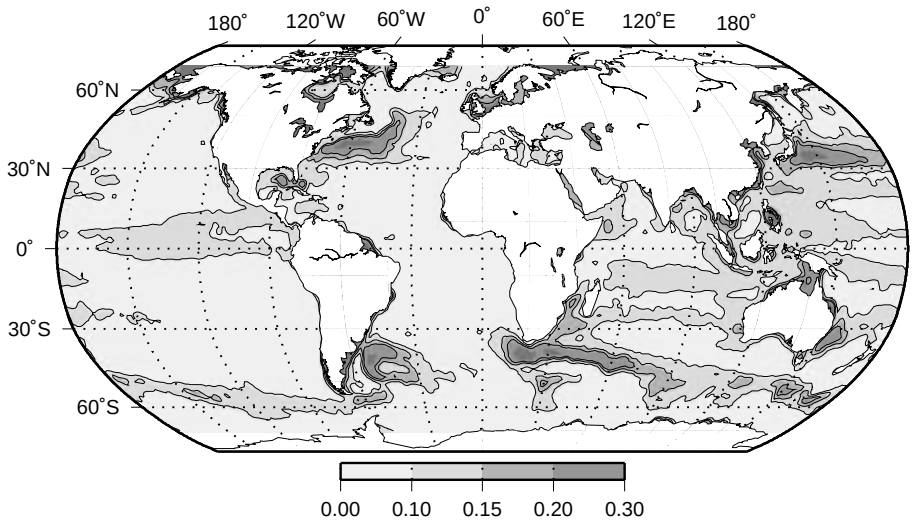

Figure 2.1: *Variability of the sea-surface heights measured by TOPEX/Poseidon over the years between 1992-2000 (m).*

2.2 Statistical tools

Filtering

To extract phenomena on different timescales, sometimes the altimeter data used in further statistical analysis are prefiltered. To remove high frequency phenomena, a running mean can be applied with a Gaussian shaped weight vector. The width of this Gaussian shape determines the filtering characteristics. For four different window-lengths, the frequency transfer functions are plotted in the left panel of Fig. 2.2. To remove the low frequency part of the spectrum, the same procedure is followed, but now the low-pass filtered data are subtracted from the original data. The remaining signal is the high frequency part of the spectrum. This has often been done as a prefiltering before MSSA analysis (to be discussed later in this section).

Empirical Orthogonal Function Analysis

Empirical Orthogonal Functions (EOF's) is a statistical technique that was first used in the social sciences to detect relations between large numbers of questionnaire data. Its applications to climate and geophysical data analysis were first examined by Lorenz (1956). EOF analysis is used to extract patterns and timeseries from a dataset X which is build up of n realizations of the state vector S. This state vector S contains m data points for each realization. This number m is usually the number of grid points. So our dataset may be written as: $X_{i,j}, i = 1..n, j = 1, m$. With the patterns and timeseries it can be desirable to describe the dominant behaviour of the dataset with as few degrees of freedom as possible. Therefore, it is necessary to define 'dominant'. When we define in our data-space the mean and variance

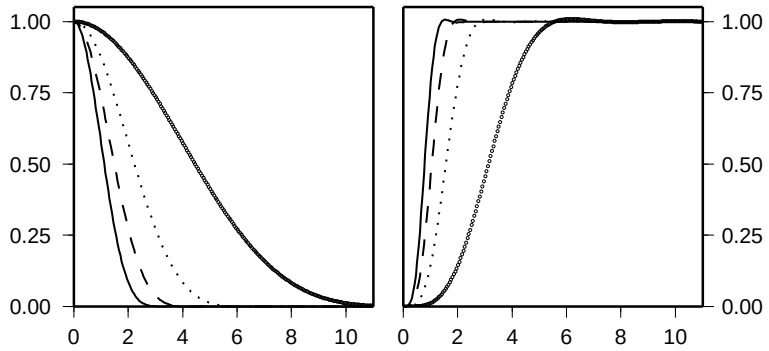

Figure 2.2: *Frequency transfer functions for (left panel) Low-pass filtering with Gaussian shaped filters of half-width 30 days (wooly line), 60 days (dotted), 90 days (dashed) and 120 days (solid); (right panel) High-pass filtering with Gaussian shaped filters of half-width 100 days (wooly line), 200 days (dotted), 300 days (dashed) and 400 days (solid). Along the horizontal axis the frequencies are plotted (in cycles per year).*

of a single timeseries by the common definition:

$$\mu_j = \frac{1}{n}\sum_{i=1}^{n} X_{i,j}, \qquad \sigma_j^2 = \frac{1}{n}\sum_{i=1}^{n}(X_{i,j} - \mu_j)^2,$$

we can obtain a measure the total variance of the dataset X by $\sum_{j=1}^{m}\sigma_j^2$. A reasonable definition of a dominant mode would be 'a single mode that describes as much of this total variance as possible'. Mode number k, characterized by a pattern $P_j^k, j = 1, m$ with the same dimension as the statevector S and an associated timeseries $a_i^k, i = 1, n$, has a variance:

$$\sigma_k^2 = \sum_{j=1}^{m}\sum_{i=1}^{n}(P_j^k a_i^k)^2.$$

It can be shown (Preiseindorfer, 1981) that maximization of this variance implies that the patterns P^k are the eigenvectors of the covariance matrix $X^T X$. The eigenvector with the largest eigenvalue is the pattern that describes most of the variance. Other characteristics of this analysis are:

- The patterns P^k are orthogonal. They can be normalized to unity so that $\sum_{j=1}^{m} P_j^k P_j^l = \delta_{kl}$. This implies an increasing constraint on all patterns following the first one.
- The timeseries a^k are also orthogonal. This implies zero-correlation at lag 0.
- The variance of the k'th EOF is given by the k'th eigenvalue λ_k of the covariance matrix.
- The fraction of the total variance that is explained by the k'th EOF (also called the contribution of EOF k) is given by $c^k = \lambda_k / \left(\sum_{l=1}^{min(m,n)} \lambda_l\right)$.

It should be noted that the EOF's are purely statistical constructs, to which no physical meaning should be attributed. Only when there is a good physical explanation for the phenomena one tries to explain with EOF analysis, the patterns found may be interpreted in terms of physical modes or processes. Another field of application of EOF's is in data compression, and it is often used as such in a preprocessing of data before more sophisticated techniques are applied, such as MSSA analysis.

Multichannel Singular Spectrum Analysis

MSSA is a multivariate time series analysis technique suitable for the detection of propagating patterns and oscillatory modes (Plaut and Vautard, 1994). It is based on the traditional Empirical Orthogonal Functions technique. We are dealing with the same dataset X, but now we don't define our state vector as the representation of the data at one moment, but take a number of lagged copies of the state vector as used in EOF analysis. So now our dataset X is not made up of n realizations of the state vector S, but of $n - M + 1$ realizations of the stacked state vector T defined as:

$$T_i = \left[S'_i\, S'_{i+1} \ldots S'_{i+M-1}\right]'$$

The procedures followed further are identical to those for EOF analysis. Again, the eigenvectors and eigenvalues of the covariance matrix are obtained. The largest eigenvalues are coupled to the modes of variability that contain most of the variance. However, as our state vector is defined in another way than that in EOF analysis, variance in this case is not the same. Variance in the MSSA analysis denotes the variance of the M times larger state vector. Therefore, the variances found by the eigenvalues cannot be interpreted in the same way as those of the EOF-analysis. Although the MSSA-modes are orthogonal too, they are so in the sense of the larger state vector. So in the traditional way of defining variance (like we did for the EOF-analysis) the modes are not orthogonal. The covariance at lag 0 of the reconstructed modes from the MSSA analysis is not necessarily zero. If we compute the variance of all individual modes in the 'normal' way, the sum of these will be larger than the original total variance. This can be considered both a positive and a negative effect. On the one hand it is more difficult to assess the strength of a mode, and to interpret the amplitudes that are given by a single mode. On the other hand, the larger number of degrees of freedom reduces the constraint the orthogonality puts on the patterns found. Two processes with (partially) overlapping patterns, but different timescales, may still be detected separately.

Oscillatory modes may be detected by MSSA analysis when the following criteria are met (Plaut and Vautard, 1994):

- Two consecutive eigenvalues are almost equal
- The corresponding MSSA-timeseries are in quadrature
- The corresponding MSSA-EOF's (containing a series of M state vectors S) are in quadrature.

These criteria follow from the assumption that when an oscillation is observed and a complete period of this oscillation is represented in an MSSA-EOF (the EOF contains a 'movie' of the

oscillation), also the same oscillation but shifted one quarter of a period will be present. This MSSA-EOF will be orthogonal to the first one, as will its corresponding timeseries. As they describe the same process, the eigenvalues will be identical as the total variance of this oscillation will be equally split up between the two MSSA-components. An oscillation that meets these criteria can be reconstructed by combining a part of the expansion into MSSA-modes. Such a reassembled oscillation is called the 'reconstructed component', usually followed by its numbers (like RC 1/2 when the first two components are reconstructed into a filtered version of the original dataset).

2.3 An example

To illustrate the use of the techniques described earlier in this chapter, an example is presented, where global sea-surface height measurements are analyzed. All TOPEX/Poseidon measurements from 1992-2000 are binned into 2.5°x 2.5°x 10 day bins. Only locations where the water is deeper than 500 m are taken into account. First, the EOF's of the unfiltered dataset are computed. The first four EOF's all contain part of the annual cycle, but all are mixed up with the strong interannual variability associated with the El Niño/ Southern Oscillation (ENSO) event of 1997 (Fig. 2.3, upper panel.). The same holds for the next several EOF's: the annual and interannual variability are split up into a substantial number of EOF's, disclarifying the picture.

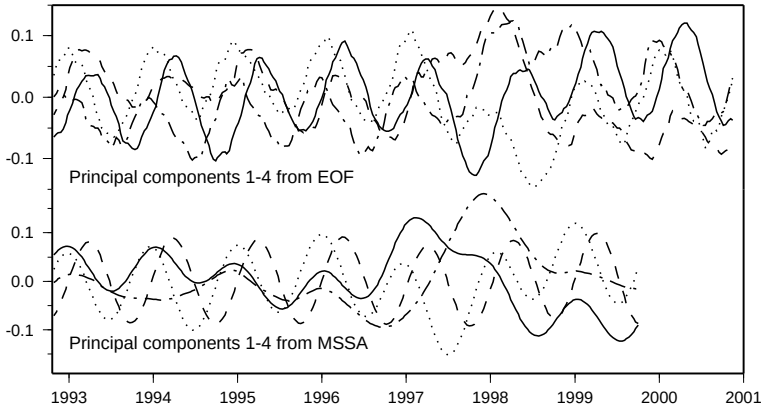

Figure 2.3: *First four principal components of the EOF (upper panel) and MSSA (lower panel) analyses of the original SSH data.*

Also the MSSA analysis is unable to extract a clear annual cycle: the first four MSSA components (plotted in the lower panel of Fig. 2.3) show more or less the same irregularity. It obviously is very difficult to obtain a good description of the annual cycle from this analysis, and things are even worse for higher frequency phenomena. It is for these reasons that on several occasions in this thesis the altimeter data are prefiltered. In our case for this example, a prefiltering with a Gaussian half width of 300 days (see section 2.2) clears up the problems with the original dataset. The low-pass filtered dataset contains mainly the interan-

nual variability. Its contribution to the total variability, (Fig. 2.4) shows that the interannual variability is indeed located primarily in the equatorial regions of the Pacific Ocean (the El Niño variability) and Indian Ocean (the variability associated with the Indian Ocean Dipole (Webster et al., 1999), of which the link to the ENSO cycle is yet unclear (Saji et al., 1999)). The dominant EOF of the low-pass filtered data shows the well-known El Niño pattern over the Pacific, and the accompanying Indian Ocean Dipole as both occurred simultaneously in 1997, the only major El Niño year captured by the T/P altimeter. The next two EOF's (not shown) represent the breakdown and buildup of this pattern, respectively.

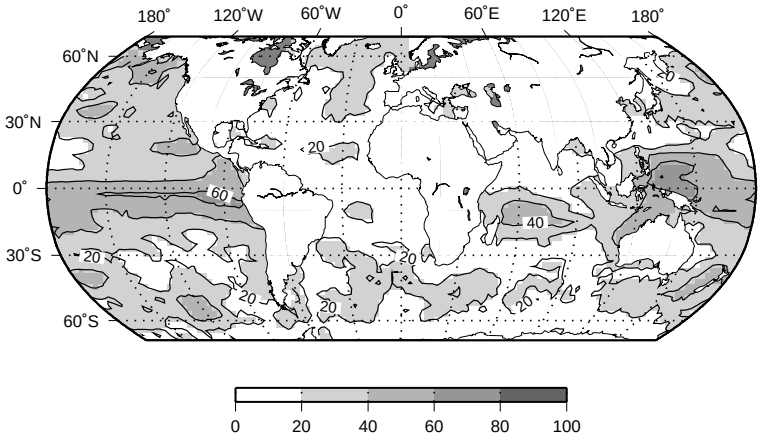

Figure 2.4: *Percentage of the total variability (%) that is on the low frequencies. This is mainly the ENSO-associated variability (see table 2.3).*

In table 2.3 the results of the three analyses are summarized. Clearly the main effect is in the filtering. It has separated the interannual variability from the seasonal signals, and allows the statistical procedures to resolve the annual and semi-annual signal far better.

The high-pass part of the data now enables an undisturbed look at the annual cycle. The first two EOF's of this dataset clearly show an annual behavior. We are now also able to resolve the semi-annual cycle from this dataset. The third and fourth EOF contain this (propagating) signal. Both the annual and semi-annual modes also show up first in the MSSA analysis. The first principal components of the EOF and MSSA analysis are shown in Fig. 2.5. In this case, the MSSA analysis was not really necessary as it does not give much information that we could not get from the EOF-analysis. But several reasons may alter this in other circumstances:

- Propagating patterns are often not well described by EOF's due to the orthogonality constraints. In this example, the two dominant oscillations are strong enough to also show up as the first number of EOF's, which are not very much constrained by the preceding EOF's. Usually this is not the case.

- When the period of the oscillation is not clear on beforehand, the MSSA technique may bring out modes of variability that were unnoticed from the EOF analysis alone.

	EOF			MSSA	
Dataset	k	c^k	description	k	description
Original	1-4	50%	Annual+ENSO	1	Annual+ENSO
	5-7	15%	ENSO	2	ANNUAL
				3	Annual+ENSO
				4-6	ENSO
low-pass	1	35%	ENSO		
	2	15%	ENSO -post-		
	3	10%	ENSO -pre-		
high-pass	1-2	15%	Annual	1-2	Annual
	3-4	6 %	Semi-annual	3-4	Semi-annual

Table 2.3: *Three ways of analyzing the global SSH dataset (2.5° resolution). EOF and MSSA components are listed according to their dominant signal or frequency. With the original data, the interannual (mainly ENSO) variability is mixed with the other components, disabling a clear separation of the other signals. This is circumvented by prefiltering of the data.*

An oceanographic example of this approach can be found in Schmeits and Dijkstra (2000), where a 9 months cycle in the Gulf Stream region was described. There was no reason to expect this frequency on beforehand, as it seems to be set by internal ocean dynamics and not by e.g. the annual forcing.

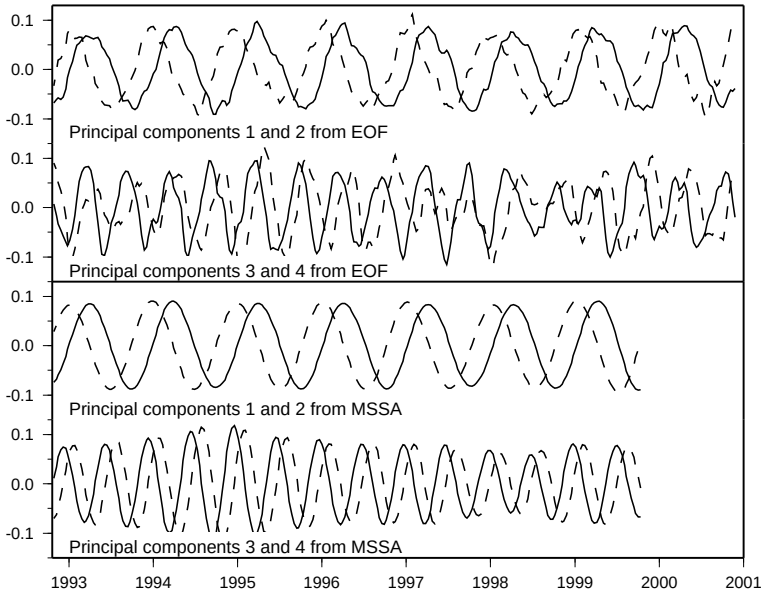

Figure 2.5: *Like in Fig. 2.3, the first four principal components of the EOF and MSSA analysis are plotted.*

The variability in the annual cycle of global SSH variability is plotted in Fig. 2.6a, and shows the effects of thermal expansion (which explains the relatively uniform presence of variability) and the relatively strong annual signals in the equatorial bands of the Pacific and Indian Oceans. In Fig. 2.6b the same is plotted for the semi-annual mode, showing that this frequency is primarily found in the equatorial bands of all three oceans. The timeseries of this mode suggests equatorial Rossby and Kelvin waves at the semiannual frequency in all three basins.

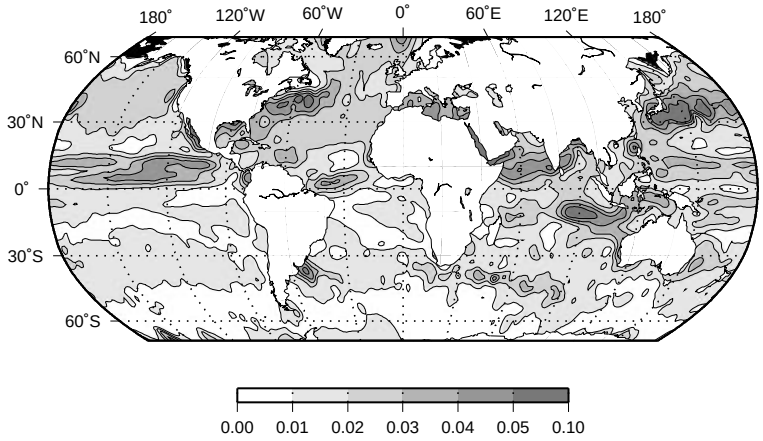

(a) the annual MSSA mode

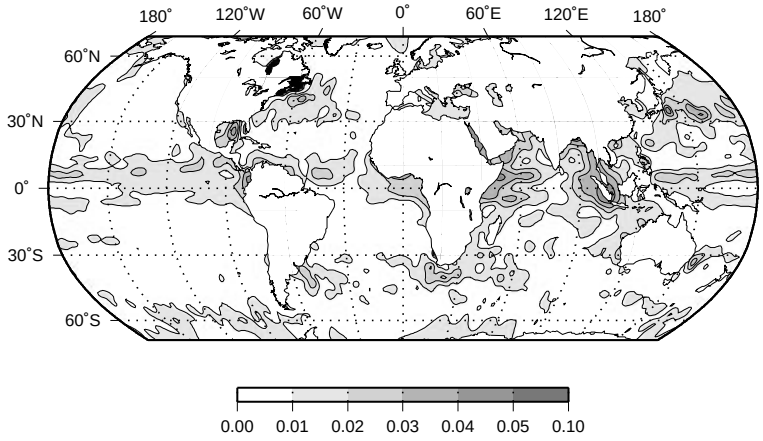

(b) the semi-annual MSSA mode

Figure 2.6: *Variability of the reconstructed MSSA modes 1&2 (the annual mode) and 3&4 (the semiannual mode) of the high-pass filtered SSH data (in m).*

Chapter 3

Translation, decay and splitting of Agulhas rings in the southeastern Atlantic Ocean

All Agulhas rings that were spawned at the Agulhas retroflection between 1993 and 1996 (a total of 21 rings) have been monitored using TOPEX/Poseidon satellite altimetry and followed as they moved through the southeastern Atlantic Ocean, decayed, interacted with bottom topography and each other, or dissipated completely. Rings preferentially crossed the Walvis Ridge at its deepest parts. After having crossed this ridge they have lower translational speeds, and their decay rate decreases markedly. Half the decay of long-lived rings takes place in the first 5 months of their lifetimes. In addition to the strong decay of rings in the Cape Basin, about one third of the observed rings do not seem to leave this region at all but totally disintegrate here. The interaction of rings with bottom topography, in particular with the Vema Seamount, is shown frequently to cause splitting of rings. This will enhance mixing of the rings' Indian Ocean water into that of the southern Atlantic. This localized mixing may well provide a considerable source of warm and salty Indian Ocean water into the Atlantic overturning circulation.

3.1 Introduction

The Agulhas current is the western boundary current to several nested anticyclonic gyres in the South Indian Ocean. On the basin scale it is constituted by the wind-driven subtropical gyre of this ocean. On a smaller scale it is fed by a distinct subgyre concentrated in the southwestern part of the Indian Ocean (Stramma and Lutjeharms, 1997), which encloses an even tighter eddy-driven recirculation cell (Feron et al., 1998). Major contributions to the Agulhas current's volume transport come from these subgyres. For instance, the Agulhas transport has been estimated to increase from 65 Sv at 32°S to 95 Sv at the southern tip of Africa (Gordon et al., 1987).

Having become detached from the African continent around 35°S, the Agulhas current continues as a free jet in a west-southwesterly direction. Around 20°E it makes a strong anticyclonic turn back into the Indian Ocean, while conserving its potential vorticity (De Ruijter and Boudra, 1985; Ou and de Ruijter, 1986). The location of this retroflection loop is highly variable, as monitored by infrared imagery (Lutjeharms and Van Ballegooyen, 1988) and by radar altimetry (Feron et al., 1992; Wakker et al., 1990). Intermittently, the westward progradation of the retroflection loop is terminated by the shedding of a large Agulhas ring when the current loops back upon itself. This event may be triggered by meanders in the Agulhas current, causing the shortcut between the current itself and the Agulhas Return current (Lutjeharms and Van Ballegooyen, 1988; Van Leeuwen et al., 2000).

The rings shed from the Agulhas current consist of relatively warm and salty Indian Ocean water (Olson and Evans, 1986; Gordon et al., 1987) compared to the ambient South Atlantic waters. Together with direct Agulhas leakage (Gordon, 1985), they constitute a distinctive source of energy and salt for the Atlantic. This feeds a net equatorward transport of these quantities in the South Atlantic and may establish a key link in the global thermohaline circulation (THC) (Gordon, 1986; Weijer, 2000). From hydrographic and tracer data, obtained on a number of cruises, estimates of direct Agulhas current leakage range between 2 and 10 Sv (Lutjeharms, 1996). Estimates of the interocean volume transport by Agulhas rings range between 0.5 and 1.5 Sv per ring, salt flux estimates range between 0.7 $\times 10^5$ kg/s and 6.3 $\times 10^5$ kg/s, and heat flux estimates between 10^{-3} and 2.5×10^{-2} PW (1 PW $= 10^{15}$ W) per ring, depending on ring size and whether the anomalies are calculated with respect to their direct surroundings (De Ruijter et al., 1999; van Ballegooyen et al., 1994). However, if the Indian Ocean water input is (partially) compensated by North Atlantic Deep Water (NADW), then the heat flux estimates increase by an order of magnitude. Assuming complete compensation by NADW for a total volume flux of 14 Sv, Gordon (1985) has obtained a heat flux estimate of 0.5 PW. Based on six rings shed per year (see also below) they contribute about one third to the total estimated fluxes. These numbers are of comparable magnitude to estimates of the equatorward heat flux across 30°S (Fu, 1981; Schlitzer, 1996). This has contributed to the development (Gordon, 1985; Broecker, 1991) of the concept of a global thermohaline overturning circulation in which a key role is played by Agulhas leakage.

Because of strong air-sea interaction, the positive sea-surface temperature anomalies of Agulhas rings tend to disappear quickly (Olson et al., 1992). Rings can therefore be identified from thermal infrared images only for a very limited part of their lifetime. The signature of Agulhas rings in sea-surface height (SSH) stays visible far longer, making satellite altimeter measurements very useful for monitoring the behavior of Agulhas rings over longer periods (van Ballegooyen et al., 1994; Gründlingh, 1995; Gordon and Haxby, 1990; Goñi et al., 1997).

The process of ring shedding by the Agulhas current is highly variable (Feron et al., 1992; Goñi et al., 1997). Estimates based on the 3 year Geosat period between 1987 and 1989 agree on five to seven rings being spawned per year (Gordon and Haxby, 1990; Feron et al., 1992; van Ballegooyen et al., 1994; Byrne et al., 1995). From the TOPEX/Poseidon data set (starting in November 1992), Gründlingh (1995) has estimated that five rings were shed in 1992 and that at least five were shed in 1991. Goñi et al. (1997) have given estimates of five, four, and six rings shed in 1993, 1994, and 1995, respectively. The speeds at which the rings travel in a west-northwestward direction lie between 5 and 15 km d^{-1} (Byrne et al., 1995).

They seem to slow down when getting closer to major bottom topographic features such as the Walvis Ridge. This slowing down is also expected from model results (Kamenkovich et al., 1996).

After being spawned most Agulhas rings translate in a northwestward direction, changing to a more western course between 25°and 35°S. Most rings stay south of 20°S and also north of the subtropical convergence (Gründlingh, 1995; Goñi et al., 1997). Garzoli et al. (1999) have defined an "Agulhas Eddy Corridor" confining rings to their northwestward direction until 30°S and diverging north of that. Goñi et al. (1997) placed the "Ring Corridor" more to the south, indicating the change of the rings' paths to more westward directions around 5°east. Their corridor is consistent with a maximum in the eddy kinetic energy of the area, which stems almost completely from Agulhas ring activity.

So far, studies on the fate and decay of Agulhas rings have focused on long-lived ones (Byrne et al., 1995). These rings penetrate the interior of the South Atlantic subtropical gyre and their water may thus conceivably recirculate in the subtropical "supergyre" that connects the South Atlantic and Indian Oceans (De Ruijter, 1982; Schmidtz, 1995). As such, they may not contribute directly or immediately to the warm water limb of the Atlantic Ocean overturning circulation. Such an immediate contribution is expected to result predominantly from their decay in the Benguela current region, i.e. in the Cape Basin off southwestern Africa, between the continent and the Walvis Ridge. A class of rings that seems to have gone unnoticed thus far consists of those that do not make it across the Walvis Ridge and that decay completely in the Cape Basin. Such rings may mix completely into the overturning circulation, providing it with a significant direct source of extra heat and salt. Therefore, in this chapter the earlier analyses using satellite altimeter data (Gründlingh, 1995; Byrne et al., 1995; Goñi et al., 1997) are extended by an analysis of 5 years of data from the TOPEX/Poseidon altimeter, collected between 1993 and 1998. Focus is on the translation, decay and splitting of all identified rings and on estimating the number and size of rings that disappear from the altimetric signal. All Agulhas rings formed between January 1993 and December 1996 have been followed on their way through the South Atlantic Ocean.

3.2 Data and Methods

The TOPEX/Poseidon altimeters cover the World oceans between 65°N and 65°S every 10 days, with a spatial resolution of ~ 7 km along track but with an intertrack spacing of ~ 300 km at the equator. A coverage at this resolution means that mesoscale features with a diameter of 250 km, moving though the ocean, may temporarily not be resolved and may thus disappear from view. The precise locations of, for instance, Agulhas rings can therefore not be known all the time. Nevertheless, by interpolating between members of a series of mappings, one can usually get a reliable estimate of their trajectories. Only measurements that show some consistency in the height anomaly of the rings, or in their horizontal dimensions, have been considered reliable in this analysis. It is therefore expected that most of the time the measured position is within 50 km, or half a degree, of the actual center of the ring. A sudden drop in both height and diameter of a ring has been regarded as a "hole-in-the-net" incident where resolution of the feature has been partially lost.

All available data provided in the TOPEX/Poseidon altimeter pathfinder data set for the

mentioned period have been used. The area under investigation includes the South Atlantic Ocean between 45°and 20°S. A mean ocean surface was computed from the measurements between November 1992 and November 1996 and subtracted from the measurements. This defines, but may underestimate, the intensity of the anomalies. All conventional corrections (instrumental, atmospheric, tidal and inverse barometer) have been applied to the measurements. The data processing used to create the path-finder dataset can be found on the WWW: http://neptune.gsfc.nasa.gov/krachlin/opf/algorithms.html. For each 10 day cycle the data have been taken together and a surface has been fitted through them. These surfaces do not completely represent the state of the ocean at one instant but suffer some time distortion resulting from the 10 day cycle needed to collect all the data. Removing this time distortion adds little, but removes a substantial part of the variability and thus visibility of the rings (Gründlingh, 1995).

Only anomalies generated at the known location (Lutjeharms and Van Ballegooyen, 1988) of the Agulhas retroflection were selected as ring candidates. The tracks of these Agulhas rings were then determined from consecutive maps, as described above. For a number of rings the individual satellite tracks have, furthermore, been examined in detail to obtain the actual measured SSH anomalies in every cycle.

We have determined the first time an anomaly is visible as a distinct entity on the altimetric maps and considered this as the moment of spawning. As the rings are shed in arguably the most variable area of the world ocean, the Agulhas retroflection, this is no easy task and is never quite objective. To detect the events in a more objective manner, the correlation method proposed by Feron et al. (1992) has been used. In this method an analysis is carried out of a time series to establish the decorrelation time of altimetrically derived SSH anomaly fields. The fields are obtained by a Gaussian interpolation in both time and space of the described altimeter data onto a regular 1°by 1°by 10 days grid. Decorrelation scales of 1.4°in space and 3.5 days in time were used. The correlation between each field and its successors is computed, and the time when this correlation drops below 0.5 for the first time is defined as the decorrelation time. The rate of change of the decorrelation time contains information about sudden changes in the SSH fields. A jump in decorrelation time is associated with a ring shedding event (Feron et al., 1992).

Clearly, the crucial assumption being made here is that SSH anomalies in the southeastern Atlantic Ocean that are explicitly initiated at the Agulhas retroflection are indeed Agulhas rings and nothing else. Since this project did not contain a seagoing component, we were unable directly to verify most of the anomalies as rings. However, there exists ample evidence that the Benguela current in this region is a broad and sluggish background drift with little inherent variability itself (Garzoli and Gordon, 1996; Garzoli et al., 1996). The preponderance of variability in the Cape Basin has therefore been demonstrated to arise from passing Agulhas rings only. A number of the type of anomalies we identify here as Agulhas rings have been investigated hydrographically by others (Arhan et al., 1999; Goñi et al., 1997; van Ballegooyen et al., 1994)) and have been demonstrated to be rings. Three of the set of features specifically used in our study were fortuitously surveyed at sea and unambiguously shown to be rings by Arhan et al. (1999). Two more were thoroughly measured by a range of observational methods, and described by Garzoli et al. (1999). Another two that are not included in this investigation as they were shed before the start of the TOPEX/Poseidon period have been measured at sea and identified as Agulhas rings by Garzoli et al. (1999). These are also

described by Clement and Gordon (1995). A number of these type of anomalies have, furthermore, been verified by their characteristic thermal expressions at the sea surface from infrared observations (Gründlingh, 1995) or have been correlated with current meter measurements (Garzoli et al., 1997). This large number of authentications gives us strong confidence that all the SSH anomalies we follow in this investigation have a very high likelihood of being Agulhas rings.

3.3 Agulhas Rings

3.3.1 Ring Shedding

By the methods described in section 2 we estimate that 21 rings were shed at the Agulhas retroflection between November 1992 and December 1996. The time series obtained by the decorrelation method were used to verify each visually identified ring-shedding event. These spawning events occurred irregularly, but the average number of five rings per year seems to be a fairly steady value. We determine that in 1993, 1994, 1995 and 1996, 4, 6, 5, and 5 Agulhas rings were shed, respectively. These numbers agree very well to the results of Goñi et al. (1997). Small differences are caused by the subjective way of defining when exactly a ring is pinched off: visual inspection of snapshots of SSH or SSH-derived quantities such as the depth of the 10°C isotherm does not enable the exact timing of the events within a month or so. To reduce the subjectivity involved in the visual inspection, the decorrelation method can be used for the timing of ring-shedding events. Three periods of over 4 months without any ring shedding were observed: in the second half of 1993, between August 1995 and January 1996, and again between February and June 1996, as illustrated in Fig. 3.1. A relative change in decorrelation time of 30% with respect to the previous observation is chosen to distinguish peaks. All jumps in decorrelation time thus defined may be associated with a ring-shedding event. The peak at the end of 1993, which comes half a year after the shedding of three rings without a corresponding jump in decorrelation time, is an exception. The data suggest that during the second half of 1993 more rings were shed but were reabsorbed by the retroflecting current shortly afterward. This would cause the decorrelation time to stay short as there is still a lot of mesoscale activity. The area used to evaluate correlations was fairly large (between 0°-30°E and 50°-20°S). It is therefore remarkable that the ring-shedding events seem to dominate the described signal for such a large area. This phenomenon is currently subject to further investigation.

On four occasions, two Agulhas rings were shed almost simultaneously or within 3 weeks. On three of these occasions the rings left the region in completely different directions (93C/93D, 94E/94F and 95B/95C in Fig. 3.2). It could therefore seem that the trajectories the rings take after spawning are indeterminate, but an analysis of their paths shows that this is not the case.

3.3.2 Ring Paths

All rings formed between November 1992 and December 1996 have been tracked as long as their SSH signatures permitted. The tracks of all 39 rings are given in Fig. 3.2 (besides the

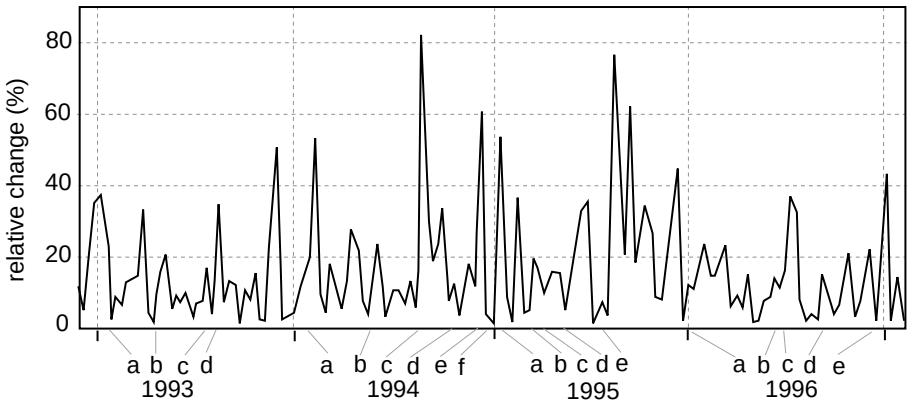

Figure 3.1: *The relative change in decorrelation time between altimetry-derived SSH anomaly fields around South Africa. A maximum means that there is a sudden change in the SSH field, which is associated with a ring shedding event (Feron et al., 1992). This holds for almost all of the higher peaks. Below the horizontal axis, the ring shedding events are indicated at the time they can be visually identified in the series op SSH maps.*

21 rings discussed before, 5 older rings are tracked, as well as 13 rings that are split off from other ones, as will be discussed in section 4). A tendency to avoid the shallow parts of the Walvis Ridge as noted by Byrne et al. (1995) is suggested by the tracks given in Fig. 3.2, although rings with a very steady west-northwestward movement are not observed to have this tendency. A number of rings (93C4, 93C, 94B2, 94D, 94F and 96A; Fig. 3.2) show a tendency for a greater meridional component in their movement on reaching the Walvis Ridge.

The corridor for rings suggested by Goñi et al. (1997), following the isolines of eddy kinetic energy, is partially confirmed by our data. The main routes of Agulhas rings are within this corridor, but a substantial number of rings nevertheless travels north of this corridor. Out of 39 observed rings, 12 are not confined by the corridor. Of these, 7 belong to the class of dissipating rings discussed below. The Agulhas Eddy Corridor drawn by Garzoli et al. (1999) lies considerably too far to the north. No rings would be allowed to cross south of 30°S, which is, in fact, done by two thirds of the rings that cross the Walvis Ridge.

From the conservation of potential vorticity one would expect a northward topographic steering when a ring encounters a ridge on the seafloor. We do observe this effect in a number of cases (rings 93C, 93C4, 94A3, 94D, 94E, 96A4 and 96B; Fig. 3.2) but clearly not in all. A possible explanation for this difference is given by the modeling results of Beismann et al. (1999). In their quasigeostrophic two layer model, rings that reach the ridge early in their lifetimes show the effect of northward translation on passing the ridge, whereas rings that have spent more time in the Cape Basin do not. The cause of this difference is the loss of barotropic structure that occurs with age. The older, more baroclinic rings are unable to feel bottom topography in the model. This explanation is not confirmed by our observations, as also older rings (like rings 93C4 and 94A3 over a year after shedding) show the northward movement along the slope of the ridge. Also, some younger rings (like 94B and 94B2 at ages

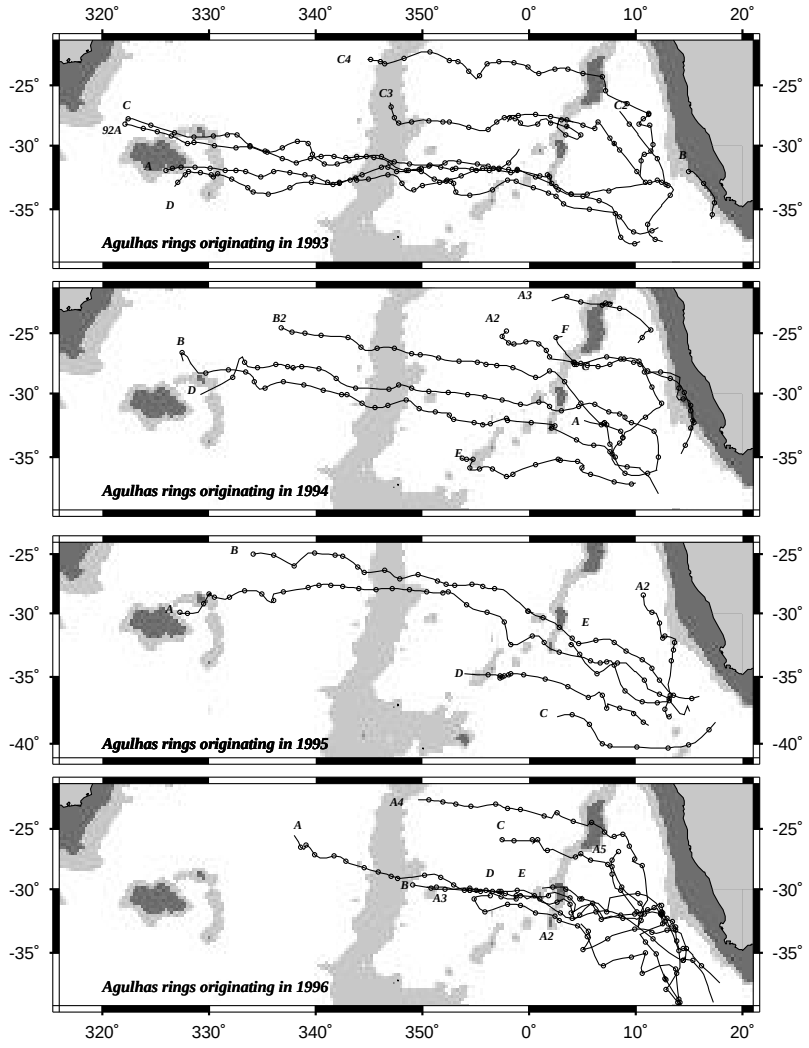

Figure 3.2: *The paths of all observed Agulhas rings for the years 1993, 1994, 1995 and 1996. Ring 92A has been included in 1993's plot. The rings that were shed from the Agulhas retroflection have been named by their year and a letter, the split off parts by the name of their parent, and a number (93C-2 is split from original ring 93C). The shaded contours are those for the 3500 and 2500 m isobaths. Dots indicate locations one month apart.*

of only half a year) pass the ridge without a clear disturbance to their paths.

The average translational speed of all the rings investigated fluctuates steadily around 4.8 km d^{-1}. We found no evidence for seasonal or interannual variations in this speed of Agulhas rings. Our estimates confirm those established by Goñi et al. (1997). However, average speeds vary by geographic location. Highest speeds occur in the eastern part of the basin, in the region east of the Walvis Ridge. For this region the mean speed for all rings is 5.2 km d^{-1} (with a standard deviation of 3.6 km d^{-1} (± 3.1). This drop has usually been attributed to the direct effect of this strong topographic feature (Byrne et al., 1995; Gründlingh, 1995), but that is not confirmed by our observations. We find that the mean speed stays low and even drops farther, to 4.3 km d^{-1} (± 2.2), for the region between the Walvis Ridge and the Mid-Atlantic Ridge. A more credible explanation for the higher speeds east of the Walvis Ridge is that the background flow in that region is stronger than elsewhere.

The influence of the background flow is also clear when one compares the mean speed of the rings on both sides of the 31°S parallel. South of it, in the heart of the wind-driven gyre, the mean translation speed is 3.5 km/day (± 1.8). To the north, where the speed of the rings is enhanced by westward advection, the mean translation velocity is 4.9 km d^{-1} (± 2.5). If we assume the background zonal flow south of 31°S to be close to zero, which is supported by the results of drifter tracking (Piola et al., 1987), and assume that the mean intrinsic drift of the rings north and south of the parallel is the same, we can derive a mean background flow of ~ 1.7 cm s^{-1} for the region roughly between 31°and 25°S. An attempt has been made also to examine whether there is a relationship between translation speed and diameter of the rings, but because of the difficulty of measuring diameters accurately, it turns out that the signal to noise ratio is too small to draw any conclusions. The same holds for a comparison of the size, the shape, and the effect of bottom topography.

3.3.3 Ring Decay

The upper age at which rings are still reliably identifiable in this data set is $\sim 2.5 - 3.5$ years. By then the rings that travel near the 30°S parallel have almost reached the other side of the basin and are lost in the mesoscale variability associated with the Brazil current. The rings taking the more northerly route are also lost after ~ 2.5 years. They will then have traveled a distance about as far as their more southern counterparts but have spent a larger part of their time in getting north. However, most rings could only be tracked for periods much shorter than 2.5 years. A substantial number of rings can be tracked for only ~ 7 months, and the split-off rings to be discussed below could be tracked for ~ 2 years if they were not dissipated before they reached the Walvis Ridge. (The rings shed or split off in 1996 are not included in these numbers, as they were not tracked after December 1997).

The decay rate of Agulhas rings has been considered to be exponential in a number of studies. Byrne et al. (1995), Gründlingh (1995), and others have made estimates of the e-folding distance for Agulhas ring decay. However, van Ballegooyen et al. (1994) have noticed that the strong decline of the SSH anomaly stopped for at least one ring after having crossed the Walvis Ridge. This latter behavior is confirmed by our results based on the close examination of 11 rings that can be tracked from their shedding at the Agulhas retroflection and that do not totally dissipate in the Cape Basin (Fig. 3.3).

The first 5 months show a strong decay of ~ 5 cm per month on average. From ten

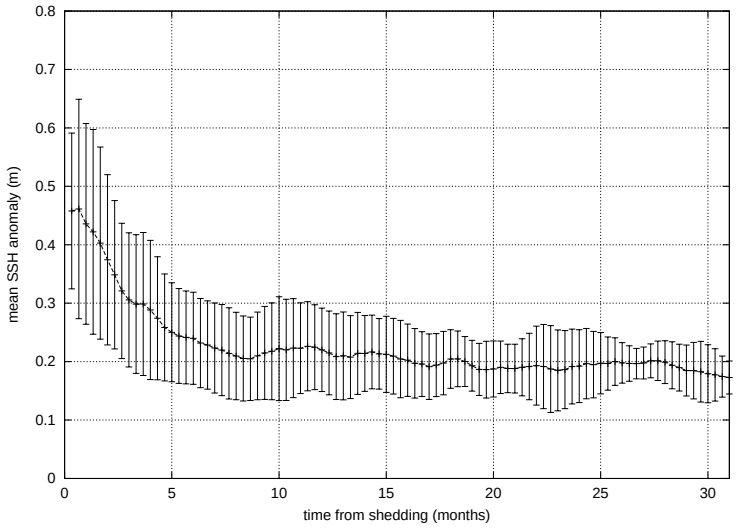

Figure 3.3: *Mean sea-surface height anomaly of Agulhas rings plotted against their age. The first five months can be characterized by a very strong decay in the Cape Basin. After ten months the rings hardly decay anymore.*

months onwards the rings keep their surface height anomalies of, on average, just below 20 cm (Fig. 3.3). In the first period after having been spawned the rings are subject to a combination of physical mechanisms, leading to strong decay. Their warm core of Indian Ocean water is strongly cooled by air-sea interaction. A large evaporative buoyancy flux adds to the increase of upper layer density. In particular, during winter this lead to vigorous convection down to over 300 m (Duncombe Rae et al., 1996; Olson et al., 1992). In the next spring, subduction and associated lateral spreading (Dewar, 1987) leads to mixing of the ring's water into its surroundings. Observed temperature and salinity characteristics on isopycnal surfaces suggest that double diffusive interleaving is also a very active process by which ring properties are mixed into the environment (Arhan et al., 1999). On top of this, rings may be strongly deformed by their interaction with each other, by the shear in the background Benguela current, and by their interaction with the bottom topography (as shown below and in section 4). Together with the small scale mixing processes this may lead to a large shear diffusion and associated decay of the rings. The Benguela region seems to act as a big blender by all the above processes.

In the next period the rings cross the Walvis Ridge, and after 10 months most rings have reached the relatively invariant regions west of the Walvis Ridge. Here there seems to be less distortion of the rings by background currents, interactions between rings, and bottom topography. Only the small-scale processes are still at work, leading to only a very slow decay (Fig. 3.3).

The effect of the Walvis Ridge on the SSH expression of Agulhas rings has been men-

tioned by Kamenkovich et al. (1996). They expected a measurable increase of the SSH elevation of up to 10 cm when the ring is approaching the higher parts of the ridge, followed by a decrease when leaving the ridge again. This is not inconsistent with our results, although the theory is not applicable to all rings measured by altimetry. Of 15 rings crossing the ridge over the shallower parts (≤ 3000 m deep), 9 rings show the mentioned increasing SSH anomaly, whereas 6 do not. This is not clearly connected to the age of the rings, although the increase does always take place when the Walvis Ridge is reached at the end of the period of strong decay (the first 3-5 months). The rings that have already reached the more or less stable value of ~ 20 cm before they arrive at the Walvis Ridge do not always show the expected behavior. This favors the assumption that the barotropic component of the rings is dissipated in the Cape Basin, taking away the rings's ability to feel directly the bottom topography. On crossing the Walvis Ridge the remaining deeper parts may be dissipated, explaining the end of the period of strong decay that is often marked by the passage of the Walvis Ridge. But, as the effect of the Walvis Ridge on the routes of the rings are not clearly related to the age of the rings, we cannot endorse this assumption right away.

3.4 Ring Splitting

In section 3, we described the decay of Agulhas rings that takes place rather continuously. However, a significant number of the rings appear to split up in the early stages of their lifetimes. In addition to the 20 rings that were shed from the Agulhas retroflection over our 4 year observational period, 13 rings were generated by splitting off from other rings. Three of the original 20 split once, one split twice, and two even split four times. Of these six rings that show splitting events, four were shed in the middle of the austral summer (during December/January). The sizes and spawning locations of these rings are not significantly different from those of the other rings.

One might well ask how reliable the interpretation of this degree of detail in unverified altimetric data is, particularly splitting events. Could the appearance of these events not be an artifact of the limited spatial resolution of the data? To date the products of only one splitting of an Agulhas ring have been explored at sea (Arhan et al., 1999). Distinct anticyclonic vortices of different dimensions and internal structure were found. Fortuitously, these particular eddies form part of our set of splitting products as well, giving us at least two hydrographic verifications. This gives us confidence that the other splitting events we have identified likewise represent real mesoscale features. The fact that the splitting products remain coherent anomalies in the altimetric data and that they may be tracked for a substantial period also argues against the idea of resolution artifacts. Such artifacts could be expected to be ephemeral.

3.4.1 Vema Seamount

Arhan et al. (1999) have reconstructed the splitting history of Agulhas rings they encountered at sea. Our analysis shows that such splitting was not an exceptional incident, but that it happens frequently. Not all splitting incidents can be attributed to a single mechanism, but bottom topography appears to play a striking role in this process (Figs. 3.4 and 3.5).

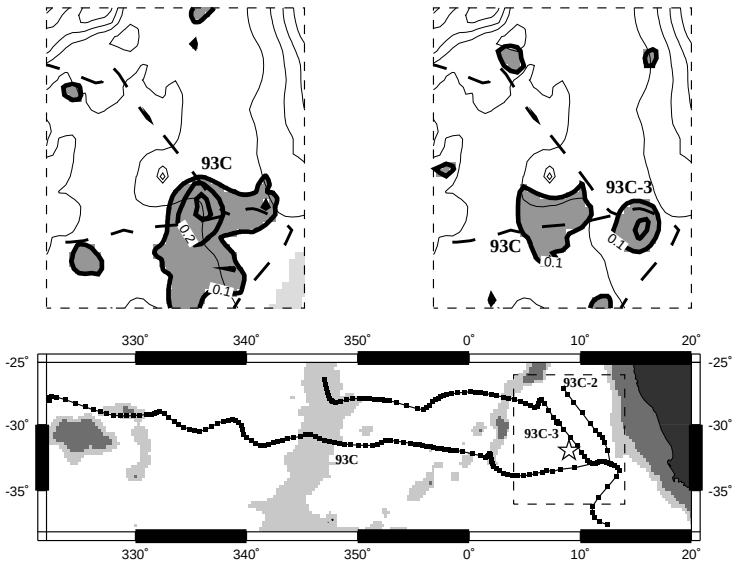

Figure 3.4: *The first ring splitting event discussed in the text. The upper two panels show the actual splitting over Vema Seamount. In the upper panel, the lighter contour lines are bottom topography, the coloured areas have positive SSH anomalies of over 10 cm. Also superimposed are the paths of both split off parts (dashed lines). The arrows identify the Vema Seamount. The left snapshot was taken in August 1993, with ring 93C approaching the Vema Seamount. Three weeks later (right panel), ring 93C-3 had been torn off. The lower panel shows the paths of the splitting ring 93C, and the split off parts 93C-2 and 93C-3.*

The role of bottom topography in the decay of coherent vortices has also been documented for meddies in the North Atlantic. Three scenarios are observed in hydrographic measurements or float trajectory data. Encountering the line of Great Meteor Seamounts on their way west, meddies have been documented to split into two pieces (Richardson and Tychensky, 1998) as we observe with Agulhas rings, but passing between two seamounts with only a partial loss of 25% of the heat and salt content to the surrounding waters has also been observed and described (Shapiro et al., 1995). Finally, also complete destruction appears to be a possible result of the interaction between a meddy and strong topographic features. This scenario is observed by Richardson and Tychensky (1998) for a strong meddy encountering Hyeres Seamount, just north of Great Meteor Seamount. Agulhas rings may show similar behavior.

Remarkably, 6 out of 13 splitting incidents we have identified in this study occurred in the direct vicinity of the Vema Seamount. The Vema Seamount rises from the deep ocean floor to within 50 m below the sea surface at (9°E, 31°S). This makes it a major obstruction for Agulhas rings, which can penetrate several kilometers deep (Olson and Evans, 1986). On encountering the seamount a ring may break up into two or three parts, which leave the region

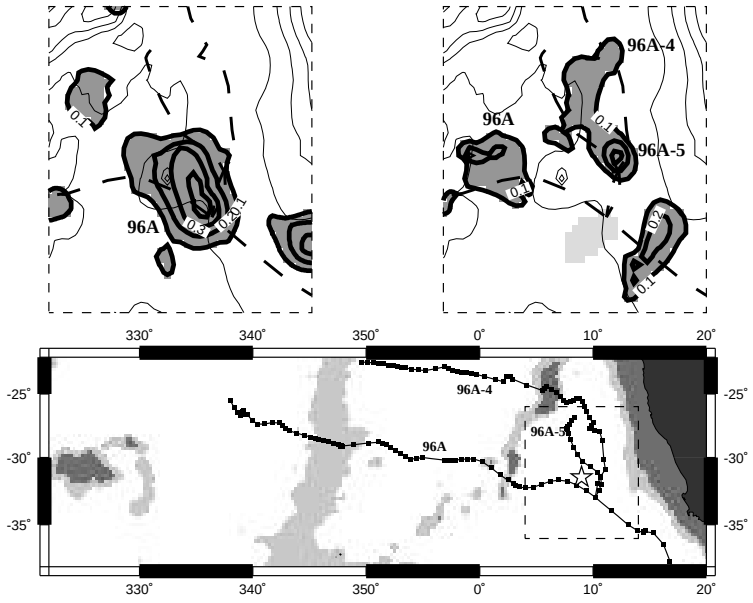

Figure 3.5: *The second splitting event discussed in the text. The upper two panels again show the actual splitting over the Vema Seamount, identified by arrows. The left snapshot was taken in the third week of October 1996, and shows Ring 96A still as one structure. Six weeks later (right panel) it had split off 96A-4, which had a very irregular shape, causing it to split again. To the south-east, a newly formed ring approached the seamount. Dashed lines show the paths taken by the original ring and its offspring. The lower panel shows the complete paths of the splitting ring 96A and the two split-off parts.*

in different directions (Figs. 3.4, 3.5). When an Agulhas ring (or part of it) has passed the seamount on its eastern flank, it is advected northward by the Benguela current (Fig. 3.6). The rings that stay west of Vema Seamount are seemingly not affected by a northward current. This supports the schematic picture of transports in the Cape Basin as given by Garzoli et al. (1999), with most of the Benguela transport flowing east of the seamount.

Although the limitations of the altimetric data prevent a detailed description of the processes involved in the splitting of Agulhas rings, two events are highlighted as examples of the effect of the Vema Seamount. The first one is the splitting of ring 93C (denoted in Fig. 3.6 by upward pointing triangles). Shed in June 1993, it initially moved in a northward direction, until it reached the vicinity of the seamount, which it was seemingly unable to pass. A smaller part did move northward, and did split off immediately when ring 93C reached the seamount (Fig. 3.4). This part, 93C-2, had an initial diameter of ~ 100 km (defined as the area of positive height anomaly) and a maximum sea-surface height anomaly of 20 cm; it left the region quickly, probably advected by the Benguela current, as the observed translation speed of 9 $cm\,s^{-1}$ is confirmed by the computed surface velocity for the CMM3-IES58 section of the Benguela Sources and Transport experiment (BEST) for August 1993 (Garzoli et al., 1996). This splitoff ring disappeared from the altimeter signal within 3 months, less

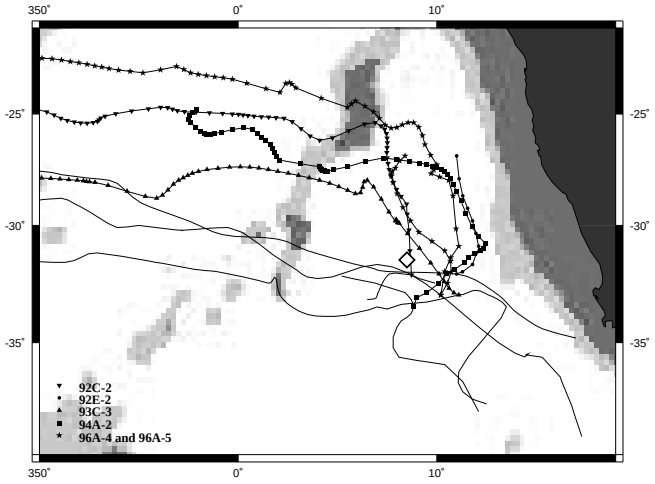

Figure 3.6: *The paths of all rings that split over the Vema Seamount. The original rings are displayed just by lines, the split off parts also by symbols. Note the northward tendency of the split-off parts, during the first period after splitting, whereas the movement of the parts that pass Vema Seamount on its west is dominated by a westward drift component.*

than 600 km north of where it was formed. The remaining (larger) ring split into two roughly equal pieces (Fig. 3.4), one of which passed the seamount to the east (93C-3), and the other of which passes the seamount to the west (93C itself). Both parts remained visible as anomalies in the altimetric data long after this: 93C-3 for another 2 years, 93C for over 3 years. By then, 93C had almost crossed the South Atlantic Ocean (Fig. 3.4).

The second splitting event, described here as a further case study, took place in March 1996 (Fig. 3.5). A large Agulhas ring (96A), shed only 2 months earlier, migrated over the Vema Seamount. Its path seemed undisturbed by the seamount, except that a major part of the ring was cut off. That cutoff part itself split into two pieces almost immediately thereafter. These two pieces continued to move north, where one of them disappeared from the altimetric signal within 6 months, and the other one crossed the Walvis Ridge to move west into the core of the South Atlantic subtropical gyre (Fig. 3.5).

3.4.2 Other Splitting Events

Not all splitting incidents identified in this data set can be attributed to the Vema Seamount. All other splitoff rings (seven in total) have been plotted in Fig. 3.7.

One ring (93C-5) split off from ring 93C-3 on crossing the Walvis Ridge and moved back into the Cape Basin before turning westward again and crossing the Walvis Ridge. On four occasions a ring split shortly after having been spawned at the Agulhas retroflection. Some of

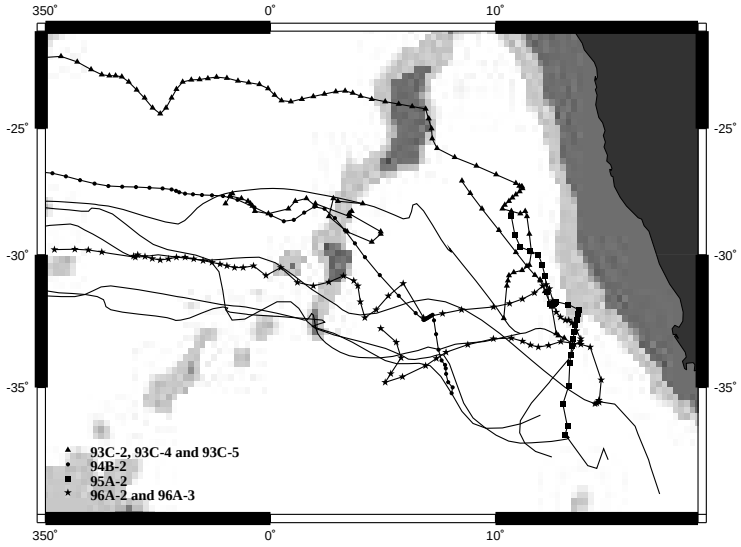

Figure 3.7: *The other splitting incidents (not over Vema Seamount). Again the paths of the split-off parts are indicated by symbols.*

these may have been two separate rings from the beginning, that exhibited one combined SSH anomaly in the altimetric signal because of a lack of spatial resolution. The two remaining splitting incidents both resulted in two very stable rings. They took place in the Cape Basin, probably because the original rings became unstable because of a previous splitting event (the case of 93C-4 after splitting off 93C-3 over the Vema Seamount) or due to interaction with another ring (as 94B interacts with 94A before splitting off 94B-2). As mentioned earlier, the low spatial resolution makes deriving a relation between initial ring size and eventual splitting impossible. Nevertheless, splitting rings do not seem to be necessarily much larger than the rings that do not split.

3.5 Dissipating Rings

Agulhas rings that cross the Walvis Ridge and move westward into the South Atlantic subtropical gyre conceivably do not contribute directly to the Atlantic overturning circulation. However, a more direct contribution could possibly be made at an earlier stage, in the Cape Basin, by mixing of heat and salt into the environment of the dissipating rings.

A number of rings disappear as SSH anomalies from the altimetric data before crossing the Walvis Ridge (Fig. 3.8). They constitute about one third of the total number of rings identified. Another 10 % disappear just after crossing the Walvis Ridge. The equatorward movement of rings may lead to a 25% reduction of the SSH signal, because of conservation of potential vorticity. However, this would not constitute a sufficient reduction in SSH

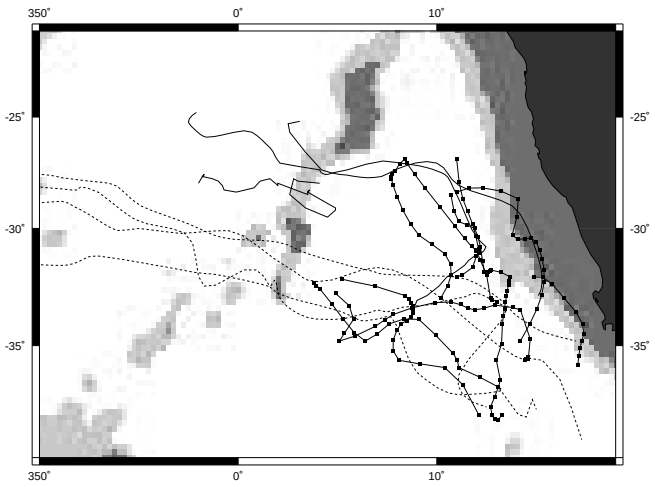

Figure 3.8: *Trajectories of all rings that disappeared from the altimetric signal over the period 1993-1996. The rings that are lost east of the Walvis Ridge are indicated by symbols, the ones that are lost just after crossing it by solid lines. The original rings of which lost rings are split off are indicated by dotted lines. Note that there are two favourite regions where most rings disappear, around (*4° *E,* 32° *S) and (*10° *E,* 27° *S).*

anomaly for them to disappear from the altimeter signal. It is therefore highly unlikely that all the anomaly disappearances can be attributed to the nature of the altimeter measurements. Although the rings do seem to show a tendency to become smaller and, usually, have less pronounced anomalies as they age, they should still remain clearly identifiable since anomalies as small as 10 cm can readily be measured. One is therefore forced to conclude that this class of "disappearing" rings consists of those that lose their coherence as features and disintegrate, with their anomalous heat, salt and vorticity contents would being dissipated at the location where one loses track of them in the altimetric observations. Even in the unlikely case of a small ring that comes to rest in the middle of a diamond-shaped hole in the altimetric net, the dissipation would still have to take place at that location, and the contribution would still be the same.

The rings that are shed from the Agulhas retroflection and that are seemingly dissipated in the Cape Basin have slightly smaller dimensions in the altimetric data than those that make it over the Walvis Ridge. The SSH anomalies were, however, not significantly lower: three of the five were ~ 40 cm. The other two were quite low, only 20 cm. This is more like the dissipated rings that had been split off by other rings: these, in general, had anomalies below 20 cm, except for ring 96A-5 which had an anomalous SSH of ~ 30 cm. All four rings with higher anomalies decayed rapidly to values around 15 cm, often within a month. The

dissipating rings either were smaller from the beginning or were subject to stronger decay in the Cape Basin because, as suggested by the data, of stronger interaction with other rings, or of deformation by structural variations in the Benguela current. Whatever the mechanism, they decayed far too rapidly to reach the more tranquil region west of the Walvis Ridge. Again, there is a bifurcation of the ring paths due to the Vema Seamount. Eight rings that later dissipated passed to the east, and three passed to the west (Fig. 3.8). The latter were all lost more or less in the same region, where they should have crossed the Walvis Ridge but failed to do so. The five dissipating rings that were more strongly advected equatorward by the Benguela current also ended up more or less in a similar region.

3.6 Discussion and Conclusions

On average, five Agulhas rings per year were shed between the years 1993 and 1997. This number varies between years, and sometimes long periods of over half a year may occur in which there are no shedding events. The paths followed by the rings vary and are influenced by the intrinsic drift of the rings themselves, bottom topography, and background flow. During their lifetimes, the rings can cross the South Atlantic Ocean in $\sim 2.5 - 3$ years, but only two thirds of the rings make it farther than the Walvis Ridge, which is usually reached within a year of shedding.

About one third of the anomalies that are observed in the southeast Atlantic Ocean and that have the Agulhas retroflection as their origin, i.e., those assumed to be Agulhas rings, are lost from the altimeter signal before the Walvis Ridge. This accounts for 25% of the rings directly shed at the Agulhas retroflection and for 60% of split off rings. The latter originate from splitting events in which an Agulhas ring breaks up into two or more pieces. This splitting is often induced by bottom topography. The Vema Seamount in particular, appears to play a substantial role: 6 out of 13 splitting events during this period took place over this seamount. The split off rings often disappear from the altimetric signal in the Cape Basin, and this disappearance may indicate that the rings are completely dissipated here and that they lose their anomalous characteristics to the surrounding waters. Bottom topography may therefore have a strong influence on the mixing and dissipation of Agulhas rings.

In the first part of their trajectories, in the Cape Basin, the remaining rings decay to a rather stable anomalous height of ~ 25 cm within ~ 5 months from their initial anomalous SSH of ~ 50 cm . It is instructive to note that the model for Agulhas rings used by (Beismann et al., 1999) shows a rapid decrease in ring energy during the first 5 months because of radiation of Rossby waves from the lower layers. This period is consistent with that found in the altimetric data. While crossing the southern Atlantic Ocean west of the Walvis Ridge, the rings hardly decay. This lack of decay may be due partially to the more quiescent environment west of the ridge, as there is less interaction with other rings and bottom topography. Shear diffusion, resulting from small-scale diffusion and large-scale deformation of the rings, may be an important decay mechanism in the Cape Basin, together with convective modification and double diffusive interleaving.

On the basis of the above numbers one can now try to make an estimate of the heat and salt fluxes into the Cape Basin and thus, possibly, the contribution of the rings to the Atlantic Ocean stability and overturning circulation. A direct contribution to the net northward

transport is unlikely to be made by rings that penetrate the interior of the South Atlantic subtropical gyre. Their properties are probably absorbed in the Atlantic-Indian subtropical supergyre. However, we have shown that a major part of the properties of the rings may be contributed exclusively to the eastern part of the basin. The disappearing rings cause about one third of the total shed volume to mix into the Cape Basin. Added to that, the rings that migrate into the heart of the subtropical gyre decay to half their surface anomaly here. This decay implies a total volume decay of at least 50%. Together, this adds up to two thirds of the total inflow into the South Atlantic by Agulhas rings.

Estimates of the associated heat and salt inputs into the Atlantic overturning circulation are hard to give (van Ballegooyen et al., 1994). We base our estimates on the range of estimates found in literature and summarized in the section 1, and on the five rings per year that shed two thirds of their properties into the Benguela Region, which leads to an estimated contribution to the meridional salt transport of $\sim 3 \times 10^5$ kg s^{-1}. The heat flux estimate ranges roughly between 3×10^{-3} PW and 0.15 PW. In the former case the Indian Ocean water of the rings is compensated by surrounding Atlantic waters (van Ballegooyen et al., 1994). The number of 0.15 PW is based on compensation of ring water by NADW as by (Gordon, 1985). The impact of such sources of heat and salt on the Atlantic Ocean is not exactly clear yet, but a study by (Weijer, 2000) suggests a strengthening of the overturning in direct response to enhanced Agulhas leakage.

Chapter 4

Upstream control of Agulhas Ring Shedding

Rings shed in the Agulhas retroflection region play an important role in the global thermohaline circulation. The shedding of these rings has been considered very irregular. In this chapter, we present evidence for remote control of the timing and frequency of the ring shedding events. This turns out to be a far more regular process, at a frequency of 4-5 cycles per year. The movement of the Agulhas retroflection, and thereby the shedding of rings, is timed by incoming eddies from the upstream regions. Eddies from the Mozambique Channel, and from the East Madagascar current reach the Retroflection region at the frequency of 4-5 times per year. The existence of these eddies can be related to incoming Rossby waves that cross the Indian ocean and reach the Agulhas current system. These may in turn be part of a basin wide oscillation. The irregularity found in ring shedding statistics can be ascribed to processes occurring between the actual shedding and the first unambiguous observation of a separated ring.

4.1 Introduction

The large Agulhas Rings that are spawned at the Agulhas retroflection form a key link in the global thermohaline circulation (Gordon et al., 1992; De Ruijter et al., 1999; Weijer et al., 1999). The interocean exchange brought about by the warm and saline Indian ocean water entering the South Atlantic is a crucial part of the warm water route for the renewal of North Atlantic Deep Water (NADW) (Gordon, 1985). Moreover, model studies show that it stabilizes the northern overturning circulation of the Atlantic Ocean (Weijer et al., 2001). Hydrographic measurements have established the Agulhas Rings as the most energetic ones in the World Ocean (Olson and Evans, 1986; van Ballegooyen et al., 1994). Intermittency in the shedding of these energetic and climatically important rings has been reported by many investigators (Feron et al., 1992; Byrne et al., 1995; Schouten et al., 2000), but has not yet been explained satisfactorily. The average number of rings seems to be a rather steady 4-6 per year, but periods of up to five months without any rings have been reported (Goñi et al.,

1997; Schouten et al., 2000). No clear seasonal, interannual or other dominant frequency in the shedding of Agulhas Rings has as yet been found. The process of the ring shedding itself has been described to some extent, based on various observational and modeling studies (see (De Ruijter et al., 1999) for a review). Theoretical and modeling studies have concentrated mainly on the local dynamics of the retroflection and ring shedding (Boudra and de Ruijter, 1986; Boudra and Chassignet, 1988). Given the geometrical configuration of the tip of South Africa, and at given inflow and outflow conditions representing the Agulhas, the local dynamics are intrinsically unsteady and involve retroflection and ring shedding (Ou and de Ruijter, 1986; Pichevin et al., 1999). Remote forcing by meanders in the upstream Agulhas current has been proposed as a triggering mechanism for shedding of Agulhas Rings (Van Leeuwen et al., 2000). A recent theoretical study has shown that different steady retroflection regimes, a viscous and an inertial one, exist for the Agulhas current (Dijkstra and de Ruijter, 2001b). Barotropic instabilities of these steady flows occur in the viscous regime with patterns related to Rossby basin modes. Finite amplitude development of these instabilities display ring-like localized anomaly patterns which travel around the tip of South Africa. This indicates that the origin and frequency of the ring formation is set by the physics of the large scale barotropic instabilities (Dijkstra and de Ruijter, 2001a).

The observational record includes local sea-surface temperature measurements (Lutjeharms and Van Ballegooyen, 1988), hydrographic investigations (Gordon et al., 1987), and satellite altimetry measurements of sea-surface height (SSH) elevations (Feron et al., 1992). The general behavior of the retroflection in relation to the shedding of Agulhas Rings has been described fairly intuitively by Lutjeharms and Van Ballegooyen (1988). The retroflection loop of the Agulhas current slowly progrades westward between 20-15° east, shedding a ring at the westernmost extension. By then the retroflection is constituted by a shortcut more eastward, which will in turn slowly move to the west. A more statistical approach, using altimetric sea-surface height (SSH) data has confirmed the overall correctness of this description (Feron et al., 1992).

The general characteristics of the Agulhas current system are that of an intense western boundary current to the large scale wind-driven circulation of the southern subtropical Indian Ocean. The total Sverdrup transport in this gyre is of the order of 60 Sv. This anticyclonic gyre shows some remarkable features. First, the transport is largely concentrated in the southwest corner of the basin, where a strong recirculation of water from the Agulhas Return current is present. Of 60 Sv, half is recirculated west of 60° E (Stramma and Lutjeharms, 1997). An even tighter recirculation, close to the African continent, has been identified by calculating a mean dynamic sea-surface height from the mean divergence of eddy vorticity fluxes measured by the Geosat altimeter (Feron et al., 1998). The mean flow field as depicted by Stramma and Lutjeharms (1997) gives an inflow of 25 Sv into the northern Agulhas current from east of Madagascar which originates from the South Indian Ocean subtropical gyre, and an additional 5 Sv from the Mozambique Channel, which draws its waters from further north and probably connects to the Indonesian Throughflow (Gordon, 1986) via the South Equatorial current. This additional 5 Sv added to the southern gyre is balanced by a 5 Sv exchange to the South Atlantic in the form of filaments and Agulhas Rings.

A recent cruise dedicated to the determination of the nature of the flow through the Mozambique Channel (the first cruise of the Agulhas current Sources Experiment, ACSEX I (De Ruijter et al., 2000; Ridderinkhof et al., 2001)) has shown that this flow is not constituted

by a Mozambique current comparable to other western boundary currents, but merely by a train of eddies (De Ruijter et al., 2002). These eddies, as suggested by SSH measurements from space were shown unambiguously to be present, and even to extend over the full depth of the channel (> 2500m) with diameters of 300-400 km. They were shown to carry water from the north, including a core of Red Sea and/or Persian Gulf water that is actively mixing with Antarctic Intermediate water. The latter penetrates northward into the channel, probably as a continuation of the Agulhas undercurrent (Beal and Bryden, 1997; De Ruijter et al., 2002).

Eddies in the Mozambique Channel were also found by Biastoch and Krauss (1999) in a $1/3^\circ$ primitive-equation model simulation. In their model, they could track the relatively shallow eddies (estimated to reach only 400m deep) until 34° S, where the Agulhas separates from the coast. There the eddies disintegrate in the model (Biastoch and Krauss, 1999), but still cause an extra interoceanic transport. Such a transport pulse might control the timing of the ring shedding at the Agulhas Retroflection (Pichevin et al., 1999). The origin of these model eddies was attributed to local barotropic instability of the modeled South Equatorial current (Biastoch and Krauss, 1999).

Besides southward propagating eddies from the Mozambique Channel, another possible source region of Agulhas variability that can be identified by analysis of the variability of the sea-surface height, lies southeast of Madagascar (Fig. 4.1), where the East Madagascar current seems to retroflects and probably also sheds rings (Lutjeharms, 1988). Gründlingh (1987) showed the occurrence of cyclonic eddies in the region southeast of Madagascar, and attributed these to meandering of the Mozambique Ridge Current. He used this name for the waters flowing westward from Madagascar towards the upstream Agulhas, which are diverted southward by the topography of the Mozambique Ridge. A later study of altimeter observations (Gründlingh, 1995) suggests that these cyclonic eddies may not be formed near the Mozambique Ridge, but that they may be propagating from the Mozambique Channel and from the southern tip of Madagascar.

These source regions seem to be connected to incoming Rossby waves from further east (Morrow and Birol, 1998). Annual Rossby waves found over the full width of the Indian Ocean seem to be excited by changes in the winds (Périgaud and Delecluse, 1992; Birol and Morrow, 2001). Also, a semiannual Rossby wave is observed over the basin, associated with eastern boundary forcing (Birol and Morrow, 2001). These signals might be associated with coastally trapped Kelvin waves coming from the north (Subrahmanyam and Robinson, 2000), thus linking the subtropical variability of the south Indian Ocean to the equatorial dynamics of the northern Indian Ocean. However, recent analysis of altimetric observations (Matano et al., 1998) and model results (Matano et al., 2001) indicate that especially the annual Rossby wave does not reach the Agulhas Region due to the blocking of these barotropic waves by topography such as the Mascarene Ridge.

In this chapter, we focus on upstream influences on the shedding of Agulhas Rings. We show that the underlying physical process controlling the progradation of the retroflection loop is much more regular than previously thought (Goñi et al., 1997; Schouten et al., 2000). Evidence is provided for upstream control of the timing and frequency of ring shedding events, both via anticyclonic eddies from the Mozambique Channel, and via SSH-anomalies from southeast of Madagascar. In the next section, we start at the Agulhas Retroflection, and follow the Agulhas current upstream, to identify the variability in the Indian Ocean far field

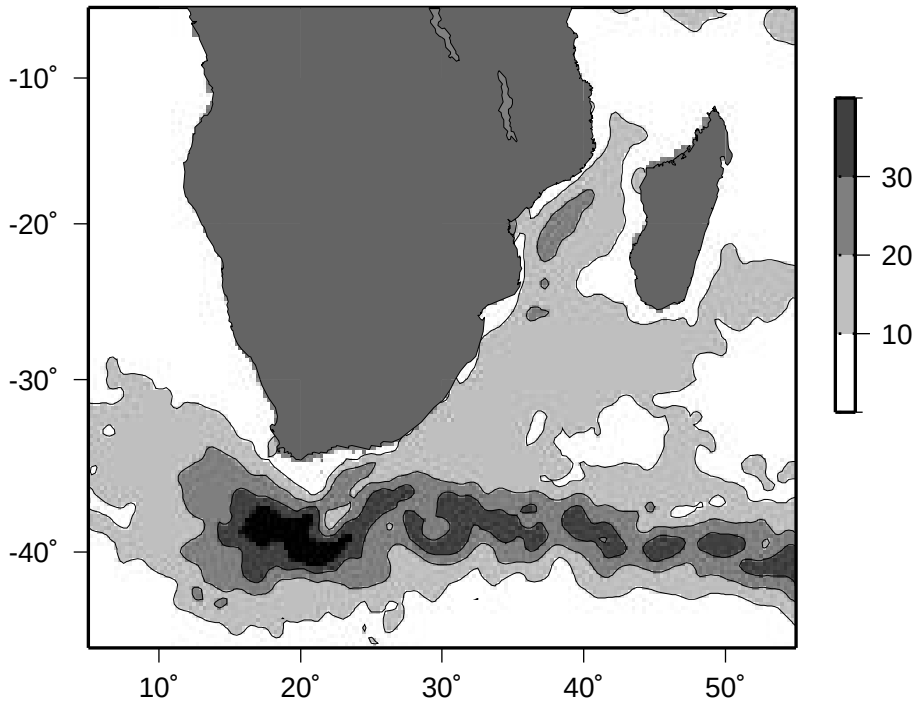

Figure 4.1: *Variability of the sea-surface height (in cm) measured by TOPEX/Poseidon during 1993-1998. Two possible source areas of variability in the Agulhas region can be identified: the Mozambique Channel and south of Madagascar. Also, both regions are connected to a band of enhanced variability in the central and eastern Indian Ocean*

that may control the ring shedding process and its frequency. We finish with a short summary of our findings, and relate this to the central question of this chapter: How and to what degree is the variability in the retroflection region, and thereby the local process of Agulhas Ring shedding, connected to, or controlled by the large scale circulation of the (southern) Indian Ocean and its variability?

4.2 Ring Shedding and the Retroflection

The frequency of ring shedding has previously been estimated by counting the number of Agulhas Rings that is eventually seen drifting into the Atlantic. This number is highly variable (Byrne et al., 1995; Goñi et al., 1997; Schouten et al., 2000). Large periods occur without any events counted at all. In this section, we show that this is not a feature inherent to the east-west movement of the retroflection, but rather a result of the behavior of the rings once they have been shed.

Fig. 4.3 shows a space-time diagram of a zonal section along 39° S (see Fig.

4.1 for the location). sea-surface height anomalies are plotted for the years between 1993 and summer 1999 (anomalies are given with respect to the University of Texas, Center for Space Research (CSR), mean sea-surface height, version of 1995). The TOPEX/Poseidon altimeter data (October 1992 - May 1995) were taken from the pathfinder dataset (further information on processing can be found on the world wide web: neptune.gsfc.nasa.gov/~krachlin/opf/algorithms.html). These data were binned into $1^\circ \times 1^\circ \times 10$ day bins. The combined TOPEX/Poseidon and ERS2 altimeter data (June 1995 - July 1999) were gridded and provided by the CLS Space-Oceanography Division in Toulouse. For details on processing, error estimation and gridding procedure see (Le Traon et al., 1998). The data are gridded to a $0.25^\circ \times 0.25^\circ \times 10$ day grid which is possible and meaningful as a result of the combined forces of ERS2 and TOPEX/Poseidon in spatial and temporal resolution respectively. All sea-surface height (SSH) anomalies are high-pass filtered with a 200-day cosine window, leaving in signals with frequencies higher than roughly three times per year. The annual and semi-annual cycle are strongly suppressed. Next, a 30-day running mean is taken. This combination is an efficient way of bandpass filtering and leaving frequencies roughly between three and six times per year unaltered. In Fig. 4.2 the average power spectrum for the gridded altimetry measurements in the region between 20°- 45°E and 45°- 30°S has been plotted (dotted line). The solid line shows the spectrum of the bandpass filtered dataset. It is clear from this picture, that no clear spectral peaks exist and no significant signals have been removed by the filtering procedure.

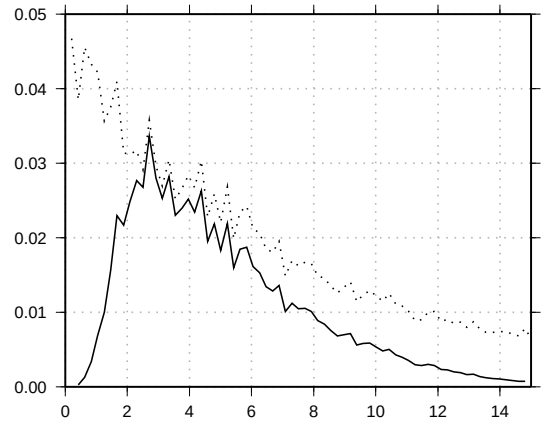

Figure 4.2: *Spectrum of the variability in the combined TOPEX/Poseidon - ERS SSH data. Along the horizontal axis the frequencies are given (cycle per year). The dotted line shows the average spectrum for all grid points in the Agulhas Retroflection region (10-35E; 45-30S). The solid line denotes the spectrum after the bandpass filtering described in the text. This filtering has been applied to produce Fig. 4.3 . For the MSSA analyses, just the high-pass filtering is applied, as MSSA effectively filters out the high frequency noise.*

The retroflection loop appears to have a very regular westward movement, at a frequency of four to five times per year (Fig. 4.3). Probably not all westward intrusions result in the full

shedding of an Agulhas Ring. Rings may reconnect to the main current, split up into several pieces in the early stages of their existence, or stay trapped behind the topographic features of the retroflection area (Arhan et al., 1999; Schouten et al., 2000). All these factors may influence the number of rings counted to leave the region, and make a 'shedding event' very difficult to define. The large range of existing estimates is thus not necessarily a result of the Agulhas current system itself being highly variable, but rather a result of the irregular behavior of the Agulhas Rings close to their spawning region in the southeast Atlantic (Schouten et al., 2000).

Not only in the filtered, but also in a plot of the unfiltered data the message is essentially the same: the retroflection of the Agulhas, here identified by the positive anomaly at 39°S, moves slowly westward with a constant speed of 13 km/day. The identification of the retroflection as a strong positive SSH-anomaly has been confirmed by comparing numerous snapshots of the anomalous SSH-field and snapshots of sea-surface temperature, on which the retroflection loop of the Agulhas current is often clearly identifiable. The signal is highly regular with a frequency of 4.5 per year. The speed of 13 km/day agrees exactly with the mean speed of westward progradation found earlier in SST measurements (Lutjeharms and Van Ballegooyen, 1988).

In (Schouten et al., 2000) three periods were identified in which no Agulhas Rings were observed to penetrate the southeast Atlantic Ocean. These results are qualitatively similar to those obtained by Goñi et al. (1997), although they used a smooth mean sea surface to provide more realistic snapshots of the total circulation. The three periods without observed ring shedding are the second half of 1993, between August 1995 and January 1996 and again between February and June 1996. These periods can not convincingly be connected to periods of less activity in the movement of the retroflection (Fig. 4.3). The first period, in 1993, coincides with two occasions of an early return to an easterly position (east of 16°E) of the retroflection. The beginning of 1996 shows two clear examples of a far westerly protrusion of the retroflection (Fig. 4.3). However, the rings counted in (Schouten et al., 2000) are usually first identified around 10°E, where they can for the first time be reliably recognized as individual rings. For the reasons described above, these rings may not exactly be the ones that have been shed around 14°E, as a lot can happen in between.

A discrepancy exists between the frequencies estimated by Lutjeharms and Van Ballegooyen (1988), and the present and previous results from SSH measurements. The present data show that the large positive sea-surface height anomalies move with a frequency of between four and five cycles per year, whereas the SST data suggested a westward progradation and sudden jump eastward of the thermal edge of the Agulhas to occur with almost double that frequency.

This may be due to the fact that in the period after shedding a ring resides close to the retroflection, where it can intermittently entrain warm filaments of the Agulhas around its periphery. That may account for the larger number of shedding counted from SST-measurements only. The altimeter measurements cannot resolve such high frequencies, although much of the high frequency noise in SSH data could be caused by these fluctuations.

The retroflection shows surprisingly regular behavior in the SSH field. The question arises whether this is mainly due to the regular local process of loop occlusion (Ou and de Ruijter, 1986; Pichevin et al., 1999), to anomalies from upstream or downstream in the recirculation gyre (eg (Van Leeuwen et al., 2000)), or to variability at the basin scale. To answer these

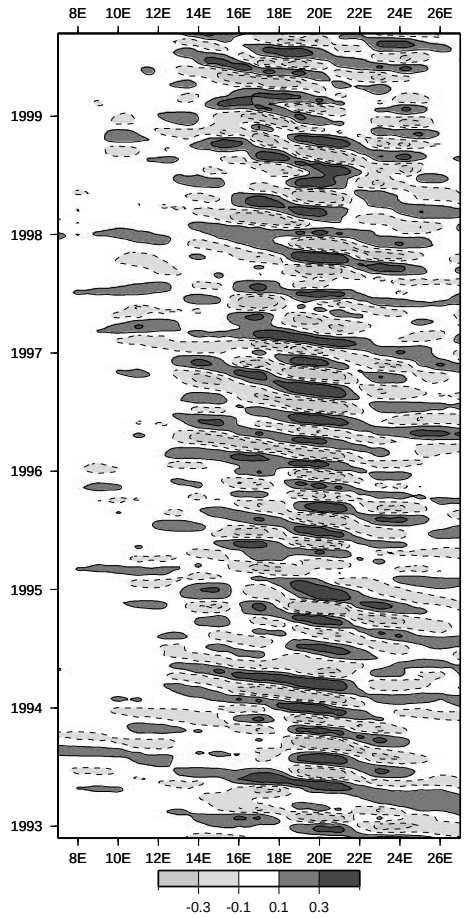

Figure 4.3: *Longitude-time diagram of filtered sea-surface height anomalies (in meter) along a zonal section at* $39^\circ S$*. Bandpass filtered sea-surface height anomalies are plotted for the period January 1993 - August 1999. Before 1995 only T/P data are used; from 1995 onward, combined TP/ERS data are used. The positive anomalies, associated with the retroflection of the Agulhas current progrades to the westward between* $22^\circ E$ *and* $14^\circ E$*. Jumps occur when the westward progradation of the centers of positive SSH anomalies end. These can be interpreted as ring shedding events, occurring* $\sim$ *4-5 times per year. The maximum at* $20^\circ E$ *should be noted, as that is the location to where the current returns after the shedding of a ring. Suddenly the anomaly that came from further east is enforced by the current.*

questions, we follow the SSH signal upstream, and show that it is connected to anomalies that appear in the northern Agulhas region. Next, we trace these back to the source regions of the Agulhas, the Mozambique Channel and the East Madagascar current. Finally, the phenomena found in those areas are shown to be connected to each other and, most probably,

to form part of a basinwide system of variability.

4.3 The Retroflection: Connection to Upstream Regions

Biastoch and Krauss (1999), using a high resolution numerical model of the region around South Africa, found shallow eddies from the Mozambique Channel to propagate southward and reach as far as 30°S. Observations during the recent ACSEX cruise (Ridderinkhof et al., 2001) have confirmed the existence of a train of large and energetic eddies that appear to reach all the way to the bottom (De Ruijter et al., 2002). In this section, we show a connection between these Mozambique eddies and the movement of the Agulhas Retroflection. Also, evidence is presented for the so-called Natal Pulse (Lutjeharms and Roberts, 1988; Van Leeuwen et al., 2000) being a manifestation of this larger scale process. The Natal pulse, a large solitary meander in the current, seems to be triggered by a Mozambique eddy on the offshore edge of the Agulhas. Thus, the Mozambique eddies influence the behavior of the downstream retroflection in several ways.

4.3.1 SSH Observations

To accommodate a clear view of the dominant processes involved in the movement of the retroflection, and its connection with upstream sources of water and dynamical properties, we have performed a multichannel singular spectrum analysis (MSSA) (Plaut and Vautard, 1994) on high-pass filtered, altimeter derived sea-surface height anomalies. These anomalies were not low-pass filtered, as the MSSA-technique effectively filters out high-frequency noise. The technique enables one to extract moving patterns from multidimensional data. We focus on a few prominent MSSA-modes (the ones with highest explained variances) rather than on modes that are selected by some significance-test such as the one proposed for SST-data (Allen and Robertson, 1996). This Monte Carlo-based test has a clearly stated null-hypothesis for sea-surface temperatures (the red noise hypothesis for white noise atmospheric forcing), but there is no physically based null-hypothesis yet for testing the statistical significance of modes found by the MSSA analysis of SSH anomalies.

The region of the Agulhas current system has been chosen sufficiently large to enable signals from outside the direct source regions to play a role in the analysis. In Fig. 4.1 we have plotted the total root mean square of the SSH anomalies. Given the close correlation between variability in the sea-surface height and the eddy kinetic energy (eg. compare (Stammer, 1997) and Fig. 4.1), the variability map in Fig. 4.1 suggests that upstream impact on the Agulhas retroflection behavior, if any, could come from two directions: from the Mozambique Channel, and from (south)east of Madagascar, as these are the two upstream regions of oceanic variability. The variability in the Agulhas return current is not likely to affect the ring shedding, as no evidence is found of regularly westward propagating anomalies in the Return current. Fig. 4.3 shows regular westward propagation starting near 25°E, and only intermittently from further downstream. This seems contradictory with results by Matano et al. (1998), but the westward wave propagation they show in the return current appears only intermittently.

On the more than four years of available data (June 1995 to January 2000) the MSSA

technique is applied. The first six resulting principal components have dominant frequencies between four and five times per year, as could be expected because of the high-pass filtering. The high-pass filtering has only removed 20 - 30 % of the total variability over the greater Agulhas region, but it has enabled us to extract modes of intermonthly variability without temporal aliasing of the annual and interannual signal. The first two oscillatory pairs that are identified are formed by the components 1/2 and 3/4 respectively. Locally the two components can describe up to 35 percent of the variance of the high-pass filtered signal. Especially in the retroflection area the explained variance is high.

To give a good first order description of the retroflection, and include the remote control variability, we reconstruct the dataset based on the first six MSSA-components. They all have frequencies of 4-5 times per year. Their variance is located not just in the retroflection area, but also in the rest of the Agulhas region. As all six modes have roughly the same dominant periods, the variability at that period is distributed between them. The most regular signal is the movement of the retroflection, which shows up as the first couple of MSSA-components. The upstream connection is slightly less regular, as is to be expected as a larger region is involved, in which also other processes play a role. Although the dominant pattern is the same in these modes, the focus is on different parts of the region, as that allows the analysis to deal with regional disturbances of the main pattern. The fraction of the variance contained in the first six modes together is over 25% over the whole region west of 40°E, reaching 75% in the central Mozambique Channel and in the Retroflection region.

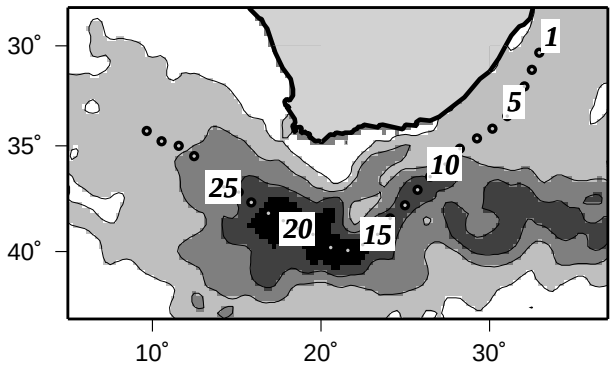

Figure 4.4: *Variability in the Agulhas Retroflection region, and the track along which the space-time plot of the upstream control is plotted. The numbers correspond to the horizontal axis of the space-time plot. This track has been chosen along the line of maximum variability.*

Together these modes form a new picture of upstream control of variability in the Agulhas retroflection and ring shedding. From the reconstructed snapshots of the ocean, built up by the first six MSSA-modes, the dominant features of the variability can be studied. Along the offshore edge of the Agulhas current, anticyclonic SSH anomalies are advected southward. These can clearly be observed in a space-time diagram (Fig. 4.5) along a line chosen through the maximum of the observed variability (Fig. 4.4). They move (Fig. 4.5) as anticyclonic anomalies in southwestward direction (locations 1-12) in the left half of Fig. 4.5, and seem to

trigger the westward shifting of the retroflection (clearly visible at the locations 13-29). The amplitudes are slightly smaller than in the original data, but irregularities in the precise timing of the phenomenon, can strongly reduce the strength of the complete reconstructed signal. So the amplitudes found from the MSSA analysis need to be considered with great care, and cannot directly be interpreted in terms of the original amplitudes. These are considerably higher in the retroflection region where they can reach up to one meter, and also in the region further north, where the anomalies on the offshore edge of the Agulhas have amplitudes of $\sim 20 - 40$ cm.

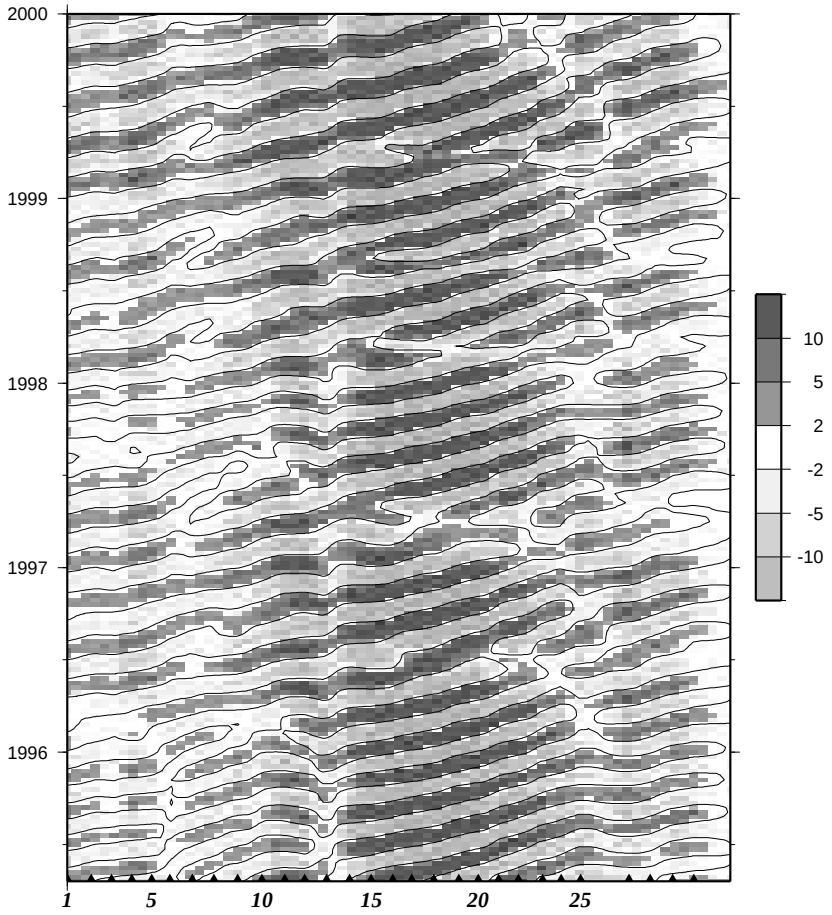

Figure 4.5: *Space-time plot of the sum of the first six MSSA-modes along the track shown in Fig 4.4. The numbers on the horizontal axis correspond to the locations shown there. Anomalies can be followed from the upstream Agulhas near* $30^\circ S$ *(point 1) to the westernmost point of the retroflection (point 29). Amplitudes are given in cm.*

4.3.2 Natal Pulse Generation

The otherwise remarkably stable Agulhas current path along the African coast is intermittently disturbed by a growing solitary meander, the so-called Natal Pulse (Lutjeharms and Roberts, 1988), which in general precedes the shedding of an Agulhas Ring by almost half a year (Van Leeuwen et al., 2000). The anomalous flow may be caused by a barotropic instability that can grow in the Natal Bight, where the continental shelf is less steep than elsewhere along the coast (De Ruijter et al., 1999). At the Natal Bight the flow is only marginally stable, so a slight strengthening or sharpening of the current can make the flow susceptible to barotropic instability. Based on altimetric data, De Ruijter et al. (1999) suggest that relatively large offshore anticyclonic anomalies may be responsible for that strengthening of the flow, and speculate that this may be due to internal variability of the recirculation gyre in the Southwest Indian Ocean. The analysis above suggests that the anomaly causing that instability is not such a regional scale phenomenon, but that it has its origin much further upstream.

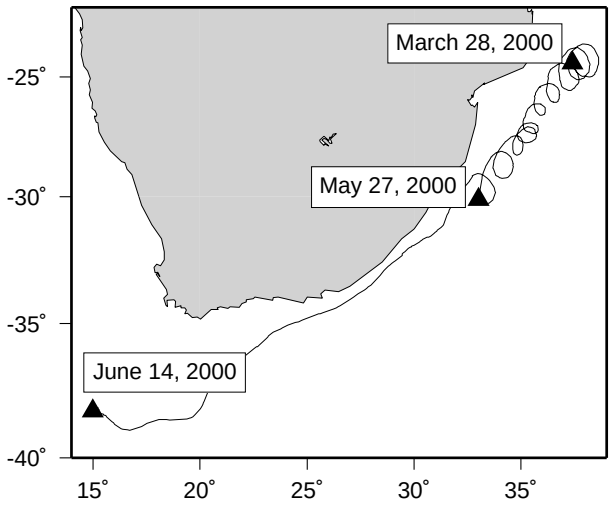

Figure 4.6: *A drifter was released inside a Mozambique eddy during the ACSEX I cruise, on March 28 (De Ruijter et al., 2002). After traveling south within the eddy for about two months, it was released to the Agulhas current near the Natal Bight by the end of May 2001. This is during the interaction of the eddy with the current illustrated in the SST-snapshots of Fig. 4.7*

The eddy that was measured hydrographically a 24 °S in the Mozambique Channel during the first cruise of ACSEX in April 2000 (De Ruijter et al., 2002) was clearly shown to have a velocity, temperature and salinity profile reaching all the way to the bottom of the channel at 3000 meter. In addition, a drifter was released in the eddy. The path of this drifter shows a swirling route southward (Fig. 4.6), as expected for water trapped in an eddy that constitutes an anomaly like those followed in Fig. 4.5. The drifter was ejected from the eddy during the period of interaction with the Agulhas current (second half of May 2000), and is further advected southward.

Fig. 4.7 shows a series of consecutive snapshots of SST in the vicinity of the Natal Bight. The first snapshot, made on May 31, 2000, clearly shows an anticyclonic eddy in interaction with the Agulhas current. The eddy can easily be traced back further north in altimeter data, and is the same one that was carrying the drifter shown above. It pulls warm surface waters from the Agulhas, enabling the clear view on its anticyclonicity. It is located slightly upstream of the Natal Bight, enhancing and narrowing the flow. Five days later, exactly at the place where the coastline recedes, and where the continental slope is less steep, a cyclonic meander starts to grow in the current (Fig. 7b). The next day, June 5, the interaction between the current and the eddy has become less intense (they are clearly separated again in the SST signal shown in Fig. 7c). On June 7 it becomes obvious that the Natal pulse is traveling south with the Agulhas (Fig. 7d).

4.4 Connection to the Agulhas sources

Fig. 4.1 suggests two possible source regions for the above identified eddies: the Mozambique Channel, and the southeast Madagascar current. In this section, we show altimetric evidence for both.

4.4.1 The Mozambique Channel

Hydrographic measurements in the Mozambique Channel fail to agree on a steady circulation. Different research cruises have led to different snapshots of the circulation in the channel (Harris, 1972; Saetre and Da Silva, 1984; Donguy and Piton, 1991), but they do agree as far as the absence of a continuous western boundary current close to the Mozambique coast is concerned. They all picture the channel as a region dominated by mesoscale current features (between 100 and 400 km wide). Eddies in the Mozambique Channel are also observed in the model simulations by Biastoch and Krauss (1999).

Recently, the ACSEX I cruise was carried out in the Mozambique Channel (De Ruijter et al., 2002). It should be noted that this cruise was carried out in April/May, which is in the season of lowest transport observed in the model of Biastoch and Krauss (1999) and in POCM (Matano et al., 2001). Hydrographic measurements were made with the focus of determining the flow structure of the channel, and resolving both the western boundary current and the eddies. No continuous southward current was found along the slope. Eddies as suggested by the SSH measurements from space were shown unambiguously to be present and even to extend over the full depth of the channel (De Ruijter et al., 2002) with diameters of 300-400 km. They were shown to carry water from the north, including a core of intermediate water from the northern Indian Ocean that is actively mixing with Antarctic Intermediate Water. The latter flows northward, most probably as a continuation into the Mozambique Channel of the Agulhas Undercurrent (Beal and Bryden, 1997).

4.4.2 The East Madagascar current

The southern limb of the East Madagascar current carries about 20 Sv southward along the coast of Madagascar (Swallow et al., 1988). At the southernmost point of Madagascar, it

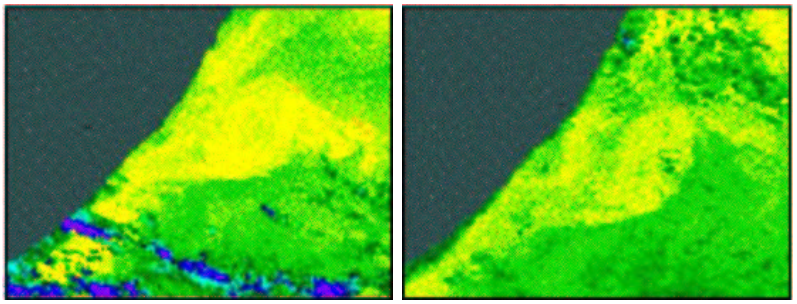

(a) May 31, 2000: The Mozambique eddy followed by a drifter (Fig.7) is in interaction with the main current.

(b) June 4, 2000: The current is pulled away from the coast, a meander is being formed.

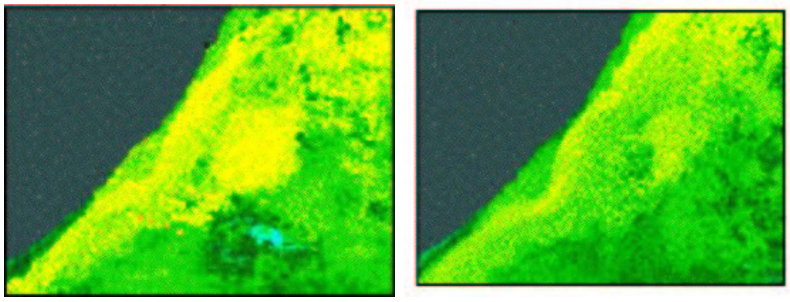

(c) June 5, 2000: The connection between the current and the eddy is weakened. The meander is moving southward.

(d) June 7, 2000: The meander is clearly visible, and moving southward. Clouds partially obstruct a view of the eddy, but its SST has also decreased due to air-sea interaction.

Figure 4.7: *sea-surface temperature snapshots of the region near 30S, off Durban. Interaction between a Mozambique eddy and the Agulhas current leads to the formation of a large meander: the Natal Pulse.*

becomes unclear what happens to the current. A purely Sverdrup-dominated balance would result in a free westward jet crossing the southern end of the Mozambique Channel, to form a direct source for the Agulhas current south of $25°$S. Observations of ship's drift in the region fail to show a univocal picture of the situation (Lutjeharms et al., 2000). Together with the high variability observed in the satellite derived SSH field, the variable ship's drift measurements indicate a region that is dominated by eddies. There is some evidence pointing at a situation more like that south of Africa: with a retroflection of the Southeast Madagascar current and the flow turning east back into the central Indian Ocean. Based on a single SST snapshot Lutjeharms and Van Ballegooyen (1988) already speculated on the retroflective na-

ture of the Southeast Madagascar current. That idea is confirmed by some of the drifters that were placed in the South Equatorial current, and showed signs of a retroflection (Lutjeharms et al., 1981). But just like in the Mozambique Channel, no uniform picture can be drawn either from hydrographic or ships drift measurements (Lutjeharms et al., 2000). Due to the large variability of the flow in this region, rings may be shed from this retroflection like they are from the Agulhas, as the local dynamical properties of the system are rather similar to those around the southern tip of Africa: a narrow western boundary current overshooting the end of the landmass (Africa or Madagascar). From the altimeter data, it becomes clear (see below) that also in this source area of the Agulhas, eddies play a role in the structure of the overall flow.

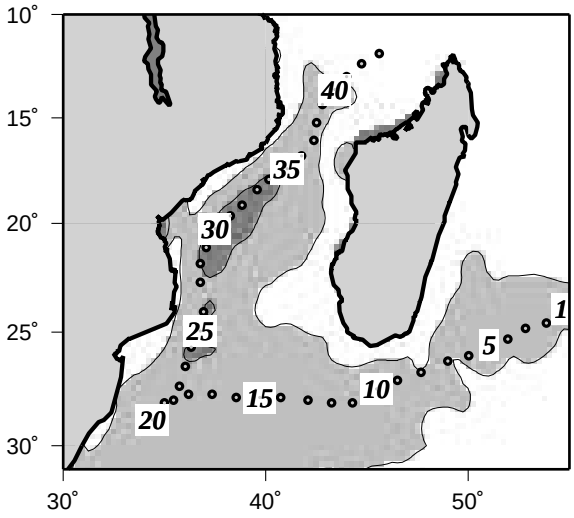

Figure 4.8: *As Fig. 4.4. Now the track along which a space-time plot is constructed has been chosen in the Mozambique channel and south of Madagascar. These tracks cover the Mozambique eddies, and the possible eddies being spawned from the Madagascar current. There is a small overlap between Fig. 4.4 and this track, to accommodate a continuous tracking of the propagating anomalies. The space-time plot itself is shown in Fig. 4.9.*

4.4.3 MSSA Results

Again we focus on the first four modes found by the MSSA analysis of the region of the larger Agulhas system, extending between $5°$E and $55°$E and between $45°$S and $5°$S (eg. see Fig 4.1). The eddies found to propagate on the offshore edge of the Agulhas current (Fig. 8), and into the Retroflection region, can be traced back to the source regions of the Agulhas. This is done In Fig. 4.9, again by constructing a space-time diagram along the lines of highest variability. At intervals of ~ 100 km the reconstructed values of the first four MSSA-modes are plotted through the Mozambique Channel and from the African coast to the southern tip

of Madagascar. There is a small overlap between the southern part of this trajectory, and the northern end of that in Fig. 4.4, so the anomalies can be clearly followed to propagate into the retroflection. Anomalies are coming from both the Mozambique Channel and southeast of Madagascar, and connect to the eddy path plotted in Fig. 4.4. The anomalous sea-surface heights are $\sim$ 20-30 cm. These relatively high values indicate that they are eddies indeed. During the recent ACSEX I cruise this eddy nature was confirmed by CTD and Lowered ADCP observations in the Mozambique Channel (De Ruijter et al., 2002). Analysis of the altimetric data gives a frequency of between 4 and 5 of these eddies per year. Southwestward propagation is in the order of 10 km day^{-1}.

4.5 Connection to the central and eastern Indian Ocean

So far, we have shown eddies from the Mozambique Channel and from the East Madagascar current to penetrate the Agulhas current System, and most probably control the timing of ring shedding at the westernmost extension of that system. But also the central and eastern parts of the South Indian Ocean seem to play a role in the upstream control of the Agulhas Retroflection. East of Madagascar (roughly between $10 - 30°$S) the SSH-variability is dominated by westward propagating baroclinic Rossby waves (Morrow and Birol, 1998). Band pass filtered altimetric data (again focusing on frequencies between 4-5 times per year) along two zonal bands throughout the width of the Indian Ocean are plotted in Fig. 4.10. The left panel shows the $12°$S parallel, that corresponds to the northern tip of Madagascar. The right panel shows the $27°$S parallel, corresponding to the southern tip of Madagascar. Both panels show clearly the propagation of Rossby waves. As was shown by Morrow and Birol (1998), the speeds agree well with the revised Rossby wave propagation theory (Killworth et al., 1997) i.e. 17 km d^{-1} at 12°S and 5 km d^{-1} at 27°S. At 12°S, the Rossby waves clearly feel the steep topography of the Mascarene ridge at $\sim$ 60°E. West of this ridge the signal is confused, but can be followed nonetheless to the African coast at 41°E. This confusion is partially caused by the strong 50-60 day periodicity of the western extension of the South Equatorial current. An MSSA analysis of this region (40°- 60°E;5°- 13 °S) yields as the first oscillatory mode (formed in this case by the first two eigenvectors) a single meander in the South Equatorial current starting at the northern tip of Madagascar, propagating westward. The dominant frequency of this mode is 55 d^{-1}, and the local contribution to the variability west of 50°E is over 40%. This MSSA mode is strongly present in 1996, 1997 and 1999, but less in 1998 and the end of 1995. The existence of this intramonthly variability was identified by local current measurements Near Cape Amber reporting 41% of the flow variance in the 40-55 day period band (Quadfasl and Swallow, 1986; Schott et al., 1988). Based on results of a single-layer model , this has been ascribed to barotropic instability of the current system north and east east of Madagascar (Kindle and Thompson, 1989). However, their model does not reproduce the 400 km waves between the tip of Madagascar and the African continent observed in the MSSA modes described above, and previously in modeling results (Périgaud and Delecluse, 1992).

MSSA-analysis of the Mozambique Channel alone yields a dominant frequency of 4 per year, and clearly a formation of eddies in the Channel, starting with an anomaly propagating from the northern part of the Channel through the narrowest part at 16°S, into the Channel

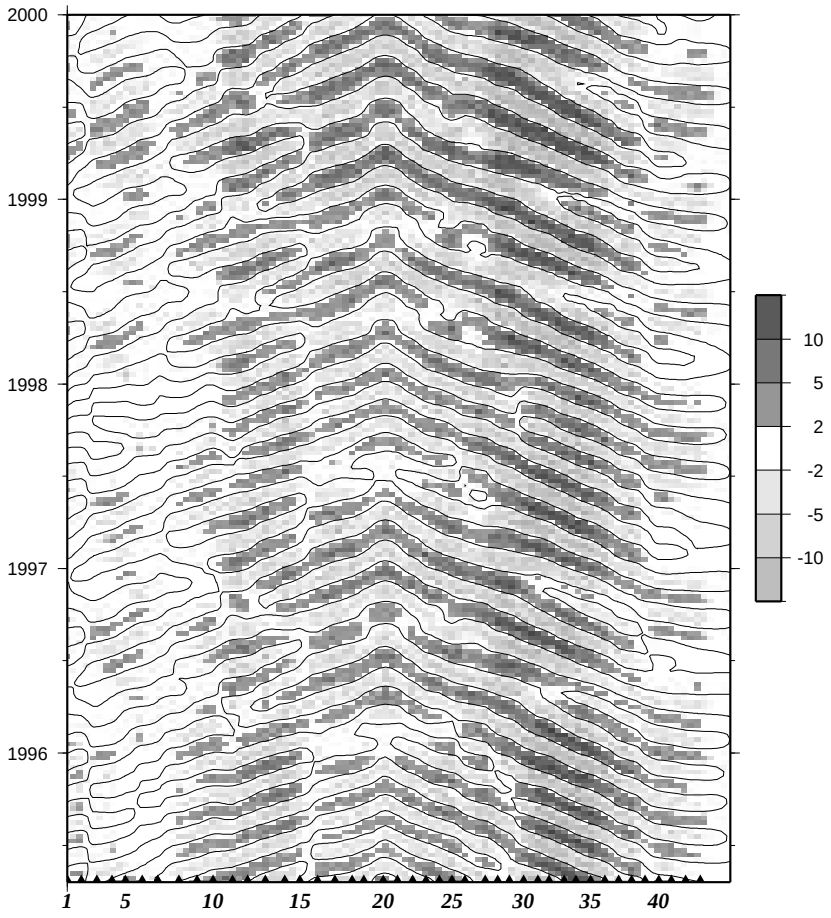

Figure 4.9: *Space-time plot through the reconstructed components 3-4 of the MSSA analysis, along the tracks shown in Fig. 4.8. Amplitudes are given in cm. The discontinuity at point 20 denotes the most 'downstream' point of the plot. From both directions incoming anomalies can clearly be followed. From the Mozambique Channel to the northern Agulhas at* 30°*S in the points (along the horizontal axis) 1-20 the translation is mainly in southwesterly direction, whereas a movement along the line 40-20 means a westerly translation.A striking feature of this plot is the apparent synchronization of both processes: anomalies from the north and the east arrive simultaneously.*

itself. Interaction of the incoming Rossby waves from the east with the high shear regions of the South Equatorial current north of Madagascar may act as a triggering mechanism for this process. The absence of local forcing (the local instability process seems to be disconnected from the Channel region, and has too high a frequency) and the correspondence in frequency are a strong indication for such a connection with the far field.

At 27°S, the Rossby waves show a significant intensification at $\sim 45^\circ$E (see also (Morrow

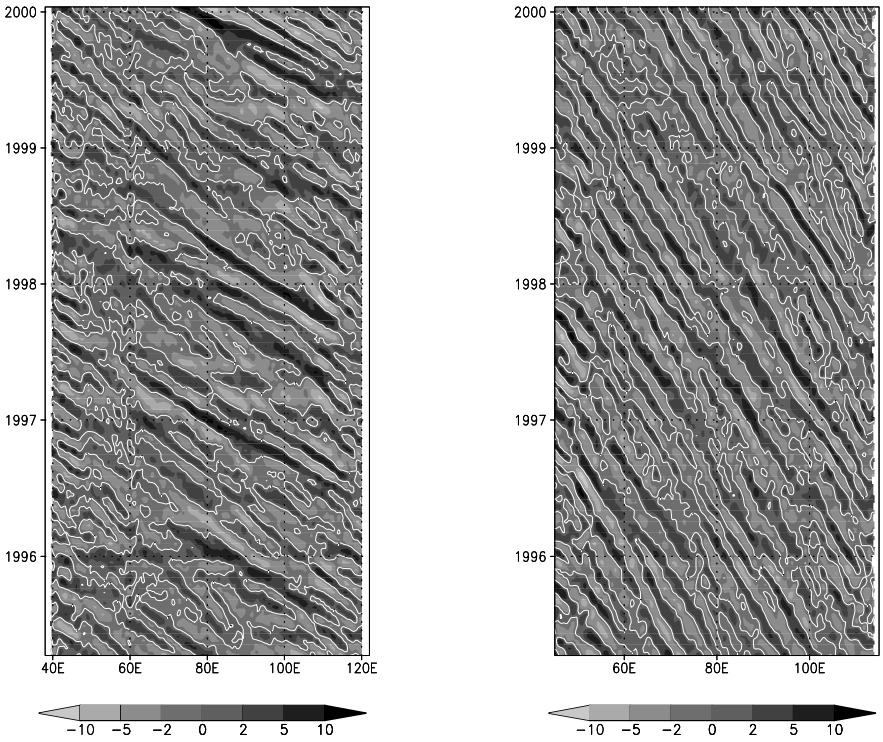

Figure 4.10: *Hovmöller plot of bandpass filtered SSH anomalies along the 12°S (left panel) and 27°S (right panel) parallels. These cross the northern and southern tip of Madagascar respectively. Note the clear movement of Rossby waves, and the different speeds of propagation for the two latitudes. Also noteworthy is the influence of bottom topography near 60°E,12°S. Amplitudes are given in cm.*

and Birol, 1998), their plate 5.). This could be due to the rising bottom (depths decrease from ~ 4000m to ~ 1500m within 500 km). But it may also be due to the interaction with the East Madagascar current, that may lead to eddy shedding at the southern tip of Madagascar. As the intrinsic drift of a freely moving eddy is very similar to the propagation speed of Rossby waves, it is very difficult to distinguish between propagating waves and eddies. However, the sea surface elevations of over 20 cm found south and west of Madagascar are too high to be solely the expression of a (linear) Rossby wave. Also, the anomalies found south and west of Madagascar are more or less circular, and those found further east have more meridionally elongated shapes. The picture thus emerges of a regular train of Rossby waves that cross the Southeast Indian Ocean at a frequency of 4 per year, are focussed, and lead to the formation of eddies in the western part of the basin.

4.6 Summary and Discussion

In this chapter, we have shown evidence for the existence of a direct link between the shedding of Agulhas Rings and incoming eddies from upstream areas, in particular the Mozambique Channel and the region south of Madagascar. The timing of Agulhas Ring shedding is controlled by the eddies traveling downstream along the offshore edge of the Agulhas current. These eddies form part of a larger system probably incorporating the whole South Indian Ocean. The zonal movement of the Agulhas Retroflection loop can be followed in altimetric measurements. It moves slowly to the west, and returns to an eastern position with a frequency of 4-5 times per year. The location of the retroflection can be traced back to the arrival of an eddy from the north. In former analyses this movement of the retroflection has been associated with the shedding of Agulhas Rings. However, Ring shedding records are far more irregular than the behavior of the Agulhas Retroflection described here. This can be attributed to the many complicating factors that dominate the signal once the rings have been shed into the Atlantic. In the first months of their life time, they interact strongly with the bottom topography, with each other, and with background currents. Also, rings may split or be recycled back into the Agulhas current (Arhan et al., 1999; Schouten et al., 2000). All these influences prevent the regularity inherent to the current itself from being observed in the Ring shedding record. Unique determination from satellite altimetry is furthermore hampered by the unknown mean background circulation, the spatial and temporal resolution of the altimetric measurements, and the limitation to the upper layer of all available remote sensing observations.

Besides the impact on the movement of the retroflection, the eddies from upstream may also control the timing of Agulhas Ring shedding by generation of the so-called 'Natal Pulse' which has been observed to be related to ring shedding almost half a year later (Van Leeuwen et al., 2000). The anticyclonic eddy on the seaward edge of the current can provide the positive transport anomaly needed to destabilize the current near Durban (De Ruijter et al., 1999).

In the Mozambique Channel, eddies are observed to propagate in southwestward direction from the northern end of the channel. These eddies have been measured hydrographically. We have shown that they can be followed in MSSA-filtered altimetric data to be the same eddies as those observed on the offshore edge of the Agulhas. This was confirmed by a drifter released in one of the measured Mozambique eddies. This drifter clearly shows the rotating path of water inside an eddy, and the southward translation that is observed for the Mozambique eddies in the five year record of altimetric data. This same single eddy has also been observed to interact with the Agulhas near Durban (in SST snapshots), triggering a large solitary southward traveling meander: a Natal Pulse.

The Mozambique eddies themselves may be connected to processes further east in the Indian Ocean, as Rossby waves are observed to cross the Indian ocean over the full zonal extent with frequencies close to that of the observed eddies in the Mozambique Channel and on the offshore edge of the Agulhas current. These Rossby waves, propagating at speeds comparing well with theoretical estimates (Killworth et al., 1997), are found in the latitude band between 10 and 30°S . Both to the north and south of Madagascar interaction of these Rossby waves with local currents (the South Equatorial and East Madagascar current respectively) may result in the shedding of eddies, as suggested by the strengthening of the anomalies in these

areas.

However, the origin of the frequency of 4-5 per year remains unclear. The forcing mechanism resulting in the Rossby waves at this frequency is not yet identified. No seasonal forcing is expected at this frequency, and atmospheric variability is mainly found at shorter timescales. A candidate explanation is that the Rossby waves are the manifestation of an internal eigenmode of the Indian ocean. Interaction of a seasonal Rossby wave with the much shorter period of the local instability of the South Equatorial current north of Madagascar leading to the observed periods is another one. Further study is presently underway to identify the origin of this phenomenon.

The interaction of the eddies from the north with the southern Agulhas current once it has become a free jet south of the African continent may be intuitively understood, but dedicated numerical studies should provide an answer to the question how and to what extent this process determines the shedding of Agulhas Rings. The eddies do not seem to be a necessary condition for the existence of Agulhas Rings, as instabilities in the retroflection have been shown to be able to produce these rings without remote forcing. Nevertheless, the eddies may very well act as the finite amplitude disturbance needed to trigger the instability after the conditions have been set by internal processes, and thereby determine the exact timing of the process.

Besides a dynamical impact, the Mozambique eddies also have distinct water mass properties that give them also a direct thermohaline dimension. In situ observations have shown that a Mozambique eddy in the southern part of the channel contained a large core of intermediate water of Red Sea and/or Persian Gulf origin, thus containing a large saline anomaly with respect to the relatively fresh surrounding water (De Ruijter et al., 2002). Red sea water has also been identified in the Southeast Atlantic ocean (Gordon et al., 1987), indicating that the eddies may indeed not only be a dynamical source of vorticity for the retroflection, but also a direct source of water at intermediate depths and above.

Chapter 5

A teleconnection between the equatorial and southern Indian Ocean

In the former chapter, we have shown that about four Mozambique Channel eddies are formed per year, and speculated on the remote origins of this four per year signal. In this chapter, these origins are further investigated. An oceanic teleconnection is suggested between wind variations over the equatorial Indian Ocean and the intermonthly oceanic variability that dominates the Mozambique Channel eddy formation. Four times per year an equatorial Kelvin wave is observed to hit Indonesia, forced by monsoonal and intermonsoonal wind variability. The signal then propagates southward along the Indonesian coast and connects to a train of Rossby waves that propagates westward across the subtropical southern Indian Ocean. On reaching the Madagascar and Mozambique Channel regions, large rings form at the same four per year frequency. These drift into the Agulhas retroflection region where they control partly the shedding of Agulhas rings. Thereby, the equatorial atmospheric changes may control a key link between the Indian and Atlantic Oceans in the global circulation of heat and salt through the thermohaline circulation. Single case disturbances of this pin-ball-like propagating signal can be traced from the anomalous equatorial events in 1994 and 1997/1998, the Indian Ocean Dipole/El Niño events, to a decrease of Indian-Atlantic ocean exchange by Agulhas rings over two years later.

5.1 Introduction

The Indian Ocean forms a major link in the global thermohaline circulation (Gordon et al., 1992; De Ruijter et al., 1999). Gordon (1985, 1986) estimated the Indian-Atlantic interoceanic exchange of warm and saline upper ocean/thermocline water at 13.5 Sv, via direct leakage of Agulhas water and the shedding of large Agulhas rings. Thereby, the Indian Ocean would be the conduit for about 70 % of the renewal of North Atlantic Deep Water (NADW)

exported from the Atlantic at deeper levels, which is estimated at 15-20 Sv (Schmidtz, 1995). This view of the Indian-Atlantic Ocean connection, the ”warm water route”, as the major renewal path for NADW, has been challenged in favor of the so-called ”cold water route”, providing the Atlantic with a renewal by entrance of cold upper ocean waters through the Drake Passage (Rintoul, 1991). Gordon et al. (1992) combined both routes into a scheme by which the cold water loops through the southwest Indian Ocean before spreading northward in the Atlantic. Chemical properties of Benguela current waters in the southeastern Atlantic were found to be derived primarily from Indian Ocean sources, rather than from Drake Passage directly. This scheme seems to be supported by recent modeling results (Speich et al., 2001). In their model, they find a contribution of 14 Sv flowing from the Indian Ocean northward through 20°N in the Atlantic. This 14 Sv is mainly composed of Indonesian Throughflow water and waters that follow the route described by Gordon et al. (1992), from Drake Passage looping through the Indian Ocean.

In several modelling studies, Weijer et al. (1999, 2001) show a considerable sensitivity of the meridional overturning strength of the Atlantic, to a thermohaline source in the South Atlantic representing the Agulhas leakage. Moreover, the input of warm and saline water at the southern tip of Africa tends to stabilize the northern overturning of the Atlantic Ocean. GCM simulations (Weijer et al., 2002) show that a strengthening (weakening) of the Indian-Atlantic exchange can result in enhanced (reduced) meridional overturning of the Atlantic within decades. Thus, by the inflow of Indian Ocean water south of Africa, climate variability over the Atlantic region may be coupled to that of the Indian Ocean at relatively short timescales.

The inflow of Indian Ocean upper and thermocline waters into the Atlantic is a complex and intermittent process (Lutjeharms and van Ballegooyen, 1988; De Ruijter et al., 1999; Goñi et al., 1997). The transport is composed of direct leakage into the Benguela region, and the shedding of large Agulhas Rings at the western end of the Agulhas, where it retroflects an turns back into the Indian Ocean. Estimates for the direct leakage range between 4 and 10 Sv (De Ruijter et al., 1999). Given the strong variability of the system, and the fact that most estimates are based on single hydrographic snapshots, this range is not a surprise. A even larger range of estimates has been made for the contribution of Agulhas Rings to the heat and salt budgets of the South Atlantic. These rings, with diameters of over 300 km, are probably the most energetic rings in the world ocean (Olson and Evans, 1986) and can reach all through the water column to the bottom at 5 km depth (van Aken et al., 2002). They carry large amounts of Indian Ocean water into the Atlantic. Estimates of the contribution of the rings are usually based on an estimate of the contribution per ring (ranging between 0.5 and 2 Sv) and an estimate of the frequency of ringshedding (between 4 and 7 per year. See (De Ruijter et al., 1999) for a detailed discussion of the various estimates.)

Although the Agulhas rings enter the Atlantic irregularly, the shedding process at the Agulhas Retroflection region appears to be more regular (Schouten et al., 2002b). This frequency seems to be controlled by incoming eddies from the Mozambique Channel and from south of Madagascar, which initiate the shortcutting of the Agulhas retroflection loop on entering the Retroflection region. The large anticyclonic features (the newly formed Agulhas rings) from then on behave very irregularly, governed by vigorous air-sea interaction (Olson et al., 1992; van Aken et al., 2002), and interaction with bottom topography or other rings (Arhan et al., 1999; Schouten et al., 2000). Also, the newly formed rings may be vulnerable to instabilities

(Drijfhout et al., 2002) and split up into smaller rings. Schouten et al. (2002b) show that besides the shortcutting mechanism by the eddies themselves, also a control mechanism via the formation of so-called Natal Pulses (Lutjeharms and Van Ballegooyen, 1988) may play a role in the upstream control of Agulhas ring shedding. These meanders in the upstream Agulhas current have been related to the shedding of Agulhas rings almost half a year later (Van Leeuwen et al., 2000), and are possibly formed by barotropic instability of the Agulhas current near Durban, where the continental slope relaxes (De Ruijter et al., 1999). The mean Agulhas current is not susceptible to these instabilities, but an intensification of the flow due to the passage of a Mozambique eddy may change this. A series of sea-surface temperature snapshots combined with in situ evidence of the presence of a Mozambique eddy supports this mechanism (Schouten et al., 2002b). As a consequence, Mozambique eddies seem to set the frequency of the basic Agulhas ring shedding at about four per year, the frequency of their occurrence. Schouten et al. (2002b), however, touch only slightly the subject of how this four per year frequency is set. They speculate that the Mozambique eddies may be related to Rossby waves coming in from the east at roughly the same frequency.

In this chapter, we provide observational evidence for an oceanic link between wind fluctuations over the equatorial Indian Ocean and intramonthly variability at dominant frequency of 4 per year in the subtropical southern Indian Ocean. We show that the equatorial signal propagates by a succession of Kelvin and Rossby waves to the region around Madagascar, where it amplifies and propagates as eddies into the Agulhas region. In this way, variability in the equatorial Indian Ocean may lead to variations of interocean exchange and associated fluctuations of the Atlantic meridional overturning circulation.

This chapter is organized as follows. First we assess the regional distribution of the four per year frequency, and investigate the possible equatorial origins of the four per year cycle (section 5.2). Statistical analysis of altimeter measured sea-surface height data shows indeed a four per year cycle, which has considerable impact on the waters near Indonesia. From there, we follow the propagation of the four per year signal southward by propagation along the Indonesian coast in the form of Kelvin waves, and westward across the southern Indian Ocean (section 5.3). In the west, the four per year signal is transformed into eddies, which drift southward into the Agulhas region (section 5.4). Finally, the results are summarized and discussed in section 5.5.

5.2 The possible equatorial origin of a four per year cycle

As already mentioned above, the upstream control of Agulhas ring shedding from the Mozambique Channel is dominated by variability with periods of around 90 days (Schouten et al., 2002b). Variability observed locally north of Madagascar by Schott et al. (1988), probably due to barotropic instability, has a higher frequency than this, with a period of around 50-60 days.

To investigate the possible source regions of the four per year variability we have filtered the frequencies between 3.5 and 4.5 times per year from six years (1995-2000) of combined TOPEX/Poseidon and ERS altimeter data. The remaining variability is plotted in Fig. 5.1a, and its relative contribution to the total variability is plotted in Fig. 5.1b. Clearly, there is considerable amplitude in this frequency range in the Agulhas region and the Mozambique

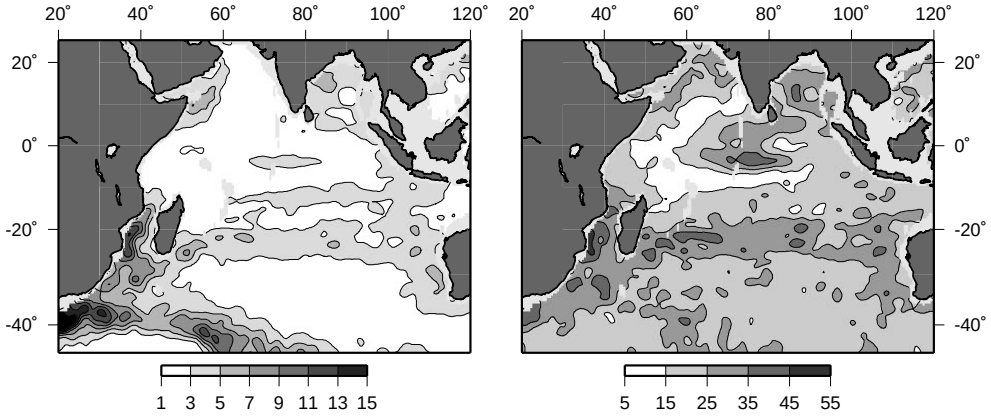

Figure 5.1: *(a) Variability of sea-surface height (SSH) in the 80-100 day period band (cm), and (b) the relative contribution of this variability to the total variability (%) over the period 1995-2000.*

Channel, where amplitudes of around 10 cm account for over 30 % of the variance. Also east of Madagascar, two bands of variability are visible across the South Indian Ocean. The first band is around 12°S, with amplitudes of over 3 cm, which does not account for a large part of the variance due to the relatively strong semi-annual, annual and interannual signals at that latitude (Périgaud and Delecluse, 1992). A stronger band of variability exists around 25°S, where also the relative contribution to the variance is over 25 %. Another clear hotspot of variability at this frequency range is found in the equatorial band, between 60°and 90°E. Here, relative contributions are found of more than 35%.

First we confirm the remotely sensed four per year periodicity in the central equatorial Indian Ocean by means of in-situ tide gauge measurements taken at the Maldives island Gan, located just off the equator. Over eight years of tide gauge measurements at this island have been plotted in Fig. 5.2a. A low-pass filtering by means of a running cosine weighted mean with a filter halfwidth of 0.8 years is also plotted in this figure. The latter shows a clear seasonal cycle, involving also interannual variability. The high-pass filtered data, obtained by subtracting the low-pass signal from the original data, shows relatively high-frequency variability. The spectrum of this high-pass filtered signal (Fig. 5.3) shows a clear peak at the four per year frequency.

To further analyse the four per year mode of variability in the equatorial band, we have analyzed six years of combined TOPEX/ Poseidon and ERS1/2 altimeter data, provided by the CLS (Collection Localisation Satellites) Space Oceanography Division, Toulouse, France. We have used the so-called Multichannel Singular Spectrum Analysis (MSSA) (Plaut and Vautard, 1994) technique. MSSA is a statistical tool to extract oscillatory and moving patterns from a multidimensional dataset. Given the dominance of propagating long waves in the equatorial ocean, MSSA may be an appropriate tool to isolate and extract the equatorial modes of variability based on their period. As we focus here on the intermonthly timescale,

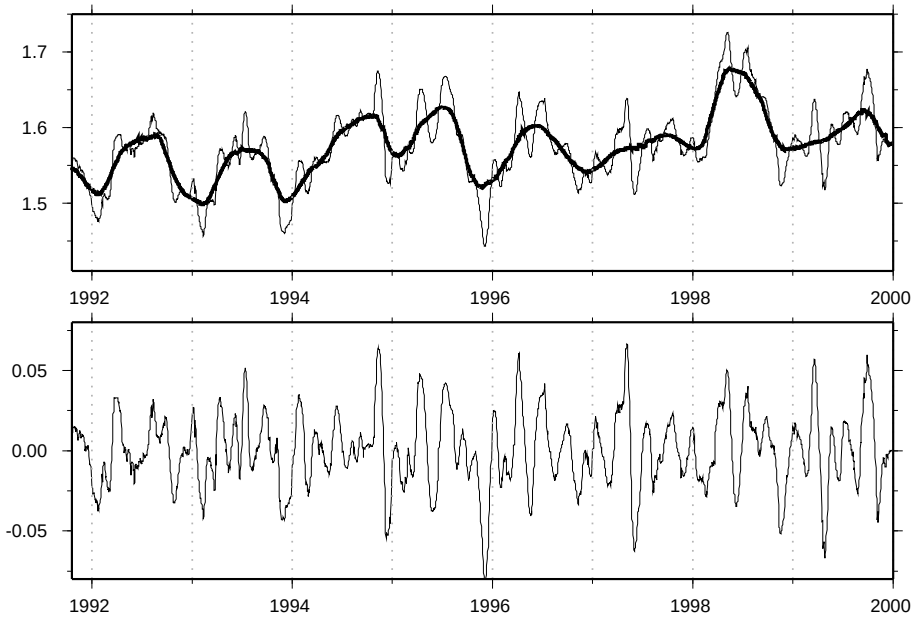

Figure 5.2: *Tide gauge SSH measurements near the Maldives island Gan (73°E ; 0.5°S). (a) Low pass filtered and (b) Remaining high pass part of the variability (in meters)*

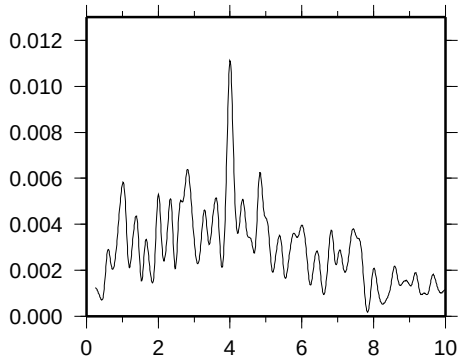

Figure 5.3: *Spectrum of the timeseries of Fig. 5.2b (cm^2). Along the horizontal axis, the frequencies are plotted (in cycles per year).*

we use a high-pass filtered version of the altimeter data. We have applied a cosine weighted running mean filter with a filter halfwidth of 200 days to remove the low-frequency part of the spectrum. Also the annual cycle is strongly damped. Such filtering does not qualitatively change the patterns of the modes found in the MSSA procedure.

The four per year MSSA mode shows an equatorial Kelvin wave that hits the coast of Sumatra (Indonesia) (Fig. 5.4a). It appears to be partly reflected as a Rossby wave prop-

agating westward, and partly as coastal Kelvin waves that propagate in poleward direction. Semi-annual Kelvin waves have been identified earlier by several authors in observational and modelling studies (Clarke and Liu, 1993; Sprintall et al., 2000). Clarke and Liu (1993) show that the semi-annual cycle of the sea level all along the Indonesian coast is dominated by a semi-annual Kelvin wave forced over the central equatorial region by the intermonsoonal westerly windbursts. Also, they show that the Indian Ocean equatorial basin is close to resonance at the semiannual frequency due to its width, close to that required for a semi-annual equatorial basin mode (Cane and Moore, 1981). Sprintall et al. (2000) present observations of the passage of an equatorial Kelvin wave, and its effects on the local circulation near Indonesia. The Kelvin wave of May 1997 was shown to strongly influence the Java current along the western coast of Indonesia, and also the circulation in the internal Indonesian seas. They also found a reversal of the flow in Lombok strait due to the passage of the Kelvin wave, followed by a strong reduction in the southward throughflow via Macassar strait. Sprintall et al. (2000) also show that the Kelvin wave is forced by the equatorial westerly wind variations. Equatorial winds also seem to be responsible for the fluctuations in coastal sea level and Lombok Strait throughflow with periods of 30-60 days (Arief and Murray, 1996; Qiu et al., 1999). These periodicities may be related to the atmospheric cycle reviewed by Madden and Julian (1994). Qiu et al. (1999) found four per year variability in their modeled sea level and throughflow, and attribute this signal also to equatorial forcing. However, they find only a very small spectral peak in the equatorial winds at periods near 90 days.

A well-known problem with MSSA is the distinction between signal and noise. It is not trivial to distinguish realistic modes that come prominently forward in the MSSA analysis, i.e. that represent realistic oscillating signals in the data, from modes that are merely constructed of noise. Allen and Robertson (1996) have shown that pure red noise may yield MSSA modes that have all the other characteristics of oscillating signals. They designed a Monte Carlo test to check whether the MSSA modes found from data are likely to be realistic, or possibly the resultant of red noise. We have performed the Monte Carlo test of (Allen and Robertson, 1996) on the original (unfiltered) data of the region between 40°- 115°E and 10°S - 10°N. Regions shallower than 500 m (mainly in the Indonesian seas) have been masked out. The results are shown in Fig. 5.5. Clearly, the annual, semi-annual and four-per-year couples of MSSA modes have eigenvalues that are above the 99% confidence interval for the red noise null hypothesis.

Another problem of the MSSA technique is the periodicity of the reconstructed signal: like with conventional Fourier analysis, irregularities of the original signal do not show up in the reconstruction of a single mode. Deviations from the 'perfect' periodic behaviour result in smaller amplitudes, and are not very well reconstructed. For instance, interannual variability of the four per year signal can not be adequately reproduced by the MSSA analysis. Another problem, intrinsic to most statistical techniques that are used to isolate signals at distinct frequencies, is that processes may be non-sinusoidal and thereby contain signals at several frequencies, resulting in dominant frequencies which are unrealistic. Especially in our case, where dominant modes exist at periods of one year, half a year and one fourth of a year, this is a possibility. To overcome these problems, and to see if what we observe in the four-per-year MSSA-mode is in reality also happening four times per year, we have spatially correlated a single snapshot from the MSSA mode (Fig. 5.4a) with the original along-track TOPEX/Poseidon altimeter data. This has several advantages: first, we avoid looking at non-

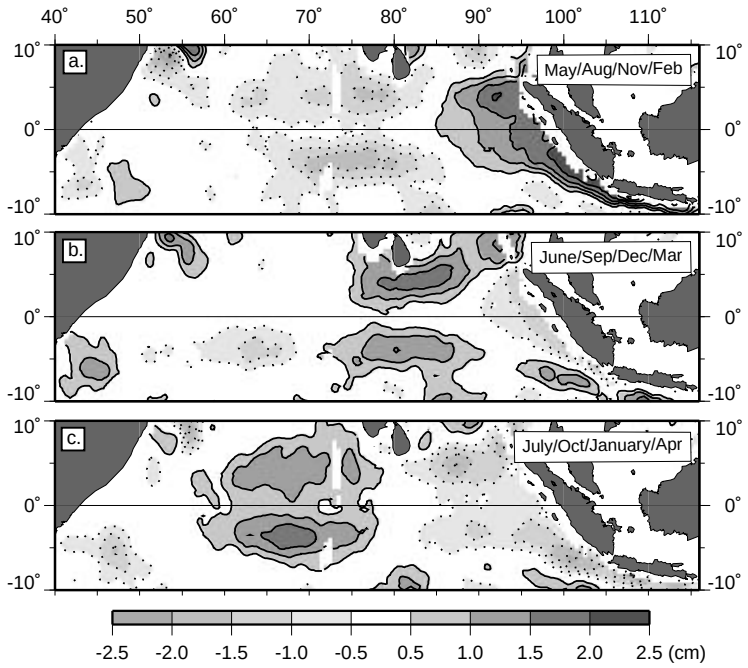

Figure 5.4: *Three snapshots from the four-per-year MSSA mode. a) an equatorial Kelvin wave has reached Indonesia, and is reflected as a Rossby wave and coastal Kelvin waves leaving in westward and poleward directions respectively. b) The Rossby wave propagates westward with speeds in agreement with the theoretical value for the first baroclinic Rossby wave (0.53 m/s (Clarke and Liu, 1993)). c) In the western half of the basin, the waves do not seem to propagate further west than roughly 60°E. This part of the basin is dominated by the semi-annual signal. This issue is further elaborated in the discussion.*

sinusoidal behaviour of the (semi-)annual cycle, as four peaks in positive correlation indeed means that the situation depicted in the snapshot is observed four times per year. Second, we obtain a time series which represents the full temporal spectrum of the data. No filtering in the temporal domain is applied, other than that the snapshot is taken from a certain MSSA mode. This also enables us to identify interannual variability on the observed signal.

Fig. 5.6 shows the correlation between the TOPEX/Poseidon data and the snapshot from the four-per-year MSSA mode from Fig. 5.4a. This time series shows clearly the higher frequency behaviour associated with the four per year cycle, but is quite irregular over the years. There is very good correlation between the high-pass filtered tide-gauge signal at the island Gan (Fig. 5.2b) and this timeseries (0.7 at zero lag). The highest correlation found during the eight years of the T/P altimeter measurements agrees with the May 1997 Kelvin wave event described in detail by Sprintall et al. (2000), which was clearly wind-forced. Fig. 5.6 shows that this was not an isolated event, but recurring over the years. Furthermore, there is also very good agreement between the time series of Fig. 5.6 and the flow through Lombok Strait as determined from in-situ pressure gauge measurements (Chong et al., 2000).

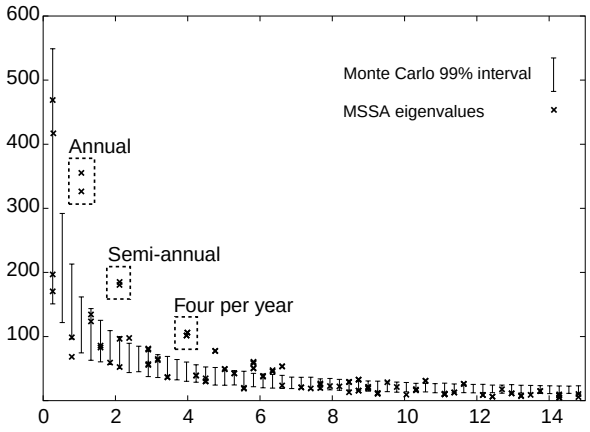

Figure 5.5: *Results from an MSSA analysis of the unfiltered SSH data from the equatorial Indian Ocean, and a n=200 Monte Carlo experiment testing against red noise (Allen and Robertson, 1996). The 99 % confidence intervals are plotted. Frequencies the horizontal axis are given in cycles per year.*

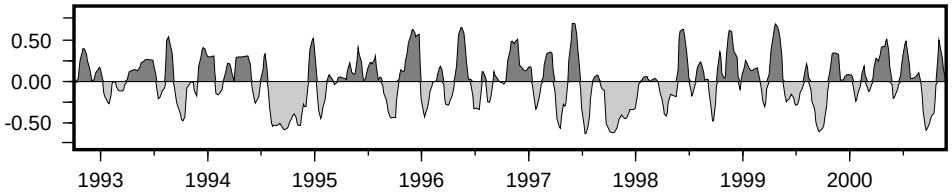

Figure 5.6: *Correlation timeseries, obtained by correlating the eastern half (east of 70°E) of the spatial pattern of Fig. 5.4a with the original along track T/P altimeter measurements.*

This is shown in Fig. 5.7. Sprintall et al. (2000), using the same data, show that the main discrepancy between the two (the eastward flow in January 1997 without a corresponding peak in the Kelvin wave signal) is caused by alongshore winds along the coast of Java. Fig. 5.6 also shows two major disturbances of the four per year signal: during the second half of 1994 and 1997 no Kelvin waves seem to reach the coast of Sumatra. These periods are characterized by strong anomalous easterly winds, associated with the build-up of the Indian Ocean Dipole events (Webster et al., 1999; Saji et al., 1999) and El Niño conditions. These strong easterlies (and the absence of the intermonsoonal westerlies) prohibit the formation and propagation of Kelvin waves in the eastern part of the equatorial basin (Fig. 5.8).

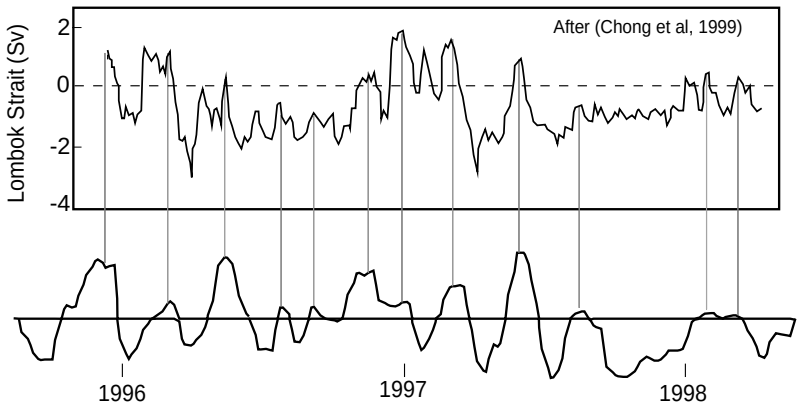

Figure 5.7: *In the upper panel, the throughflow through Lombok Strait is shown (into the Indian ocean gives negative values). The lower panel shows the timeseries of the arrival of the equatorial Kelvin wave (Fig. 5.6) for the corresponding period.*

5.3 Propagation of the signal to the subtropical region

On arrival at the Indonesian coast, the equatorial Kelvin waves are partly reflected as Rossby waves, but also propagate as coastal Kelvin waves, traveling in northward and southward direction along the Indonesian coast (Subrahmanyam and Robinson, 2000; Clarke and Liu, 1993; Sprintall et al., 2000). In this section we show altimetric evidence for the southward traveling Kelvin wave, as well as for its impact on the southern subtropical Indian Ocean.

5.3.1 The coastal Kelvin wave

The importance of coastal Kelvin waves for the local dynamics of the Indonesian seas and the throughflow between Pacific and Indian Oceans has been studied by numerical modeling experiments (Sprintall et al., 2000; Qiu et al., 1999), as well as in-situ measurements (Sprintall et al., 2000; Chong et al., 2000).

The model experiments of Qiu et al. (1999) demonstrate the potential influence of the gaps between the Indonesian islands on the southward propagating Kelvin waves. In their reduced gravity model, all Kelvin wave energy enters the Indonesian seas via Lombok Strait, the first open passage in their model topography. In reality, this is the first deep passage, as Sunda strait between Sumatra and Java is less than 25 m deep (see Fig. 5.9 for passage locations). Although the absence of bottom topography may cause their model to overestimate the effect, the Kelvin waves have been observed to enter through Lombok strait (Sprintall et al., 2000). Pressure gauge measurements on the major throughflow passages (Chong et al., 2000) show strong variations of the Indonesian throughflow at annual, semi-annual, and four per year timescales. Especially the geostrophic flow through Lombok strait seems to be dominated by the four-per-year signal, which has the same amplitude as the annual signal. Further south, at Sumba strait, the near four-per-year frequency still dominates the spectrum, although amplitudes are lower. At Savu strait, no semi-annual or four-per-year signal is observed in

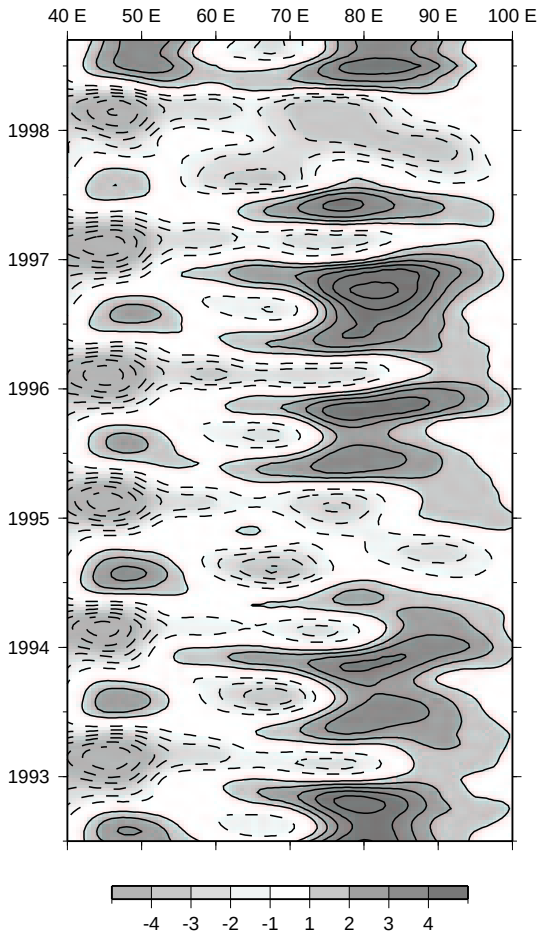

Figure 5.8: *Zonal winds (in m/s, from the NCEP reanalysis (Kalnay et al., 1996)) along the equator over the Indian Ocean. Between 60°and 90°E the semi-annual westerly windbursts occur in June and November. In 1994 and 1997 the autumn windburst is missing: anomalous easterlies prevail, associated with the El Niño and/or Indian Ocean dipole events of those years.*

the geostrophic throughflow (Chong et al., 2000).

In Fig. 5.9 we show 6 consecutive snapshots from the average 90 days cycle in the four-per-year MSSA mode, each 10 days apart. The first plot shows the equatorial Kelvin wave impinging on the western coast of Sumatra, Indonesia. On the two following plots the coastal Kelvin wave is seen to propagate along the coastline, with a speed of approximately 80 km/day. The propagation speed estimated from the altimetry is considerably lower than estimates from tide gauges and other direct observations, which are twice as large (Arief and Murray, 1996; Sprintall et al., 2000). This may be due to the poor sampling time of the altimetric measurements. The waves travel too fast to be completely resolved by the

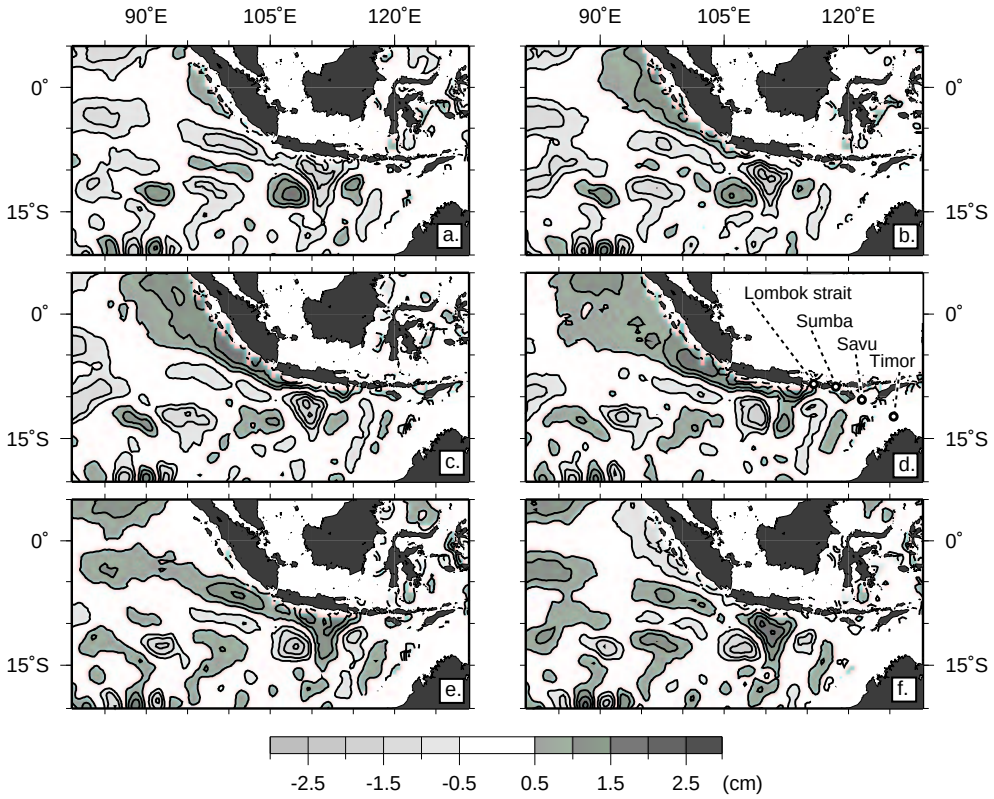

Figure 5.9: *Six snapshots of the coastal Kelvin wave traveling southward along the Indonesian coast, and leaving in westward direction as a Rossby wave. The amplitudes (cm) are unrealistically low, as this is the average 90 days cycle from the MSSA mode. Irregularity of the signal strongly reduces the observed amplitude. In a) an equatorial Kelvin wave reaches the coast of Sumatra. In b.,c.,d. the coastal Kelvin waves propagate southward and northward. In e.-f. the Rossby wave is leaving the coast over its full meridional extent between 10°S and the equator. The Kelvin wave seems to be halted at Lombok strait.*

altimetric observations, and their effect is smeared out over a somewhat larger period. The decrease of the semiannual signal observed by Chong et al. (2000), which also holds for the four-per-year signal (Chong et al., 2000, their Fig. 2), is consistent with our observations, and also with the modeling results of (Qiu et al., 1999). The last three snapshots of Fig. 5.9 show that the along-coast Kelvin wave propagation ends at Lombok strait. The anomaly has by then partly reflected into a Rossby wave, which progresses slowly westward. This effect of Lombok strait, the sudden transformation of Kelvin into Rossby waves, may be achieved by interaction of the Kelvin wave with local bottom topography (the continental slope suddenly deepens considerably), or by interaction with the throughflow through Lombok strait. The strait is one of the main passages for the Indonesian Throughflow, with a mean transport of 2 Sv, and an annual cycle of the same amplitude (Arief and Murray, 1996).

5.3.2 Rossby waves across the subtropical gyre

The region south of 10°S exhibits westward propagating signals at various timescales. At 10°S, variability is dominated by the annual signal. Périgaud and Delecluse (1992) already observed this signal in the 1987/1988 Geosat altimeter data, and showed a connection to windforcing east of 100°E. The spatial distribution of the amplitude of the annual SSH signal, with a maximum in the open ocean near 70°E, away from the regions with strongest forcing, was explained by Wang et al. (2001) to be caused by the interaction of local Ekman pumping and remotely forced Rossby waves: the westward propagating Rossby wave signal is cancelled out by local vorticity production by the seasonal winds, thus producing a so-called shadow zone where the effect of the annual cycle is seemingly small in spite of strong annual forcing. This can also be observed in Fig. 5.12, as the annual Rossby wave appears to propagate no further westward than roughly 90°E.

Birol and Morrow (2001) have made a comparison between the influence of wind forcing and eastern boundary processes on the Rossby wave activity in the southern Indian Ocean. They find the semi-annual variability between 20°and 30°S to be controlled by eastern boundary processes. Here we show indications that around 12°S, and also further south between 20°and 30°S, a significant Rossby wave signal at higher frequencies is also present, and that it is consistent with the equatorial wave forcing at the eastern boundary.

To explore the existence in the subtropical gyre of signals with frequencies higher than semi-annual , we have analysed the SSH variability at two locations in mid-ocean. One location (80E,12S) in the zonal band between 10°and 15°S, which is known to be dominated by annual waves (Périgaud and Delecluse, 1992), the other one at (80E,20S) in the southern band of variability, known for its predominantly semi-annual variability (Morrow and Birol, 1998). These locations were chosen not to be too close to the 90°E ridge, which influences the propagation of Rossby waves. In Fig. 5.10a the complete SSH signal of the northern location is plotted, as well as the low-pass filtered version. Fig. 5.10b shows the high-pass residuals. A clear semiannual signal is present but also higher frequency anomalies with amplitudes in the order of 5-10 cm (Fig. 5.10b). The spectrum of the complete signal (Fig. 5.10c) shows the dominant annual and semiannual frequencies, but also a rather broad maximum centered at 4 cycles per year. Clearly, the contribution of this signal is small (as was also concluded from Fig. 5.1), as the annual and semiannual signals dominate the spectrum, but its presence is clear. The same procedure was applied at the more southern location (Fig. 5.11). It shows similar high frequency SSH variability, with amplitudes of 5-10 cm. The main difference is that at this location the spectrum is less dominated by annual and semi-annual signals.

The propagation of the observed SSH anomalies is analyzed over a zonal band along 12°S, between 40°and 120°E. SSH anomalies are averaged over a meridional strip between 13°and 11°S. This signal is split into a low frequency part and a high frequency part, again using the 400 days cosine weighted running mean. The low frequency signal (Fig. 5.12) shows the annually propagating wave between 120°E and 90°E, and the dipole pattern of the Indian Ocean Dipole, with large positives between Madagascar and the 90°E Ridge near the end of 1994 and 1997, and negative phases in 1996 and 2000 (Webster et al., 1999; Saji et al., 1999). The high frequency signal, plotted in Fig. 5.13a. shows that on top of this, there are also Rossby waves propagating at this latitude band. Part of the (attenuated) annual signal is still visible, as well as semi-annual Rossby waves. But also at the higher frequencies Rossby

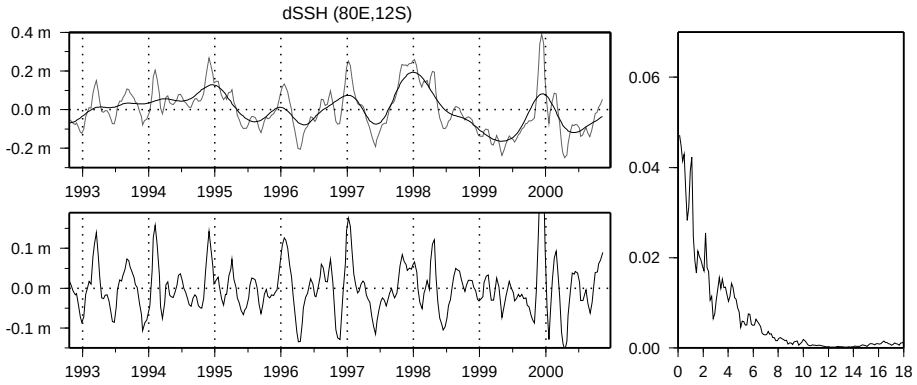

Figure 5.10: *The SSH signal at (80°E,12°S) (thin line in a.) is decomposed into a low-frequency part (thick line in a.), and a high frequency part (b.) which has considerable amplitude, clearly not only on the semi-annual frequency. (c.) Spectrum of the complete signal (the dotted line in a.). the frequencies along the horizontal axis are plotted in cycles per year.*

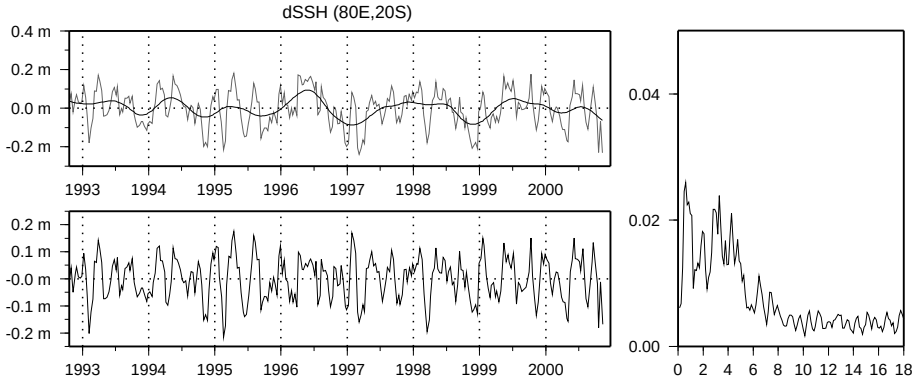

Figure 5.11: *As Fig. 5.10, but now for (80°E,20°S).*

wave propagation is observed. About four Rossby waves per year cross the basin. East of 60°E, consistent propagation is clear. The Mascarene ridge around 60°E disrupts the Rossby wave propagation (as is also suggested by Fig. 5.1), but also between the ridge and the Island of Madagascar at 50°E propagating waves can be observed. The 90°East Ridge seems to cause only a small distortion to the propagating waves. Between the tip of Madagascar and the African continent, also westward propagating waves are visible, but their frequency is higher, due to the barotropic instability of the South Equatorial current with a period of about 55 days (Schott et al., 1988).

The westward propagation speed of the Rossby waves is estimated from the slope of the isolines in Fig. 5.13 to be 19 km/day. This is in good agreement with estimates from the modified Rossby wave propagation theory presented by Killworth et al. (1997). The effect of vertical velocity shear they include in their Rossby wave propagation theory is particu-

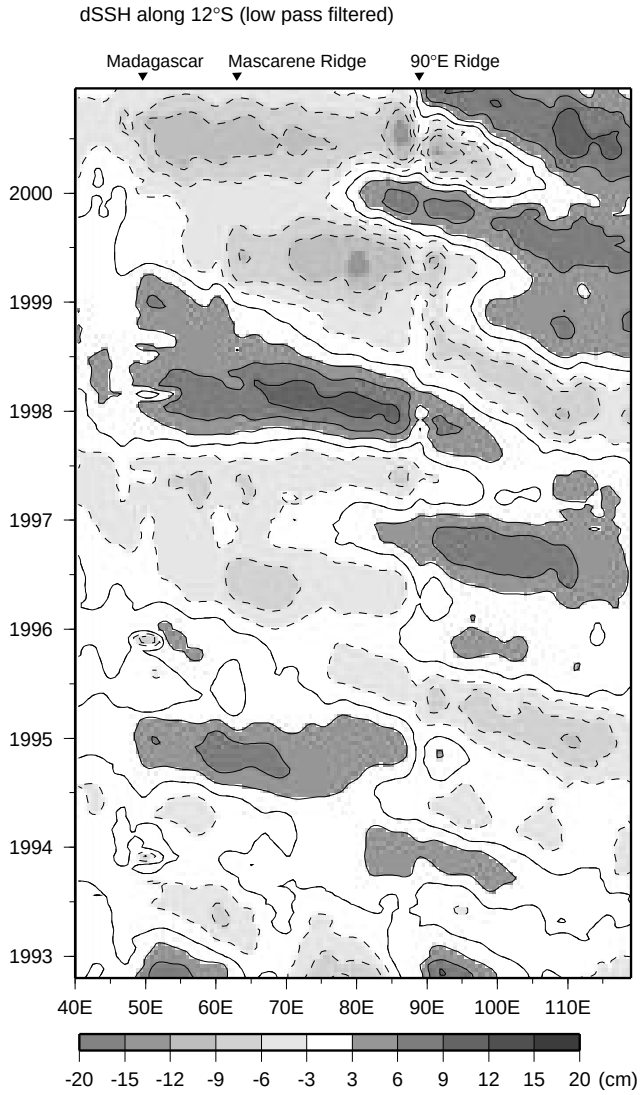

Figure 5.12: *Space-time diagram of SSH along the 12°S parallel. The low frequency part of the signal shows mainly annual and interannual variability and is dominated by the two large Indian Ocean Dipole or El Niño/Southern Oscillation events of 1994 and 1997, and annual Rossby wave propagation east of 90°E. The locations of Madagascar, the Mascarene Ridge, and the 90°E Ridge are indicated along the top.*

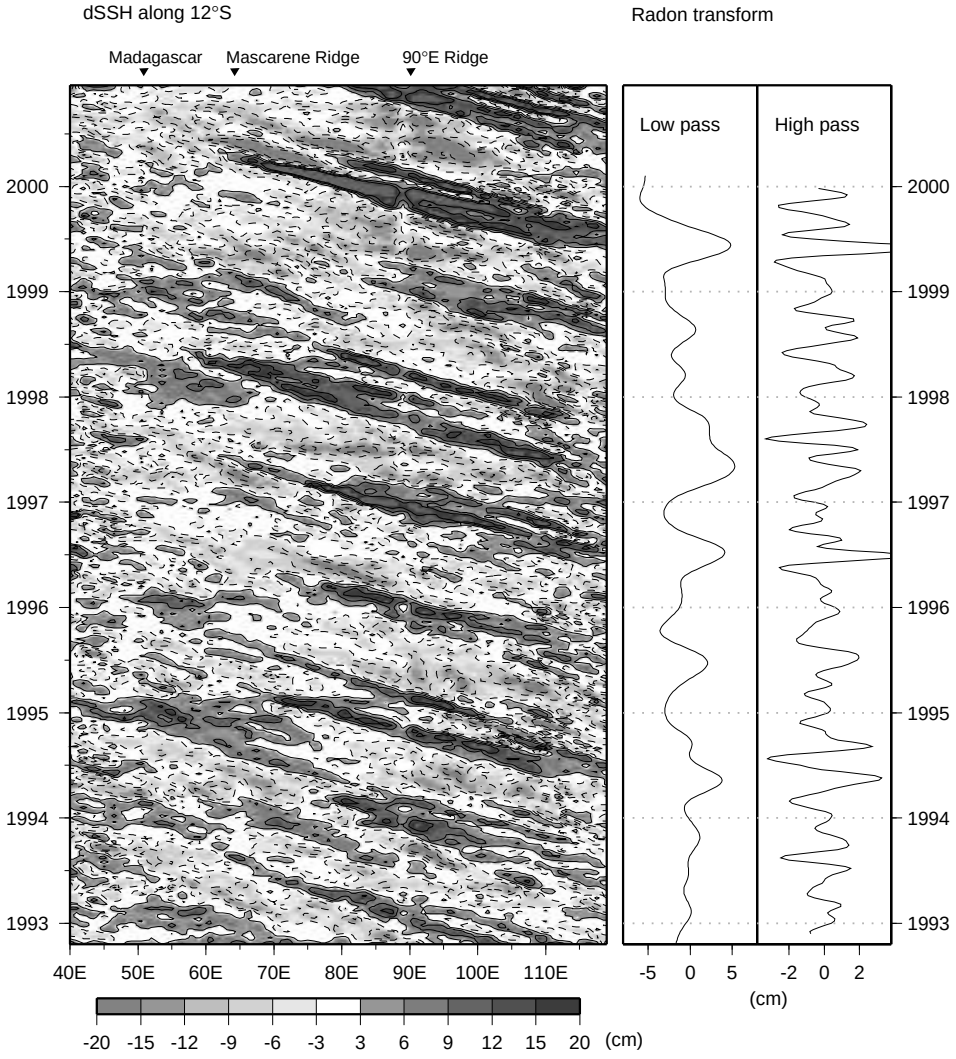

Figure 5.13: *(left) The high frequency part of the time-space diagram of SSH along 12°S (see Fig. 5.12). (right) Radon transform of the signal on the left. A, realistic, Rossby wave propagation speed of 19 km/day is derived from the left hand panel to define the direction of the transform. The Radon transformed signal is again filtered in a low frequency part (showing mainly annual and semi-annual signals) and a high frequency part (showing about four Rossby waves per year). The three main topographic obstacles along the 12°S latitude (Madagascar, the Mascarene Ridge and the 90°East Ridge) are indicated at the top of the left panel.*

larly important in this part of the world ocean. The propagation speed of baroclinic Rossby waves is almost doubled by this effect with respect to the standard propagation speeds for propagation through the β induced background potential vorticity gradient.

To have an objective measure of the Rossby wave signal, which can then be compared to the incoming forcing signal from the Indonesian coastal Kelvin wave, we have computed the Radon transform of the sea-surface height anomalies along 12S. The transform is the average SSH along a characteristic (in this case linear) propagation path through time and space. The waves propagate between longitudes x_0 and x_1, with characteristic speed c:

$$R(t) = \frac{1}{x_1 - x_0} \int_{x_0}^{x_1} h(x, t + \frac{(x_1 - x_0)}{c}) dx,$$

where h(x,t) denotes SSH at longitude x along 12°S, and R(t) is the radon transform. Formulated this way, the Radon transform shows the amplitude of the Rossby wave starting at x_0 at time t. In our case of the 12°S parallel, we take x_0 at 115°E, where the waves seem to be triggered by the coastal Kelvin waves, and x_1 to be 50°E, the northern tip of Madagascar. (The region thus also includes the disrupting signal west of the Mascarene ridge, where Fig. 5.12 shows that linear propagation along the 12°S parallel is a questionable assumption.)m

The timeseries of the transform is plotted next to the space-time diagram in Fig. 5.13. It has been split into a low-pass and a high-pass component. There is a significant correlation of 0.4 at a lag of 10 days between the high-pass component and the Kelvin-wave arrival time series shown in 5.6, if we consider the Rossby wave to be forced at 115°E. This corresponds to a propagation speed for the propagation of the coastal Kelvin wave more realistic than what we derived from the MSSA analysis shown in Fig. 5.9. The lag of 10 days corresponds to a propagation of about 200 km/day, if the time series of Fig. 5.6 is taken as the moment the Kelvin wave hits Indonesia. Close inspection of Fig. 5.4a shows that this is not fully the case, as the Kelvin wave is already propagating along the coast, rendering a somewhat lower Kelvin wave propagation speed.

5.4 Impact on the upstream Agulhas and interbasin exchange

5.4.1 Connection to the Mozambique Channel

Pedlosky (2000) showed that the main factor determining the transmission of waves 'through' an island, is in the integral constraint on the islands' streamfunction. Basically, the demand of pressure continuity around the island gives that just one streamfunction value can exist at the island. In a closed basin, this is also the total flow around the island. In the case of Madagascar, this is not directly applicable, as the Indonesian Throughflow provides an extra source which has to leave the Indian Ocean basin, without taking part in the circulation around the island. However, this does not affect the applicability of the results of Pedlosky (2000) to our case. An incoming Rossby wave pattern should fit within this boundary condition on the island, to produce a resultant wave on the western side of the Island. The sea-surface height anomalies, acting as a streamfunction anomaly for the upper layer geostrophic current, have to be in phase at the northern and southern extrema of the island. In that case, communication

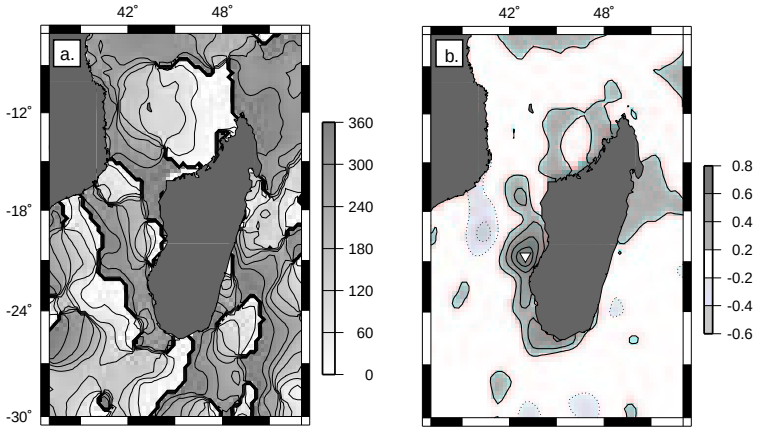

Figure 5.14: *Rossby waves seem to propagate west of Madagascar. For the four per year Fourier coefficient, the incoming SSH field from the east seems to satisfy the conditions needed for Rossby wave generation in the Channel. a) shows the phase (in degrees) of the 4-per-year harmonic of SSH anomalies around Madagascar. The distance between two contour lines, 30 degrees, corresponds to a time lag of 15 days. The point-correlation in (b.) shows that over most of the eastern part of the channel, the SSH anomalies are significantly correlated. (the correlation with the location indicated by the white triangle is plotted.)*

by coastal Kelvin waves will not lead to a destructive interference, but to the forcing of a Rossby wave within the Channel. The direct correspondence with the theoretical studies (Pedlosky, 2000; Pedlosky and Spall, 1999) may be nontrivial, as we are dealing with a dispersive wave field impinging on the island, and not with a beta plane.

The phase of the four-per-year harmonic of SSH anomalies in the region around Madagascar, as shown in Fig. 5.14a suggests that the theoretical framework for the interaction of Rossby waves and an island (Pedlosky, 2000) applies to this case. The four-per-year cycle seems to be in phase at the northern (Cape Amber) and southern extrema (Cape Ste Marie) of the island (zero contour in Fig. 5.14a), as well as in the middle of its western coast, consistent with the theoretically expected formation of a Rossby wave in the Channel. From there on, propagation of the waves in southwestward direction is suggested by the phase-lines. This is further confirmed by the point-correlation plot in Fig. 5.14b, showing the correlation of the high-pass filtered SSH anomalies with a single point at (43°E,23.5°S) near Madagascar (the white triangle in Fig. 5.14b) . Most of the region along the west coast of the island and the central Mozambique Channel, south of 15°S, are highly correlated.

Besides the transmission of the Rossby waves through the island, a second important feature of the theoretical framework (Pedlosky and Spall, 1999) is the value of the stream-function on the island, which denotes the total flow through the Mozambique Channel. This flow should thus be modulated at the frequency of the incoming Rossby waves. A recent

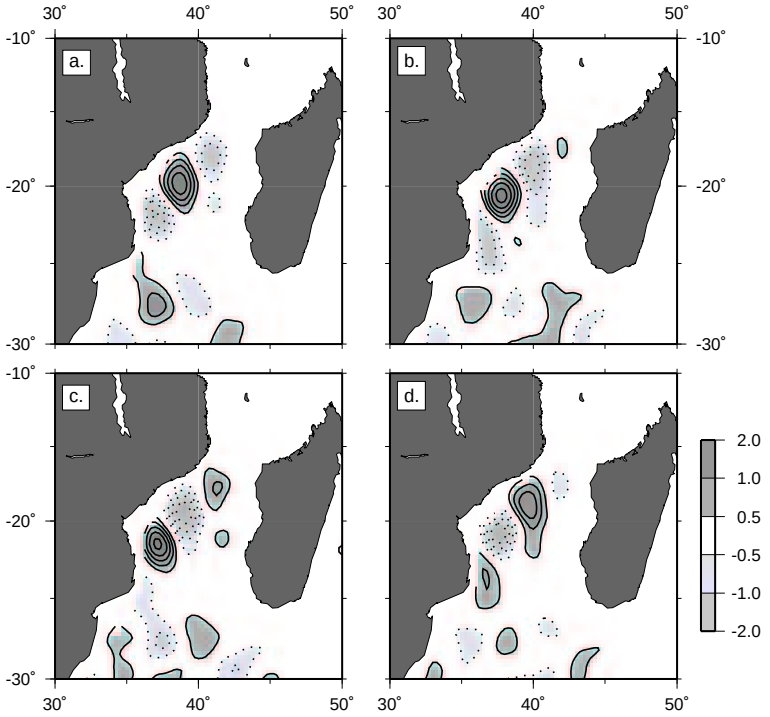

Figure 5.15: *Four phases in the mean cycle of the 90-days reconstructed MSSA mode in the Mozambique Channel, each 20 days apart. Amplitudes are given in cm. Mozambique Eddies are being formed in the Channel just south of the narrow section at 16°S, and propagate southward.*

research cruise in the channel has shown that the flow through the Mozambique Channel is dominated by southward propagating eddies, rather than a continuous western boundary current (De Ruijter et al., 2002). Satellite altimeter observations show that the frequency of eddy generation and propagation is also about four per year.

The four-per-year MSSA mode in the Mozambique Channel (Fig. 5.15) shows west-southwestward propagation of anomalies . As also observed by Biastoch and Krauss (1999) and Schouten et al. (2002b), this may be a combination of a Rossby wave and southwestward propagation of eddies. The amplitudes in this figure are again strongly reduced due to the irregularity of the signal. In reality, the eddies have SSH signatures of several decimeters. They have surface velocities of up to 2 m/s and reach all the way to the bottom at over 2500 m depth (De Ruijter et al., 2002).

To investigate the nature of the irregularity of the eddy generation in the Mozambique Channel, we have used the same correlation technique as applied earlier in the equatorial band. We have computed the spatial correlation of the TOPEX/Poseidon measurements over the complete period of observation (1992-2000) and the snapshot from the average 90-days

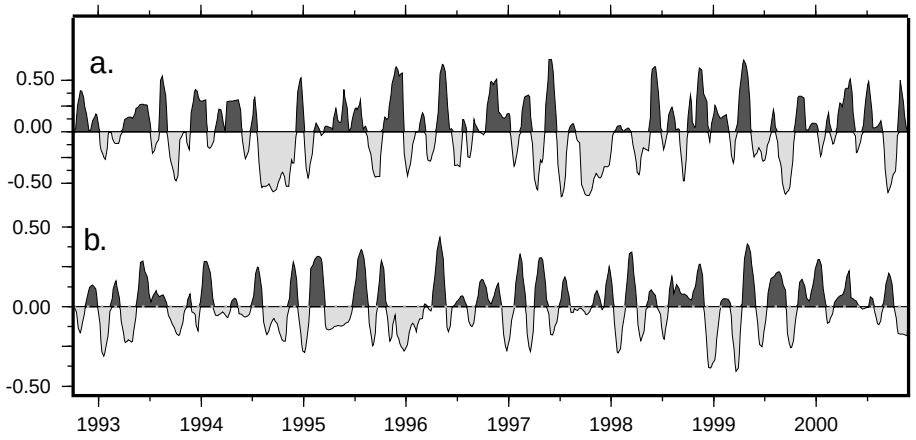

Figure 5.16: *Two time series, showing irregularities in the forcing and forced signals observed in the Mozambique Channel. (a.) timeseries of the equatorial Kelvin wave, arriving at Indonesia (same as Fig. 5.6; (b.) time series of the formation of Mozambique eddies. See the text for discussions of these quantities.*

cycle shown in Fig. 5.15a. The resulting timeseries is shown in Fig. 5.16b.

The pattern of Fig. 5.15a was selected for the computation of the correlation because in that phase of the 90-days cycle, a new eddy is generated in the Mozambique Channel. The SSH anomaly is positive all along the coast of Madagascar (the zero contour line is not shown), associated with a maximum in southward geostrophic transport through the channel. The lagged correlation between the timeseries denoting the arrival of an equatorial Kelvin wave at the Indonesian coast (Fig. 5.16a), and the birth of a new Mozambique eddy (Fig. 5.16b) shows a clear peak at 1.25 years (Fig. 5.17). The correlation of 0.35 is significant a the 99 % confidence level. This lag is consistent with several weeks travel time of a coastal Kelvin wave along the Indonesian coast, and 1.1 years needed by a first mode baroclinic Rossby wave to cross the Indian Ocean at 12°S..

This consistency between statistical and dynamical time lag strongly supports the evidence for a dynamic link between the equatorial Kelvin waves, and the formation of eddies in the Mozambique Channel at the frequency of four per year. Moreover, if such a dynamic link is real, then also the large equatorial anomalies, associated with the major Indian Ocean Dipole/ENSO events of th 90s, should propagate to the Mozambique Channel. That is indeed what Fig. 5.16 reveals: both events, in 1994 and 1997, are clearly visible as anomalously long periods of no Kelvin wave arrival at Sumatra (Fig. 5.16a), consistent with anomalous easterlies over those periods in the eastern equatorial region. The IOD-anomalies propagate across the basin. At a lag of 1.25 years a gap also appears in the formation of Mozambique eddies (Fig. 5.16b).

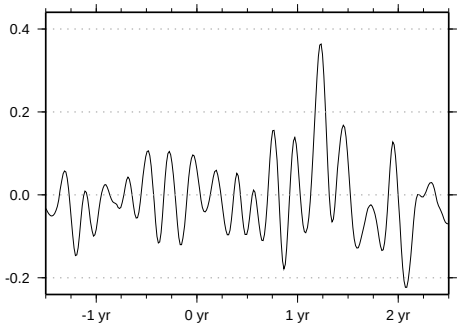

Figure 5.17: *Lagged correlation between the equatorially forced Kelvin wave near Indonesia (Fig. 5.16a), and the Mozambique eddy-shedding timeseries (Fig. 5.16b). The significant correlation after 1.25 years is consistent with the travel time of the signal by coastal Kelvin waves and baroclinic Rossby waves along 12°S.*

5.4.2 Connection to Agulhas ring shedding

Based on their frequency of four per year, the Mozambique eddies carry about 15 Sv of surface, thermocline and intermediate waters southward into the Agulhas region (De Ruijter et al., 2002). Besides a direct impact by their transportation of relatively warm and saline Indian Ocean waters southward, the eddies also have a dynamical impact on the Agulhas system. They seem to control the timing and frequency of Agulhas ring shedding (Schouten et al., 2002b). As mentioned earlier, this is partly achieved by the triggering of growing cyclonic meanders in the upstream Agulhas, followed by the formation of Agulhas Rings almost half a year later (Van Leeuwen et al., 2000). Moreover, the rings seem to provide the preferred locations for early retroflection of the Agulhas, thereby controlling the timing of ring shedding events (Schouten et al., 2002b, for details). In Fig. 5.18 a time-space diagram is shown, obtained from through a reconstruction of the first four MSSA modes of high-pass filtered SSH anomalies. The Mozambique eddies can be followed southward through the Mozambique Channel (i-ii in Fig. 5.18, and along the offshore edge of the Agulhas current (ii-iii). The timing of the incoming eddies from the Mozambique Channel seems to be related to the east-west movement of the retroflection around 22°E (iii-iv). The latter movement is associated to the shedding of Agulhas Rings that drift into the South Atlantic (Lutjeharms and Van Ballegooyen, 1988).

5.5 Summary and discussion

In this chapter we have shown evidence for a link between the equatorial waveguide and the subtropical region of the South Indian Ocean. Kelvin waves from the equatorial Indian Ocean are observed to reach Indonesia, propagate southward as coastal Kelvin waves, and initiate Rossby waves at midlatitudes. These Rossby waves can then be observed to cross

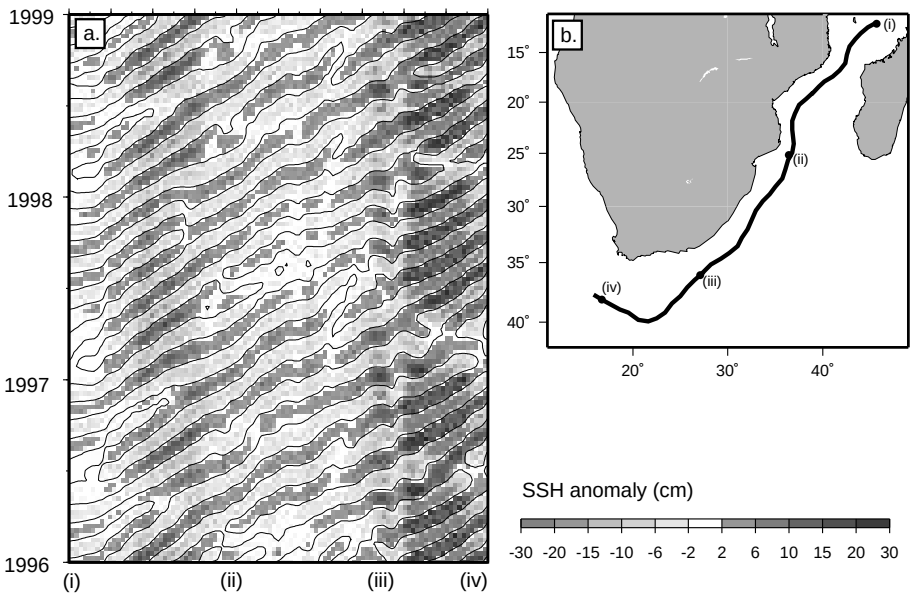

Figure 5.18: *(a) SSH anomalies from the first four modes of an MSSA analysis on high-pass filtered data are plotted along a track trough the Mozambique Channel, and south along the offshore edge of the Agulhas current (the track is plotted in (b), and goes through the main axis of variability) . Four locations along the path are indicated by letters, which correspond to those below the space-time diagram in (a.). Between iii. and iv., the positive anomalies plotted are no longer the Mozambique eddies themselves, but the retroflection loop of the Agulhas current.*

the Indian Ocean, and arrive at Madagascar little over a year later. We have shown a statistically significant correlation between the shedding of eddies in the Mozambique Channel, and the timeseries of Kelvin wave arrival at Indonesia. The time lag of this correlation is consistent with the travel times of the waves mentioned above, suggesting a dynamical link. The Mozambique Eddies have been shown to propagate southward and to be closely related to the east-west movement of the Agulhas retroflection once they have reached the tip of the African continent.

However, a number of issues is still unclear. First, the generation of the four per year cycle in the equatorial band is not clear. This will be discussed below. Second, the mechanisms by which the coastal Kelvin waves initiate Rossby waves along the latitudes between 10°and 15°S has remained unclear. The roles of the Pacific-Indian Ocean throughflow, bottom topography, and possibly local eddy formation (Bray et al., 1997) are left for future study. Third, the four per year cycle shows up prominently in the central part of the subtropical gyre (in a band of variability centered at 20 °S (see Fig. 5.1 and 5.11). In this discussion, we will show the Rossby wave nature of these anomalies. Their role in the large scale picture is not clear yet. Finally, the interplay of Rossby waves, mean currents and topography (both bottom topography and continental geometry) resulting in the formation of Mozambique eddies is another link in the chain of events presented in this chapter which needs further study.

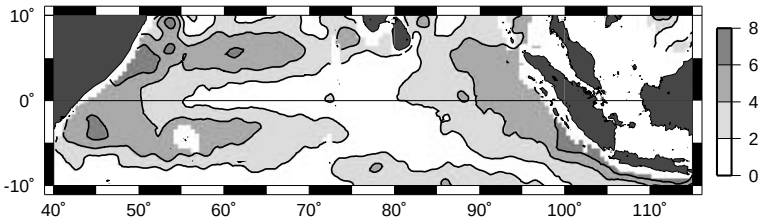

Figure 5.19: *The amplitude of the semiannual harmonic (in cm), fit to six years of altimetric data (1995-2000).*

5.5.1 The semi-annual cycle at the equator

The semiannual cycle is an important constituent of variability over the equatorial Indian Ocean (Fig. 5.19). The variability is concentrated in the western part of the basin and along the eastern boundary, with mean amplitudes over 5 cm. The signal in the western part of the basin may be associated with the semi-annual adjustment to the monsoon regimes.

The eastern boundary is forced by a semiannual equatorial Kelvin wave that propagates eastward in April/May and September/October (Clarke and Liu, 1993), after the switches of the monsoons, and enforced by the semiannual westerly windbursts occurring in April/May and October/November over the central equatorial Indian Ocean. These semiannual westerly windburst are thought to be the main contributors to the oceanic equatorial jets known as Wyrtky Jets in Spring and Fall (Han et al., 1999). Observations of semiannual eastward jets with Kelvin wave characteristics in the western part of the equatorial band (Luyten et al., 1980) -where no semiannual direct windforcing is observed- suggest that also reflection of equatorial Rossby waves plays a role in the buildup of the equatorial jets. This role is confirmed by modelling (Visbeck and Schott, 1992) and observational (Le Blanc and Boulanger, 2001) studies. Also, the equatorial basin modes (Cane and Moore, 1981), used to explain the strength of the semi-annual oceanic response (Clarke and Liu, 1993; Han et al., 1999) requires the reflection of Rossby waves into Kelvin waves at the western boundary. The main observational characteristics of the semi-annual SSH variability are present in a couple of MSSA components for the equatorial Indian Ocean region that form an oscillatory pair, and clearly stand above the red noise null hypothesis (Fig. 5.5). Monthly plots of this semi-annual MSSA mode are shown in Fig. 5.20.

In February and August, anomalies develop in the western half of the basin, and propagate westward. In April/October we see the result of the equatorial Kelvin wave traveling eastward and reaching the coast of Sumatra within six weeks after its generation. By May/November these waves have resulted in coastal Kelvin waves travelling in north- and southward direction, and a reflected Rossby wave propagating westward, as expected from long equatorial wave theory (Cane, 1979; Gill, 1982).

Surprisingly, the semiannual MSSA mode does not show the westward propagation of the Rossby waves through the eastern part of the equatorial basin. This appears to be captured by the four-per-year MSSA mode, of which monthly plots have been shown in Fig. 5.4. This

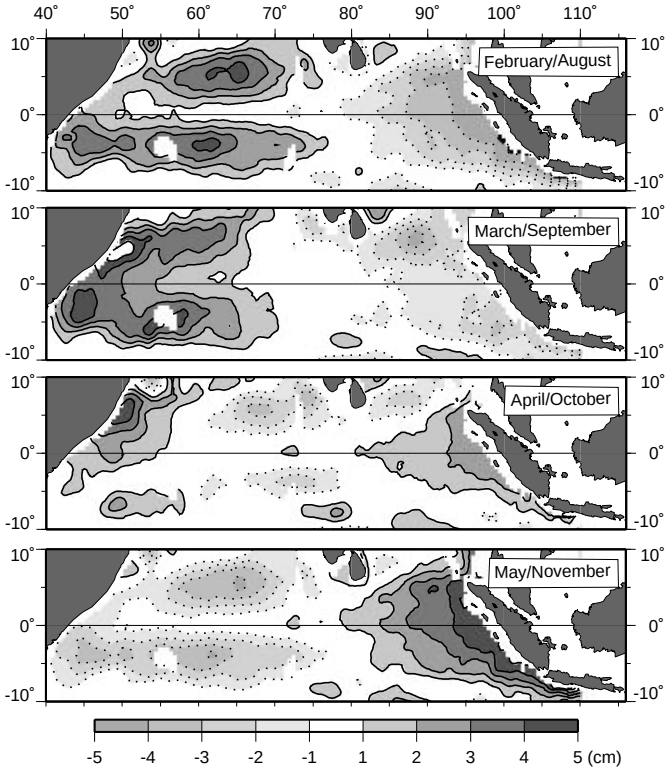

Figure 5.20: *Four steps in the semi-annual mode of SSH variability. Solid (dotted) contours denote positive (negative) anomalies. In February/August Rossby waves are generated in the western half of the basin. In March/September these waves have propagated to the African coast, where they reflect as equatorially trapped Kelvin waves. These cross the basin at the equator, and reach the Indonesian coast within six weeks (April/October), consistent with the propagation properties computed by Clarke and Liu, [1993]. In May/November there is a clear build-up of water against, and propagating along, the Indonesian coast.*

suggests that not just the semi-annual cycle is forcing equatorial Kelvin waves that reach the Indonesian coast, but that there are also other processes that cause the higher frequency of the Kelvin wave signal and its reflected Rossby waves in the eastern half of the equatorial basin. As the origins of these waves seems not to be in direct wind forcing, reflection of the semi-annual Rossby waves against the Maldives ridge could provide the frequency doubling mechanism. The Maldives form a chain of numerous small islands and atolls between the equator and roughly 10°N. As the first mode Rossby wave has its amplitude maximum SSH anomaly near 3°N and S, the northern limb is largely blocked. However, analytical estimates by Cane and Moore (1981) give a minor effect of the ridge on the propagation of the Rossby waves. Han et al. (1999) find a negative effect of the ridge on the strength of the semi-annual cycle, most likely caused by reduced resonance of the semi-annual equatorial basin mode in

their model.

5.5.2 Interbasin exchange

Paleoclimatic observations provide evidence for a fast coupling of North Atlantic Climate variability to that over the Indian Ocean, on century (Verschuren et al., 2000), millennia (Zonneveld et al., 1997; Van Campo et al., 1987) and Milankovitch time scales (Beaufort et al., 1997; Cayre et al., 1999). Three mechanisms have been proposed to explain these connections: changes of the global thermohaline circulation, of the atmospheric circulation patterns over the northern hemisphere, and variations in ice/snow coverage of Central Asia and Tibet. All three mechanisms are used to describe how the glacial/interglacial periods over the North Atlantic sector may have modified the climatic boundary conditions of the Indian Ocean. Most observations suggest weaker monsoon activity over the equatorial Indian Ocean region during glacial periods, and strong intensification of (southwest) monsoon activity during deglaciation and interglacial periods (Zonneveld et al., 1997; Marcantonio et al., 2001). On the other hand, Cayre et al. (1999) find enhanced primary production in the central equatorial Indian Ocean during glacial periods, which is attributed to stronger equatorial winds, inducing upwelling near the Maldives. Also, Verschuren et al. (2000) show how colder episodes in more recent history (the past 2000 years) were accompanied by periods of enhanced precipitation over equatorial eastern Africa. A link to the thermohaline circulation was suggested by Berger and Wefer (1996). They used observations of tropical foraminifera (*Globorotalia menardii*). This species was not found in the Atlantic Ocean during the last glacial maximum, but was reintroduced during the deglaciation, likely from the Indian Ocean, where the species is observed in records from the glacial period. This suggests a temporary breakdown of the interbasin exchange south of Africa during the last glacial maximum, and a restart of Agulhas leakage during deglaciation. Zonneveld et al. (1997) state that this theory is unlikely, as sea-surface temperature reconstructions for the southwest Indian Ocean show lower temperatures during the glacial periods (Van Campo et al., 1987), which would not be an indication of less outflow of tropical (warm) water.

The tropical-subtropical link presented in this chapter suggests a new way to interpret the paleoclimatological data that show connections between the Indian Ocean Monsoon regime and the climate fluctuations over the North Atlantic regions. The Indian Ocean may not just have its boundary conditions set by the climatic fluctuations over the North Atlantic, but may also play an active role in the generation of those fluctuations. Via control of the interbasin leakage from the Indian to the Atlantic Oceans, anomalies in the equatorial wind systems over the Indian Ocean may, when these anomalous conditions last for several years or decades, modify the overturning characteristics of the Atlantic (Weijer et al., 1999), and thereby influence climate conditions over the North Atlantic Region. Combined with the response of the winds over the Indian Ocean to North Atlantic climate fluctuations (such as changes in snow/ice coverage over the Asian continent) this may form a destabilising feedback mechanism favoring transitions between glacial and interglacial periods. An explanation for the seeming contradiction between suggested interbasin leakage fluctuations, increasing SST values in the Mozambique Channel measured during the last deglaciation period and lower SST values in the central Mozambique Channel (Van Campo et al., 1987) during glacial periods, may be the manifestation of the absence of Mozambique eddies, with reduced transport of

warm tropical waters southward through the Mozambique Channel. The anomalous behavior of the Agulhas current during much of the year 2000 (early retroflection of the Agulhas in an extremely eastern position, no shedding of Agulhas Rings, less eddies in the Mozambique Channel, combined with stronger westward transport southwest of Madagascar) may have given us a glimpse of the conditions during the last glacial maximum.

Chapter 6

Modification of Rossby waves across the subtropical gyre

6.1 Introduction

In chapter 5, a description has been given of the connection between wind variations over the equatorial Indian Ocean system, and the shedding of Agulhas Rings. This description contains several unresolved issues. One of these is the prominence of the four per year cycle in the southern part of the subtropical gyre. A direct link between the equatorial dynamics and the Mozambique Channel was suggested to be formed by Rossby waves along the more northern route around 12°S. However, also the band of variability south of 20°S was shown to exhibit strong variability at the intraseasonal timescales, particularly the four per year frequency (Fig. 5.1). Another issue not solved in the preceding chapter was the interplay of the waves with the topography and background current systems around Madagascar. A relation between Rossby waves coming in from the east and the formation and propagation of Mozambique Channel Eddies was shown statistically, but the dynamics remained unclear. Based on these observations, the main questions addressed in this chapter are:

- What causes the variability at intraseasonal timescale south of 20°S? In relation to this question, we investigate why there is so little of this signal around 15°S, and why there seems to be an intensification of the signal near 60°E.
- Can we explain the weakening of the four per year signal at the Mascarene Ridge?

This chapter is organized as follows. In 6.2 we investigate the intraseasonal Rossby waves that cross the subtropical gyre. Observations are presented showing the Rossby wave nature of the two bands of variability (Fig. 5.1). Theory on the propagation of Rossby waves through a background current field is combined with hydrographic data to explain the meridional structure of the variability (the two bands of Fig. 5.1). In 6.3 the transfer of energy from the northern to the southern band is investigated. Model results show how this may be accomplished, and what may cause the weakening of the four per year signal west of the topography of the 90°East Ridge, the Mascarene Ridge and Madagascar itself. In 6.4 the

interaction of the Rossby waves with the island and local current characteristics is studied by use of altimetric observations, assisted by current meter measurements. The results of this chapter are summarized and discussed in 6.5.

6.2 Rossby waves in the subtropical gyre

We suggested an explanation for the lag of 1.25 years (Fig. 5.17) between the generation of a coastal Kelvin wave along the Indonesian coast by the splitting of an equatorial Kelvin wave and the birth of an anticyclonic eddy in the Mozambique Channel by the time it takes for a Rossby wave to propagate through the northern band of enhanced variability (Fig. 5.1). This signal appears to be strongly attenuated west of the Mascarene Ridge. The bottom topography of the southern Indian Ocean is shown in Fig6.1. The southern band of variability does not show this attenuation, so it is likely that this band also plays a role in the information transfer. This has motivated us to study the nature of this band of variability.

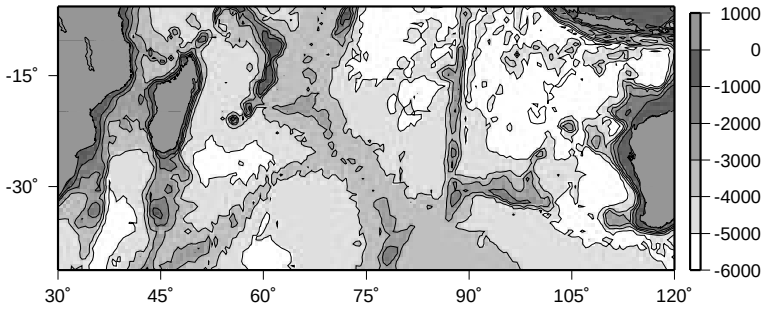

Figure 6.1: *Bathymetry of the southern Indian Ocean. Topographic features mentioned in this chapter are Madagascar (at 45°E), the Mascarene Ridge (60°E), and the 90°E Ridge.*

The altimeter data in chapter 5 showed Rossby wave propagation through the subtropical gyre. Modes 7/8 of a MSSA analysis of the southern Indian Ocean form an oscillatory pair with a period of 90 days. Its amplitude is plotted in Fig. 6.2, and a snapshot of its reconstructed component (i.e. the reconstructed field for a certain date, based on only the two MSSA components that form the 90 days periodic signal) shows a regular 'train' of anomalies propagating westward between roughly 90°E and Madagascar (Fig. 6.3).

The realistic nature of these altimetrically derived Rossby waves in the South Indian Ocean is further confirmed by in-situ measurements of the upper ocean thermal structure by Expendable Bathythermographs (XBT's). These are employed by voluntary observing ships, and thus mainly confined to commercial shipping routes in this region. The XBT's measure most of the upper kilometer of the ocean, thereby reaching well below the thermocline. We show an XBT track between Perth (Australia) at (32°S,117°E) and Mauritius (20°S,57°E), which crosses most of the subtropical gyre (Fig. 6.4). The XBT data were obtained from the Global Temperature-Salinity Profile Program (GTSPP) Database (http://www.nodc.noaa.gov/GTSPP/gtspp-home.html). The lower panel of Fig. 6.4 shows the observed temperature field in the upper 850m. Depth variations in the isotherms appear all over

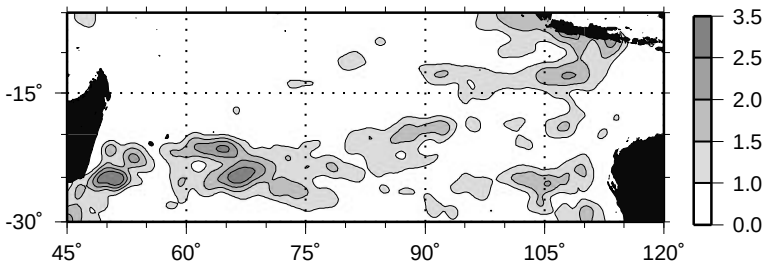

Figure 6.2: *Sea surface variability (in cm) represented by two MSSA components that form an oscillatory MSSA mode with a period of 90 days. Amplitudes are relatively low because of the irregularity of the signal (see also chapter 5).*

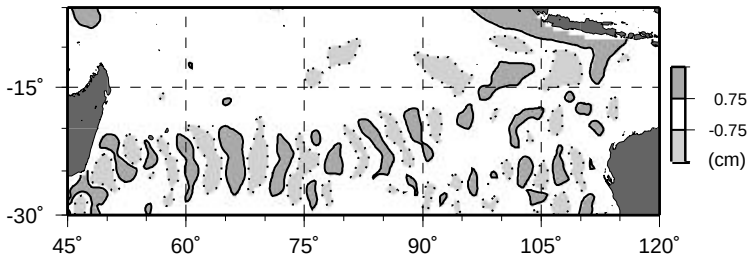

Figure 6.3: *A snapshot from the reconstructed component of the 4-per-year MSSA mode of SSH anomalies.*

this depth range, and mirror the altimetrically observed SSH anomalies from the upper panel.

The fact that the amplitude of the waves is still considerable in the temperature signal below the thermocline, is in good agreement with a first baroclinic Rossby wave mode. We have computed the first baroclinic mode for the stratification observed at a World Ocean Circulation (WOCE) CTD station at (80°E,20°S). The vertical structure of the amplitude of the horizontal velocities is plotted in Fig. 6.5 (dotted line). Assuming a temperature dominated linear equation of state, which is not unreasonable for the depth-range we are looking at (100-800 m), we can take the slope of the isotherms,

$$\alpha = \frac{\partial T/\partial x}{\partial T/\partial z},$$

as a measure for the slope of the isopycnals, and thus for the vertical shear of the horizontal velocities. The velocity shear profile averaged over the XBT-section in Fig. 6.4 is shown in Fig. 6.5. Both lines have been normalized with their 250m depth value. Below the thermocline (at 250 m), the decreasing amplitude of the observed velocity profile agrees reasonably well with the decrease of the first baroclinic Rossby mode. However, the relatively small amplitude above the thermocline suggests that there may be a contribution by the second vertical mode, which changes sign at the thermocline (250m). Another effect that may explain part of

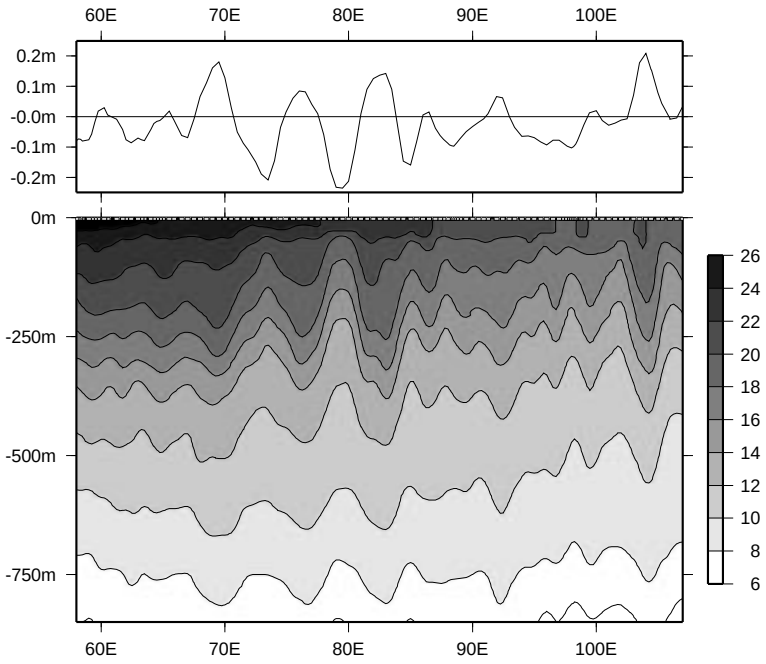

Figure 6.4: *XBT temperature measurements made in December 1995 between Mauritius (20°S,57°E) and Perth (32°S,117°E). In the upper panel the sea-surface height anomalies are shown. Anomalous SSH-elevations and the vertical excursions of the isotherms are strongly correlated.*

the difference between the two profiles is the effect of salinity. The South Indian Ocean south of 15°S is characterized by a strong subsurface salinity maximum. This maximum (for the WOCE station used it is located around 220 m depth) implies steeper (less steep) isopycnals than isotherms below (above) the salinity maximum. The velocities above the thermocline are therefore slightly underestimated, whereas those below it are overestimated. To conclude, the altimetrically observed westward propagating anomalies have a vertical structure that seems to be consistent with that of a first mode baroclinic Rossby wave.

6.3 Why are there two separate bands of variability?

As shown in chapters 4,5 and above, the variability of SSH in the two zonal bands crossing the subtropical gyre (Fig. 5.1) is most likely related to baroclinic Rossby waves that propagate westward. A question is why there are two bands of variability, separated by a low energy band roughly between 15°and 20°S. Also: why is the observed four per year signal intensified near 60°E in the southern band? These questions are addressed below, by exploring the propagation characteristics of baroclinic Rossby waves.

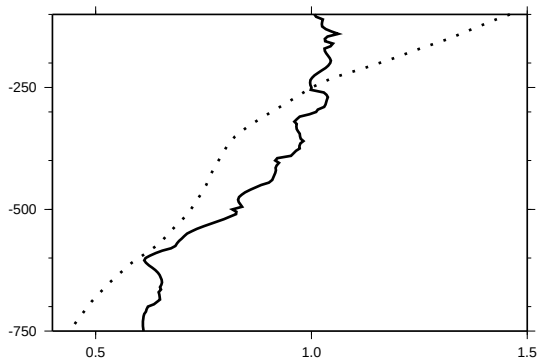

Figure 6.5: *Vertical profiles of the shear of the horizontal velocity estimated from the XBT-data in Fig. 6.4 (solid line) and the first baroclinic Rossby mode (dotted line). The velocities have been divided by their value at 250m depth, yielding comparable nondimensional quantities.*

Linear free waves

In a two layer ocean, linear Rossby wave theory leads to the following dispersion relation for zonally propagating baroclinic Rossby waves with frequency ω and horizontal wavenumber l (Pedlosky, 1987):

$$\omega = \frac{-\beta l}{l^2 + \frac{1}{R_d^2}},$$

where β is the local meridional derivative of the Coriolis parameter and R_d is the local internal Rossby radius of deformation given by $R_d = \frac{\sqrt{g' H_0}}{f_o}$ in which $g' = g\frac{\rho_2 - \rho_1}{\rho_1}$ and f_0 is the Coriolis parameter and H_0 is the depth of the unperturbed first layer. The phase propagation of the waves is given by

$$c = \frac{\omega}{l} = \frac{-\beta}{l^2 + \frac{1}{R_d^2}},$$

indicating westward phase propagation. The group velocity of these waves, and thus the propagation of their energy, is given by:

$$c_g = \frac{\partial \omega}{\partial l} = \beta \frac{l^2 - \frac{1}{R_d^2}}{\left(l^2 + \frac{1}{R_d^2}\right)^2}.$$

This can both be positive (eastward propagation) and negative (westward propagating), depending on the wavelength. In case the group velocity is eastward, the waves are relatively short and likely to dissipate quickly. The westward propagating waves are the long Rossby waves observed throughout the World Ocean (Chelton and Schlax, 1996). Given the stratification of the water column and its latitude, long and short Rossby waves may be separated

by the length scale where the group velocity vanishes:

$$\frac{\partial \omega}{\partial l} = 0 \Leftrightarrow l^2 = \frac{1}{R_d^2},$$

leading to a wavelength of

$$L = 2\pi R_d$$

This lower bound for the wavelength of westward propagating Rossby wave energy is related to the upper bound for the associated frequency:

$$\omega_{\max} = \frac{1}{2}\beta R_d$$

Chelton et al. (1998) computed the geographical distribution of the first internal Rossby radius of deformation from an atlas of temperature and salinity measurements. We have used their values to investigate where, according to this theory, the four per year signal may propagate as a first mode baroclinic Rossby wave group given the bounds on frequency and wavelength from above. As the variation of the Rossby radius is strongly dominated by the variation of the Coriolis parameter, the upper bound on the frequency implies westward propagating Rossby waves can only exist equatorward of a certain latitude. The resulting minimal period at which long Rossby waves can exist in the South Indian Ocean, computed from the values for R_d of Chelton et al. (1998), is shown in Fig. 6.6. Fig. 6.6 gives a suggestion of what may separate the observed northern band of variability (north of 15°S), from the band of variability further south: the maximum southern latitude to where a four per year signal may induce long Rossby waves is located close to the 15°Sriri parallel.

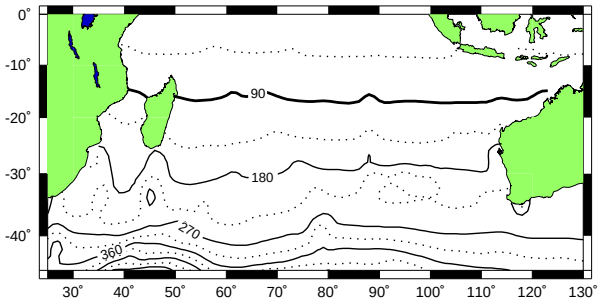

Figure 6.6: *Minimum period at which a first mode baroclinic Rossby wave can exist in the South Indian Ocean in the absence of (baroclinic) background flow (based on the internal Rossby deformation radii given by (Chelton et al., 1998)). Contour lines are drawn every 45 days. The 90 days line is drawn thicker)*

The more southern band of variability (Fig. 5.1) was shown in the previous chapter to have even stronger variability at the four per year timescale. So although the linear theory seems to explain why the intraseasonal signals are not showing up directly south of 15°S, it is not yet clear why they return further south. An explanation for this may be found in the background flow field.

Modification by vertical shear, long wave limit

Analyses of altimeter observations have shown the propagation of Rossby waves to be faster than predicted by linear theory (Le Traon and Minster, 1993; Killworth et al., 1997; Morrow and Birol, 1998). Especially away from the tropics the observed speeds are often found to be 1,5-2 times faster than expected from linear theory. A major cause for these discrepancies was pointed out by Killworth et al. (1997). They showed that the vertical shear of the background velocities has a significant effect on the propagation speed of baroclinic Rossby waves. The vertical distribution of the background velocity was shown to have a somewhat surprising effect on the propagation of the waves: the propagation speed of the first vertical mode Rossby wave is not affected by a background velocity field which has the same vertical shape, but it is affected by background velocities distributed otherwise over the water column (particularly with the shape of the second vertical mode). The effect of vertical velocity shear can be interpreted as a pseudo-topographic effect, due to the sloping of the isopycnals. The slope in the isopycnals induces a potential vorticity gradient equivalent to that induced by the variation of the Coriolis parameter. When the sloping isopycnals are the result of flow in the upper layers, the advection of the Rossby waves by this flow has the opposite sign of the effect on the wave propagation induced by the vorticity gradient. In the long wave limit, the effects cancel out each other. However, when the isopycnals are sloping due to flow in the lower layers, the effects do not cancel out.

We have computed the contribution of the first baroclinic mode to the total zonal baroclinic geostrophic velocities (Fig. 6.7) derived from the ocean atlas compiled at the WOCE Hydrographic Program Special Analysis Center in Hamburg, Germany. The baroclinic flow is projected on the first vertical mode based on the local stratification. The projection divided by the total flow yields the contribution of the first vertical mode. From these contributions, it becomes clear that the southern band of variability runs through a region where the vertical profile of the first mode is not dominating the vertical profile of the zonal background velocity, and the first baroclinic Rossby wave propagation therefore may be subject to a perturbation due to the background flow.

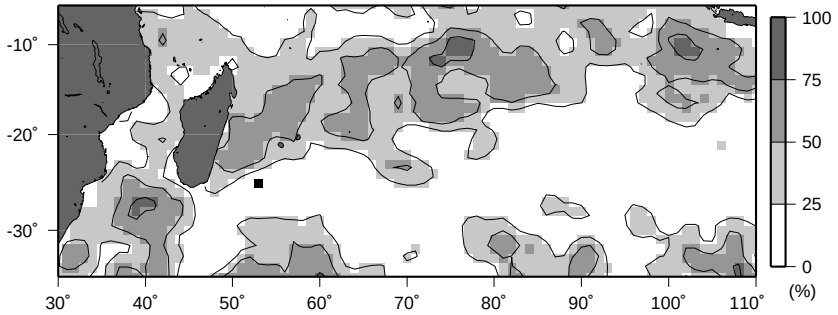

Figure 6.7: *Contribution of the first baroclinic mode to the baroclinic geostrophic velocities in zonal direction. High contributions of this mode indicate regions where the vertical shear of the background flow does not affect much the propagation speed of the first baroclinic Rossby wave.*

But can these modifications to the unperturbed case explain the observations of Rossby

waves at the four per year frequency around 20°S? The minimum zonal length scale for long Rossby waves is not altered by the addition of zonal flow, but the phase propagation and group speed are. The presence of a westward flow with a mode 2 structure around 20°S could thus speed up the propagation speed and enable the existence of such waves. This is exactly what Killworth et al. (1997) find: east of Madagascar, between 20°and 30°S they find a band where the baroclinic zonal flow is dominated by a mode 2 structure (with eastward flow near the surface and westward flow at deeper levels, independent of a barotropic component to the flow, which may alter the absolute flow, but not its vertical shear.

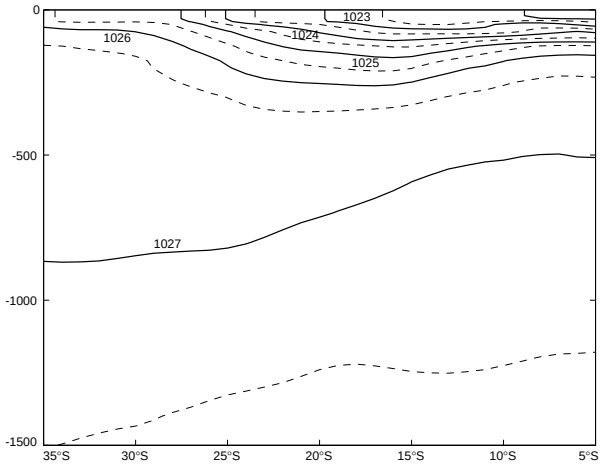

Figure 6.8: *Potential density along the 80°E meridian. Between 30°and 20°S the upper 500 m show downward sloping isopycnals, associated with eastward baroclinic flow, in contrast to the deeper levels where the baroclinic flow is generally westward. An unknown barotropic component determines the absolute direction of the total flow.*

Modification by vertical shear; two layer model

The results of Killworth et al. (1997) can be applied only in the case of very long waves (length scales $L >> 2\pi R_d$, about 300 km in our ocean region). The zonal length scale of the observed waves as extracted from the altimeter data (see Fig. 6.3) is about 600 km, so the long wave assumption of Killworth et al. (1997) can not be made without introducing large errors.

To be able to interpret the four per year variability in the zonal band between 20°and 30°S, we have evaluated the Rossby wave propagation characteristics in a two-layer quasi-geostrophic case. We use the simple two-layer model with meridionally uniform zonal velocities first used by Phillips (1954). The derivation of the group speed of baroclinic Rossby waves in this model is included in the appendix at the end of this chapter, and leads to the

following dispersion relation:

$$\omega = u_2 l + \frac{(u_1 - u_2)l^3 - \beta l}{\left(l^2 + \frac{1}{{R_d}^2}\right)}$$

where u_i is the zonal flow velocity in the i'th layer, l is the horizontal wavenumber, βd the meridional gradient of the Coriolis parameter, and R_d is the internal Rossby radius of deformation of the upper layer. Using $x = l^2 {R_d}^2$, the group speed of the baroclinic Rossby waves becomes:

$$c_g = \frac{\partial \omega}{\partial l} = \frac{u_1 x^2 + 3u_1 x - u_2(x-1) + \beta {R_d}^2 (x-1)}{(x+1)^2}$$

Without vertical shear (so $u_1 = u_2$) this yields the unperturbed group speed, which is simply that of the linear free waves added to the uniform background flow:

$$c_g = u_1 + \beta {R_d}^2 \frac{(x-1)}{(x+1)^2}.$$

In the presence of a baroclinic flow, the group velocities are modified further. Representing the velocity in the second layer relative to that in the upper layer, so the total velocity in the lower layer is $u_2 = u_1 + u_2'$, we may rewrite the modified group speed as:

$$c_g = u_1 + \left(\beta {R_d}^2 - u_2'\right) \frac{x-1}{(x+1)^2}$$

To estimate the group speed of baroclinic Rossby waves in the southern band of variability, we use observed data to evaluate the above expression for our case. We have used the estimates of the local Rossby radius of deformation given by Chelton et al. (1998). As the thermocline is located around 200-400 m around 25°S, we have used $H_1 = 400$ m, and computed realistic values for ρ_1, ρ_2, and the velocity profile along 25°S from the WOCE hydrographic data. Fig. 6.8 shows a meridional section of potential density. The upper 1300 m between 35°S and 5°S along the 80°E meridian are plotted, but this structure is observed over most of the subtropical gyre, east of roughly 50°E. The slope of the isopycnals shows that between 20°and 30°S the vertical derivative of the baroclinic flow changes sign somewhere near the thermocline: the fingerprint of the second vertical mode. The associated geostrophic velocities relative to a zero velocity at the surface are plotted in Fig. 6.9.

Based on the observation that 25°S crosses the heart of the subtropical gyre, we have chosen no surface speed as a reference. Surface drifters might provide a reference at the surface, but drifters are subject to both geostrophic and Ekman currents. Also, mean surface speeds derived from surface drifters are biased towards the larger current velocities: the mean velocity extracted from drifter-tracks is a Lagrangian transport-averaged mean, rather than time-averaged, more so when the drifters get further away from their deployment locations. As the South Indian Ocean is not a densely sampled region, surface drifters may not give a reliable estimate of the surface velocities there. Drifters show small westward mean speeds along 25°S.

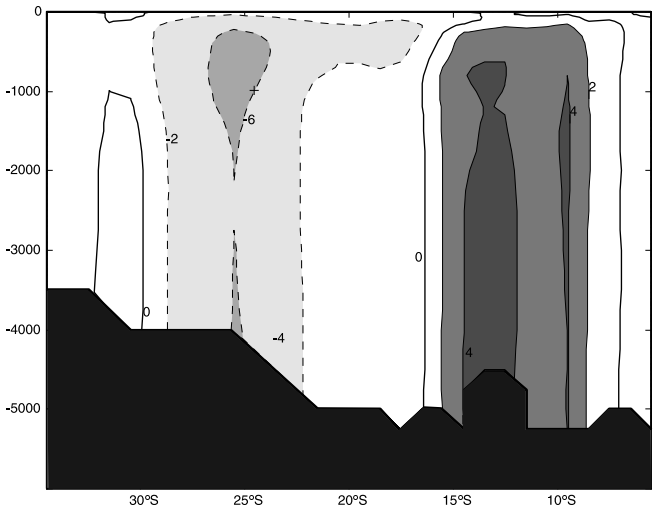

Figure 6.9: *Geostrophic velocities at 80°E, relative to a zero velocity at the surface (temperature and salinity data are from the WOCE hydrographic atlas). Positive values denote eastward flow.*

The velocities in the upper and lower layer were estimated by averaging the geostrophic velocities over the appropriate depths (i.e. above and below the thermocline). The local estimates of the group speeds were averaged over the 25°S parallel, between 50°and 115°E. For wavelengths of 600 km (which is the wavelength of the observed 90 days mode shown in Fig. 6.3) this gives a group speed of -0.06 m/s. This result hardly changes using different depths for the thermocline: depths between 200 and 500 m all yield group speeds between -0.07 and -0.06 m/s. The phase velocity estimated similarly from the dispersion relation above, is -0.08 m/s, which is in agreement with the 90 days period and a 600 km wavelength. It is concluded that westward propagation of Rossby waves (and Rossby wave energy) of four per year frequency is possible indeed in the southern band between 20°and 30°S due to the vertical shear in the background velocity.

However, this only holds in the presence of a zonal flow with the correct characteristics. Although such flow is observed over most of the region between 20-30°S, it is varying locally, which may complicate the wave propagation: conditions determining the energy propagation may vary 'en route'.

6.4 The influence of topography

We have carried out a few preliminary numerical simulations to investigate the interaction of four-per-year Rossby waves with topographic features in the south-western Indian Ocean. Our goal is to investigate the possible connection between the two bands of enhanced variability across the subtropical region (Fig. 5.1). Can the topography of the basin influence the propagation of Rossby waves in a manner that may explain the observed attenuation of the

signal west of the topographic features (see Fig. 5.1) ? And can the topography induce southward transport of Rossby wave energy, thus providing a source of energy for the southern band of variability, observed south of 20°S in the Indian Ocean?

The bottom topography of the South Indian Ocean is dominated by large, meridionally oriented ridges (see Fig. 6.1). These ridges have been shown to influence the propagation of (seasonal) signals between the eastern and western part of the basin (Matano et al., 1999). The interaction of Rossby waves with an island or submarine ridge has been studied in a β-plane model by Pedlosky and Spall (1999). They studied the effect of an island (or meridional ridge) on the structure of the normal modes in the basin. Their results can not be readily transferred to our application, as we are dealing with an area where the variation of β with latitude seems to be of crucial importance (see the preceding section). Still their results are instrumental in explaining some of the observed phenomena.

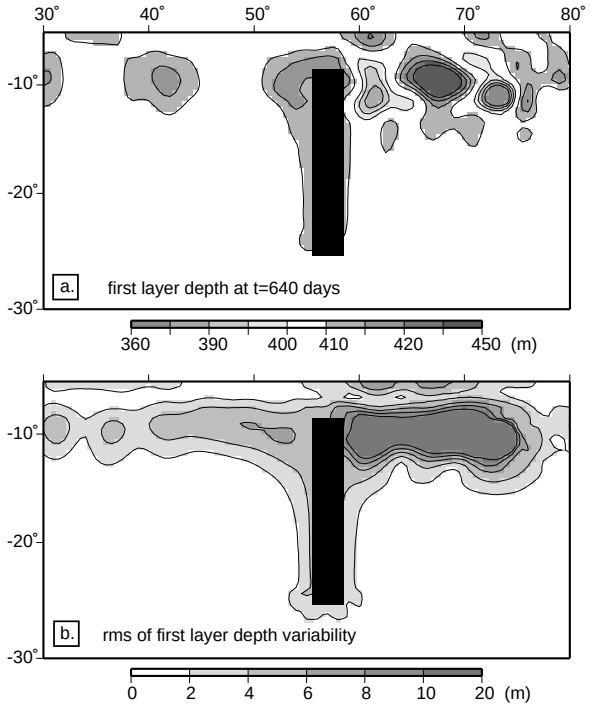

Figure 6.10: *Propagation of Rossby waves that are forced at (70°E, 12°S). The stratification in this experiment is such, that energy at the four per year frequency can propagate westward only north of 15°S. (a) a snapshot of the depth of the first layer. The unperturbed initial layer depth is 408 m. (b) Variability of the depth of the first layer over a 10 year model run.*

A two-layer version of the Miami Isopycnal Coordinate Ocean Model (MICOM) (Bleck and Boudra, 1981; Bleck and Smith, 1990) was used on a 1°x 1°horizontal resolution. As the Rossby radius of deformation ranges between 40 km at 30°S and 200 km at 5°S, this low resolution does not permit the formation of eddies. The densities and initial layer depth of

the first model layer were based on the observations around 20°S in the Indian Ocean (e.g. see Fig. 6.8). With $g' = 0.02m/s^2$ and $H_1 = 408$ m the propagation speed for the first baroclinic long Rossby wave ranges between 10 cm/s at 5°S and 1.7 cm/s at 30°S.

In a first idealized experiment, we study the interaction of a Rossby wave with a rectangular island (or ridge) of large meridional extent (see Fig. 6.10) . The Rossby wave propagation characteristics are realistic in the sense that the limiting latitude at four per year frequency is at 15°S (as in Fig. 6.6). A flat bottom at 5000 m is taken. Rossby waves are forced around (75°E, 10°S) at a frequency of four per year by a variable windforcing. Over a 3°x 3°region, a windforcing is applied which alternates between a strongly divergent and strongly convergent pattern, respectively lifting and deepening the thermocline.

The long Rossby waves propagate westward and on reaching the island force a coastal Kelvin wave which travels around it in anticlockwise direction. North of roughly 15°S, where the group velocity of the baroclinic Rossby waves is westward, Rossby waves are subsequently emitted from the western side of the island at the same frequency of four per year. These features are visible in the snapshot in Fig. 6.10a and the variability over 10 years of the depth of the first layer in Fig. 6.10b. The amplitude of the waves west of the island is much smaller than east of it, probably related to the Kelvin waves that carry energy southward and partial reflection and dissipation of the reflected Rossby waves.

In a second experiment, we have increased the density of the second layer, enhancing g' to 0.08. This changes the Rossby radius of deformation, and thereby pushes the latitude southward of which the group velocity of the 90 days periodic Rossby waves becomes eastward. It now lies south of our domain, so that Rossby waves at that frequency may propagate energy westward over the full domain. The rationale behind this approach was so simulate the possibility of southward energy transportation by the meridional ridges or island: in the South Indian Ocean, Rossby wave propagation at the four per year frequency was observed to be possible in the band between 20°-30°S. As it is difficult to simulate the effect of the vertical shear in this model, we artificially increase the Rossby radii to allow westward Rossby wave energy propagation further south than the original limiting latitude.

This is clearly observed in Fig. 6.11a, showing a snapshot of the first layer depth after 8 months of integration. A Rossby wave has been emitted from the western part of the island like in the first experiment, but now over the full meridional extent. The orientation of the patterns in the eastern part of the basin is due to the interference of long and short Rossby waves. The emittance of Rossby waves from the western boundary of the island, however, occurs independent of the waves to the southeast: in a run where the eastern boundary was chosen much further eastward to delay the arrival of Rossby waves at the southern half of the island, the Rossby wave emittance from the western part of the island was similar (not shown).

These two experiments show that meridional islands act as an antenna for Rossby waves. When the island crosses the latitude of zero group velocity for the incoming Rossby wave signal, no Rossby waves are emitted from the southern part of the island (in the southern hemisphere). For the part of the island where Rossby wave energy may propagate westward, this is observed. These results are not inconsistent with those obtained by Pedlosky and Spall (1999); Pedlosky (2000). They show that a necessary condition for communication between the regions east and west of the island, is that the incoming field from the east allows a single value for the streamfunction on the island: when the incoming waves at the

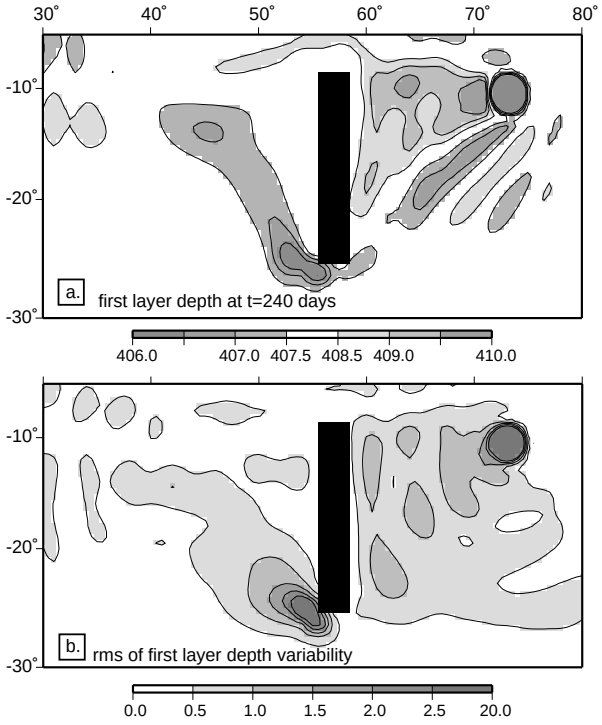

Figure 6.11: *Like 6.10, but now the density of the second layer has been increased, to enable the four per year Rossby wave energy to propagate westward throughout the basin. The patterns east of the island are complicated by the superposition of long Rossby waves and short Rossby waves emitted from the island and from the forcing region.*

southern and northern ends of the island 'agree' on the value of the streamfunction, a flow around the island is established which communicates information to the western basin. As the southern extremum of our island is generally not forced, it will follow the condition put by the incoming field at the northern tip of the island. The communication along the coast is established by the observed coastal Kelvin waves. Further comparison between the results of Pedlosky and Spall (1999); Pedlosky (2000) and our simulations is complicated by the dispersion of the waves in our model, due to the variation of β.

6.5 Summary and discussion

In this chapter, the propagation and modification of Rossby waves in the subtropical gyre of the South Indian Ocean was studied. We observed a four per year Rossby wave signal in the zonal band of stronger sea-surface height variability between 20°- 30°S. The Rossby wave nature of this signal was confirmed by in-situ temperature observations. We have seen in the preceding chapters, that the zonal band between 10°and 15°S also shows Rossby waves at

this period. However, the four per year signal at this latitude was observed to be attenuated west of the topographic features along its path: west of the 90°E ridge the signal is attenuated, and this is again observed at the Mascarene Ridge. The questions investigated in this chapter thus were: Can we explain the distribution of the four per year signal, with two bands of enhanced variability, separated by a band of low Rossby wave activity at this frequency, and can topographic features such as the Mascarene Ridge explain the attenuation of the Rossby wave signal, and cause the southward transport of Rossby wave energy?

From theoretical and observational treatment of Rossby wave propagation characteristics it was shown that unperturbed linear Rossby wave theory allows long baroclinic Rossby waves with a frequency of four per year only north of roughly 15°S. At this latitude, the group speed of the four per year Rossby waves becomes very small, and the energy is likely to be dissipated. Killworth et al. (1997) introduced a modification of the standard linear theory, including the effect of vertical shear of the background velocity field. Given the flow characteristics in the region of the southern band, with negligible or small eastward velocities at the surface, and westward flow at depth, this effect would increase westward phase velocities in the region south of 20°S, and probably enable the four per year Rossby wave to propagate energy westward. However, the assumptions used by Killworth et al. (1997) (i.e. the long wave approximation) make their modified theory inapplicable to our problem: for waves with zonal length scales of 600 km, the long wave approximation is no longer valid. Therefore, we investigated the Rossby wave propagation in a two-layer quasi geostrophic model context, taking into account the background flow in both layers. Using realistic values for the vertical shear, Rossby radii, and density distribution, we obtain a westward group speed for the four per year Rossby wave of -0.06 m/s. It should be noted that we approximate the surface flow by zero. This, however, seems to be a good approximation, as the phase velocity derived from our dispersion relation agrees well with the observed -0.08 m/s. Small surface velocities in either direction do not prevent the group speed to be westward.

Next, the energy transfer between the two bands was investigated using a numerical model. We simulated the effect of meridionally elongated topography on the propagation of Rossby waves. Both attenuation of the wave signal west of the topography, and southward transportation of energy along the western coast of the island was observed in the simulations. In may therefore be concluded that the ridges of the south Indian Ocean may indeed be instrumental in the forcing of the southern band of variability. This is also suggested by the variability plot of the 90 days MSSA mode in the south (Fig. 6.2): the signal seems to become organized only west of the 90°East Ridge, and to be significantly strengthened at the southern end of the Mascarene ridge near 65°E.

Appendix: Rossby waves in the Phillips (1954) model

The quasi-geostrophic model used by Phillips (1954) considers an ocean consisting of two layers with uniform zonal velocities u_1 and u_2. Pedlosky (1987) derives an expression for the phase velocity of propagating disturbances of the interface between the two layers. Using $u_2' = u_1 - u_2$, $F_i = 1/R_{d_i}^2$ where R_{d_i} is the internal Rossby radius of deformation for the i'th layer, and l the horizontal wavenumber, his formula 7.11.6 may be written as:

$$c \;=\; u_1 + u_2' + \frac{u_2'\, l^2 \left(l^2 + 2F_2\right) - \beta \left(2l^2 + F_1 + F_2\right)}{2\, l^2 \left(l^2 + F_1 + F_2\right)}$$

$$\pm\; \frac{\left(\beta^2 \left(F_1 + F_2\right)^2 + 2\, \beta\, u_2'\, l^4 \left(F_1 - F_2\right) - l^4\, u_2'^2 \left(4F_1F_2 - l^4\right)\right)^{1/2}}{2\, l^2 \left(l^2 + F_1 + F_2\right)}$$

Assuming a thin upper layer compared to the lower layer ($H_1 << H_2$) we may neglect F_2 with respect to F_1 (as $F_2/F_1 = (R_{d_1}/R_{d_2})^2 = H_1/H_2$). If we also assume the length scale of the disturbances to be on the order of magnitude of the internal Rossby radius of deformation in the first layer (about 300 km in our case) we may also neglect F_2 with respect to l^2. This strongly simplifies the latter equation to:

$$c = u_1 + u_2' + \frac{u_2'\, l^4 - \beta \left(2l^2 + F_1\right)}{2\, l^2 \left(l^2 + F_1\right)} \;\pm\; \frac{\left(\beta^2 F_1^2 + 2\, \beta\, u_2'\, l^4 F_1 + l^8\, u_2'^2\right)^{1/2}}{2\, l^2 \left(l^2 + F_1\right)}$$

$$= u_1 + u_2' + \frac{u_2'\, l^2}{2\, \left(l^2 + F_1\right)} - \frac{\beta \left(2l^2 + F_1\right)}{2\, l^2 \left(l^2 + F_1\right)} \;\pm\; \frac{\beta^2 F_1^2 + u_2'\, k^4}{2\, l^2 \left(l^2 + F_1\right)}$$

which leads to:

$$c_+ = u_1 + u_2' + \frac{u_2'\, l^2 - \beta}{l^2 + F_1}$$

$$c_- = u_1 + u_2' - \frac{\beta}{l^2}$$

Here, we focus on the first solution (c_+) which describes the baroclinic Rossby waves. The dispersion relation follows easily from the above and, using $F_1 = 1/R_d$, where R_d is the internal Rossby radius of deformation in the upper layer (we do not use that of the second layer anymore), is written as:

$$\omega = \left(u_1 + u_2'\right) l + \frac{u_2'\, l^3 - \beta\, l}{\left(l^2 + \frac{1}{R_d^2}\right)}.$$

Chapter 7

Variability in the Mozambique Channel

In chapter 4 we studied the upstream control of the Agulhas Retroflection, and found this to be related to eddies from the Mozambique Channel. Statistical analyses showed a link between such eddies and the movement of the retroflection, which is in turn related to the shedding of Agulhas Rings. We speculated on the formation of the Mozambique Eddies, as Rossby waves were observed to reach Madagascar at the same timescales as observed in the eddy formation and propagation. In chapter 5 this upstream control of the Agulhas Retroflection was related to a mode of variability that involves much of the Indian Ocean (Schouten et al., 2002a), and a statistical relation was found between the sea-surface height variability at the eastern boundary, where the Rossby waves are generated, and the appearance of eddies in the Mozambique Channel. In this chapter, we present observations of individual eddies, to complement the statistical analyses of chapter 4. Also, some basic statistics on the Mozambique eddies are derived which could not be obtained from the results in chapter 4. Next, we investigate the SSH variability in the Mozambique Channel, in particular focussing on the relation between local instability processes observed north of Madagascar, incoming Rossby waves from the east, and Mozambique eddy formation in the central region of the channel.

7.1 Eddies in the Mozambique Channel

the flow in the Mozambique Channel is dominated by large anticyclonic eddies. This was suggested in the past from in-situ observations (Harris, 1972; Saetre and Da Silva, 1984; Donguy and Piton, 1991), recent numerical model studies (Biastoch and Krauss, 1999), and analysis of altimetric measurements (Biastoch and Krauss, 1999; Schouten et al., 2002b). The dominance of the eddies was confirmed by using a combination of in-situ CTD and lowered ADCP observations, buoyant drifter tracks and satellite altimetry (De Ruijter et al., 2002). Here we provide a census of six years of measurements, indicating that roughly 4-5 eddies per year pass through the Mozambique Channel. In six years of combined TOPEX/Poseidon and ERS1/2 altimeter data, eddies in the Mozambique Channel have been tracked by manually

following the features through the Mozambique Channel. In the years 1995 to 1999 on average 4 eddies per year were followed to propagate from roughly 15°S to south of 35°S (Fig. 7.1). The eddy paths are rather uniform, and follow the African coastal bathymetry. North of the narrows, tracking is often not unambiguous due to interfering anomalies with periods of 50-60 days. Clear identification of the eddies is sometimes troublesome, as smaller features may merge into larger ones, especially in the central part of the channel between 17°and 20°S. Nonetheless, this collection of Mozambique eddies enables us to give some statistics about the mean SSH anomalies of the eddies, their size and propagation characteristics.

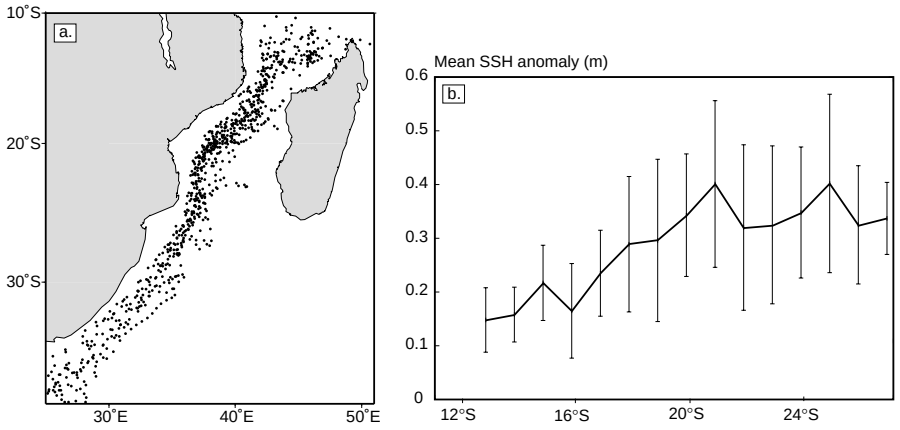

Figure 7.1: *(a) Paths of 25 Mozambique eddies that were altimetrically tracked between 1995 - 2000. (b) Mean SSH expression of the Mozambique eddies along their way south. The vertical bars show one standard deviation over the observed 25 eddies.*

The mean maximum SSH anomaly in the center of the eddies is plotted in Fig. 7.1b as a function of latitude. The eddies appear to strengthen between 12°and 20°S from 15 to 35 cm. Between 20°and 30°S they fluctuate around this 35 cm SSH anomaly. Their diameters are very constant ranging between 300 and 350 km. The southward propagation speed of the 25 eddies under examination was about 6 km/day between 12-27°S in the Mozambique Channel, with the exception of the region between 18-21°S, where on average the southward propagation was only 3-4 km/day (Fig. 7.2. Between 27 and 35°S the eddies seem to feel the advection by the the background inflow into the northern Agulhas, as they speed up to 8-10 km/day.

In April 2000, three Mozambique eddies were hydrographically sampled during the first Agulhas Current Sources Experiment campaign (ACSEX I, (De Ruijter et al., 2002)). Lowered ADCP current measurements for one eddy at 17°S, in the narrowest part of the Channel, are plotted in Fig. 7.3. The eddy has a strongly barotropic component with speeds over 10 cm/s reaching to the bottom around 2000 m depth. The SSH anomaly that was associated with this eddy was almost 20 cm, determined by satellite altimetry.

State-of-the-art numerical ocean models have met limited success in realistically reproducing the Mozambique Eddies. In the Parallel Ocean Climate Model (POCM) (Semtner

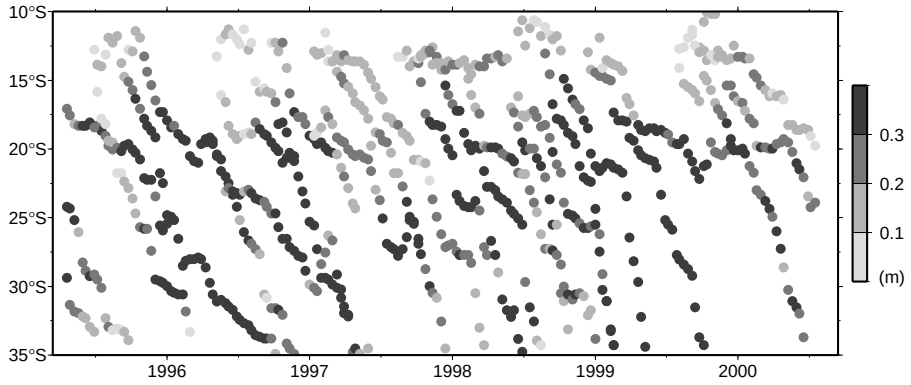

Figure 7.2: *Time/latitude plot of the 25 eddies observed in the Mozambique Channel. The gray scales denote the maximum SSH anomaly in the center of the eddy (in m). Clearly, this anomaly increases once the anomaly has passed the narrow section of the channel. It is not clear whether the anomalies in the north are already eddies, but in the Mozambique Channel it was shown (from surface drifters and in-situ observations) that they are (De Ruijter et al., 2002).*

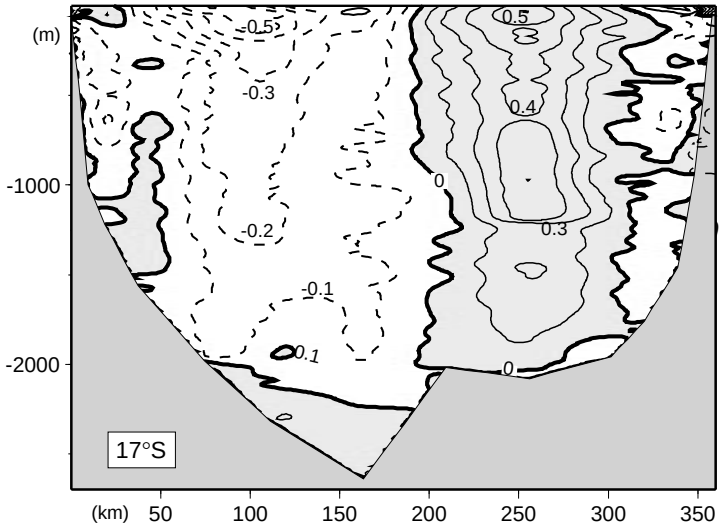

Figure 7.3: *Velocity section through an eddy taken in April 2000 in the Mozambique Channel at 17°S. Shown are the meridional velocities (m/s) observed using a Lowered Acoustic Doppler current Profiler (LADCP). Positive values denote northward flow (from De Ruijter et al. (2002)).*

and Chervin, 1992), eddies are very regularly shed in the Mozambique Channel. They are strongly surface-intensified, with meridional velocities up to 50 cm/s in the upper layers, and velocities $>$ 5 cm/s only in the upper 1000 m.

Also, the rate of eddy formation is larger in the model than it seems to be in reality: for

twelve modeled years between 1986 and 1998, 74 eddies were identified in the channel. This comes down to a periodicity of once every 60 days, comparable to 50 days found by Biastoch and Krauss (1999). The eddies in the regional model from Biastoch and Krauss (1999) are also concentrated mainly in the upper 400 m, and are formed by barotropic instability of the South Equatorial current north of Madagascar (Schott et al., 1988). Both models seem to lack a mechanism that reduces the number of anomalies to an eddy-frequency of about five in the Central Mozambique Channel, and in both models the barotropic component of the eddies is much too weak.

Combining altimetry and current meter measurements

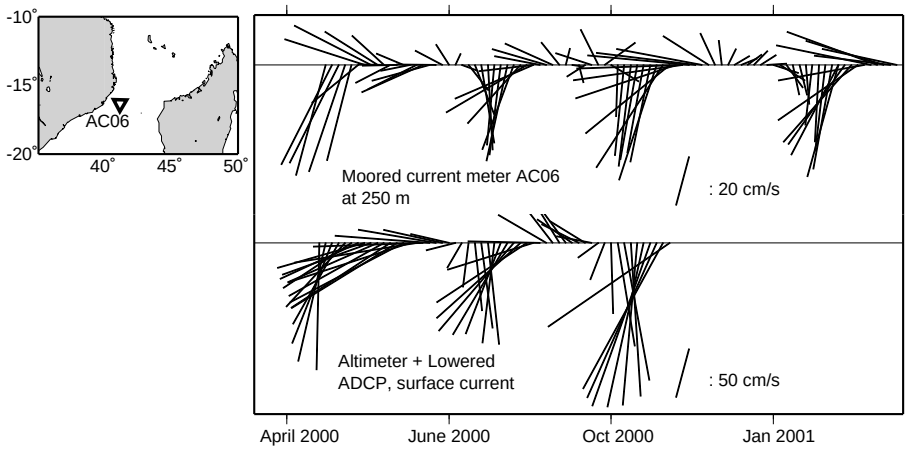

Figure 7.4: *current measurements from mooring AC06 (Ridderinkhof and de Ruijter, 2002) (upper line, see left panel for the location of the mooring) are compared to the result of the LADCP-referenced geostrophic currents measured by altimetry (lower line). There is good agreement between the two: the passage of anticyclonic vortices (of which the western half passes by the mooring) is evident from the clockwise rotation of the velocity vectors. Although the surface intensification is considerable, the eddies have a notable barotropic component.*

The passage of four eddies through the narrow part of the Mozambique Channel was documented by an array of moored current meters employed and recovered during the Agulhas current Sources EXperiment (ACSEX) I and III campaigns in 2000 and 2001, respectively (Ridderinkhof et al., 2001; De Ruijter et al., 2002; Ridderinkhof and de Ruijter, 2002). We use data from one of the moorings to verify the altimeter data. The altimeter data are then used to extend the current meter time series to a longer period, and investigate interannual changes. As the present day geoid models cannot resolve the mean state of the ocean at mesoscale resolution, we cannot derive the mean sea surface from the altimetric measurements. Therefore, only the surface current anomalies can be inferred from anomalous SSH gradients.

The geostrophic approximation was used to compute the anomalous surface currents from the gridded ERS/TOPEX/Poseidon SSH dataset provided by the CLS Physical Oceanogra-

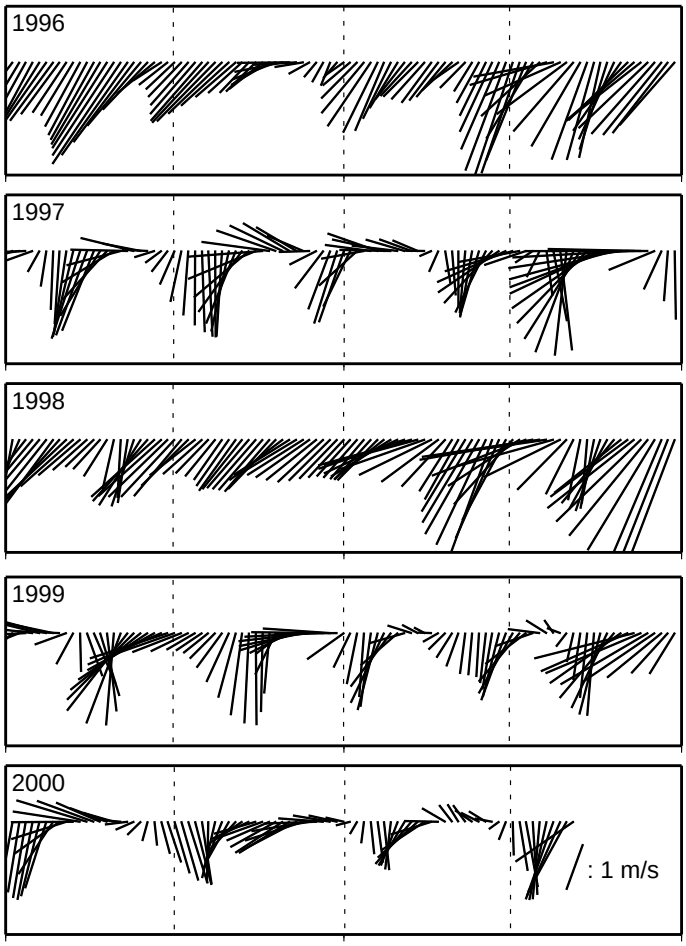

Figure 7.5: *Like the lower panel of Fig. 7.4, but now extended to almost five years of combined TOPEX/Poseidon and ERS1/2 measurements. Velocity fluctuations at the five per year frequency are dominant, mostly related to passing eddies. During the first halves of 1996 and 1998, no eddies were formed in this region.*

phy Division, France (http://www-aviso.cnes.fr) . These flow anomalies, interpolated to the time of the ACSEX I cruise, were subtracted from the total velocity as determined from the LADCP measurements during the cruise (averaged over the upper 200 m, see Fig. 7.3). The resulting 'background' flow was then added to the anomalous flow velocity timeseries obtained from altimetry. The sum of these is an approximation of the 'total' surface flow at the location of the CTD/LADCP-station.

To check the validity of this method, we have used the, independent, current measurements from a moored current meter. This was done for one of the moorings in the western

part of the narrow section of the Mozambique Channel (Fig. 7.4). Although the amplitudes are distinctly different, the flow directions in general agree very well. The amplitude of the flow at the moored current meter is lower than that of the combined altimetry/LADCP observations, because the latter is a measure of the surface flow and the current meter measurements were taken at a depth of at least 250 m. Usually the current meter was measuring even deeper than 250 m, as the flow pushes the moored current meter downward, especially during the eddy passages when strong currents occur.

Apparently, the altimeter estimates combined with the background flow determined from the LADCP-observations represent the surface flow reasonably well. This makes it possible to extend our analysis period from the one year of the moored current meter array, to several years when the combination of TOPEX/Poseidon and ERS1/2 satellite altimeters has been operational. This combination provides accurate SSH measurements with a horizontal resolution high enough to resolve the variable flow at this location using the geostrophic approximation. The resulting longer timeseries obtained from the altimeter data, is shown in Fig. 7.5. These altimetry data show that the number of anticyclonic eddies passing through the narrow part of the Mozambique Channel is irregular over the years: from 5 in 1997, 1999 and 2000, down to only two in 1998. Extended periods without eddies also appeared in the first halves of 1998 and 1996, but also these periods show velocity fluctuations at a frequency of five per year.

7.2 Southward reduction of the dominant timescale

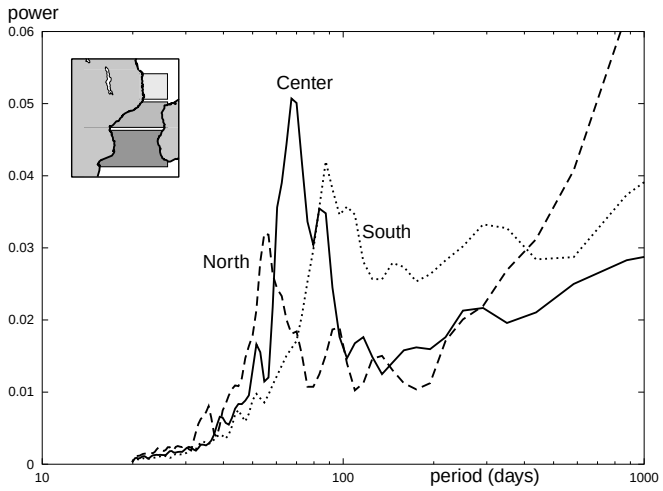

Figure 7.6: *Average SSH spectra over three regions in the Mozambique Channel. The spectra have been normalized by their total variance (the interannual signal is about the same for the three regions).*

The main source of variability in the region north of Madagascar is the barotropic instability of the South Equatorial current, which has a dominant period of 55 days (Schott et al.,

1988; Quadfasl and Swallow, 1986) At this point it is unclear why this strong signal is not propagating at that frequency of about 7 per year through the narrows of the channel: the frequency of the passage of anomalies through the narrows seems to be close to 5 cycles per year (7.5). To explore this further, we have computed the average SSH spectrum, by averaging the spectra of all individual points where SSH is observed by altimetry, in three regions in the Mozambique Channel. The three regions and their average SSH spectra are shown in Fig. 7.6.

The northern region clearly shows a peak in the spectrum at the 55 days period consistent with the earlier observations (Quadfasl and Swallow, 1986; Schott et al., 1988). However, going southward through the Channel, the dominant eddy period increases. The southern part of the Channel is dominated by four per year variability as was described in chapter 5. The SSH variability in the central part of the Channel lies somewhere in the middle, with a broader peak at frequencies between 4 and 7 per year. This is consistent with 5 eddies or flow pulses per year that seem to pass through the narrows (Fig. 7.5). A possible explanation for the slow change of the dominant eddy time scale for these three regions is presented below.

Variability of the northern region

We use altimeter data of a relatively small region between 40-55°E and 16-5°S (so north of the narrows of the Mozambique Channel) to focus on the variability of this specific region. A high-pass filter (a cosine window running mean with a half-width of 200 days) has been applied to remove the interannual and annual components. These are strong in this region (see Fig. 7.6) related to the Indian Ocean Dipole and/or El Niño events (Webster et al., 1999) that are strongly felt. We have applied the MSSA technique (Plaut and Vautard, 1994) to extract the oscillatory modes of variability for this region.

A dominant mode with a period of 55 days is found as the 5th and 6th modes, which satisfy the criteria for an oscillatory mode (Plaut and Vautard, 1994). The first two EOF's of

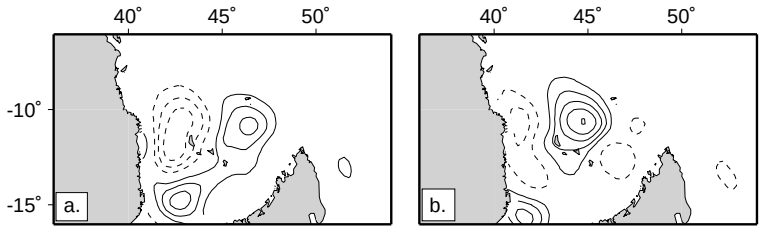

Figure 7.7: *First two EOF's of the 55 days MSSA mode of the SSH anomalies (a. and b.) for the region shown. Positive (negative) values are indicated by solid (dotted) contours. The spectrum of the timeseries associated with these EOF's is plotted in Fig. 7.10*

this oscillatory mode describe it almost completely. Fig. 7.7a,b show westward propagating wavelike features in SSH with a length-scale of 400 km west of the northern tip of Madagascar, where the South Equatorial current separates from the island and flows westward as a free jet. As the amplitude of these first two EOF's is fully concentrated in the region between Madagascar and the African continent, north of the Comores Islands at 12°S, it shows

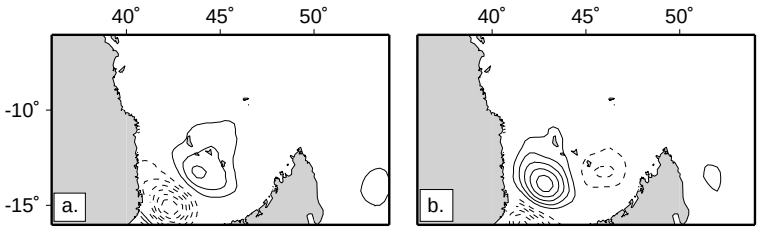

Figure 7.8: *First two EOF's of the reconstructed MSSA mode with a dominant frequency of five per year (a. and b.). The spectrum of the timeseries associated with these EOF's is plotted in Fig. 7.10.*

a regional phenomenon, most likely related to the barotropic instability of the free jet (Schott et al., 1988; Biastoch and Krauss, 1999). No clear connection seems to exist between the 55-day periodicity originating at the northern tip of Madagascar, and the observed variability further south in the Mozambique Channel.

The first MSSA mode of our northern region of the Mozambique Channel also contains longer period variability. Mode 1/2 has peak frequencies centered around 5 per year, and also forms an oscillatory mode. Fig. 7.8 shows the two dominant EOF's of the mode. They show propagating anomalies entering the Mozambique Channel through the narrows, consistent with the extended current meter record of Fig. 7.4.

The variability pattern of the 7 per year mode (Fig. 7.9) suggests a possible route for anomaly propagation via the western boundary (where the signal could be too close to the African coast to be observed) to the entrance of the Mozambique Channel. There, a separate variability maximum of the 7 per year mode is found. In the same region also the five per year mode shows maximum variability (Fig. 7.8). The two modes thus are not completely separated, and cannot be considered fully apart from each other. The pattern of variability of the 5 per year mode also suggests a connection between anomalies east and west of Madagascar. (The third and fourth MSSA-modes are concentrated along the northern part of the domain, and represent the semi-annual mode described in the discussion of chapter 5).

7.3 Dominant variability around Madagascar

The 5 per year frequency present in the dominant MSSA modes of the northern region is also the frequency with which anomalies were observed to pass through the narrow section of the Channel (Fig. 7.5), and it is therefore likely that this is also the frequency with which the anomalies are passing through the central part of the Channel. This is confirmed by an EOF analysis applied to this region. The first two EOF's of the high-pass filtered SSH data (Fig. 7.11) show the southwestward propagation of SSH anomalies through the central part of the Mozambique Channel. In-situ observations, including drifters, have shown that the positive anomalies correspond to anticyclonic eddies (De Ruijter et al., 2002). The spectrum of the timeseries corresponding to the EOF's (Fig. 7.12) shows a rather broad peak centered around 5 times per year and resembles that of the 5 per year MSSA mode from the analysis in the north (reproduced in Fig. 7.12).

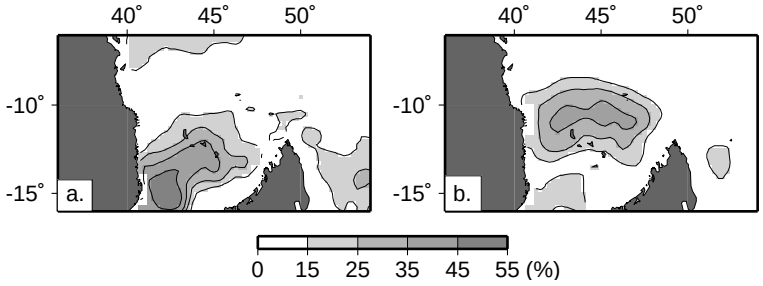

Figure 7.9: *Variability of the 5 per year (a) and 7 per year (b) MSSA components for the region shown, divided by the total variance of the high-pass filtered SSH data. The 55 days variability is mainly confined to the region north of the Comores islands, whereas the 5 per year modes shows the propagation into the central Mozambique Channel. Also, the 5 per year mode shows more variability east of Madagascar, with values over 15%.*

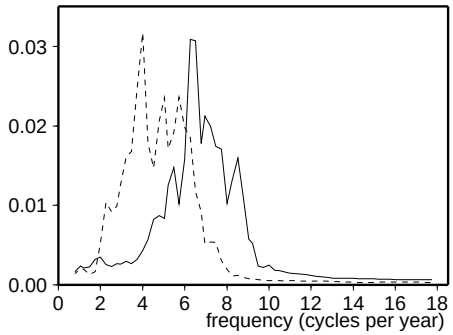

Figure 7.10: *Frequency spectra of the principal components of the 7 per year eddy mode (solid line) and the 5 per year mode (dotted line) in the northern region of the Mozambique Channel (see Fig. 7.9 for the region).*

The southern region of the Mozambique Channel showed a clear peak at the 90 days period (Fig. 7.6). An MSSA analysis of SSH data, for the southern region (see Fig. 7.6) alone, resulted in MSSA modes which showed variability not localized within the small region, but extending beyond the domain of the analysis. Therefore, we have repeated the analysis for the Mozambique Channel as a whole, also extending eastward of Madagascar to 55°E (Fig. 7.13) . This introduces the risk that processes show up on slightly different timescales than they have in reality, when they project well onto a dominant mode of variability for the complete region. This is what happens to the eddy propagation in the central part of the channel: In general, the number of such occasions is about five per year (Figs. 7.4 and 7.12) but the irregularity over the years causes it to project well on other timescales. The eddies thus show up in several MSSA modes.

In the large-region analysis of Fig. 7.13 , we find two strong modes of variability with peak frequencies of 4 per year, and variability at timescales between 3 and 5 times per year.

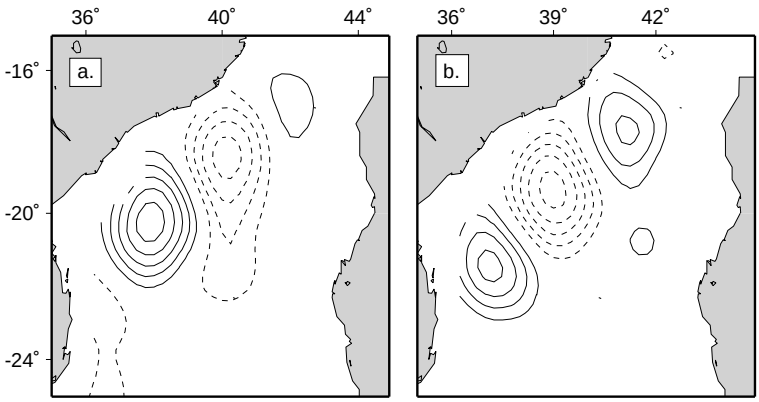

Figure 7.11: *First two EOF's of the high-pass filtered SSH data for the central Mozambique Channel. Anomalies propagate in southwestward direction, at a frequency of about five per year. The spectrum of the associated time series is plotted in Fig. 7.12*

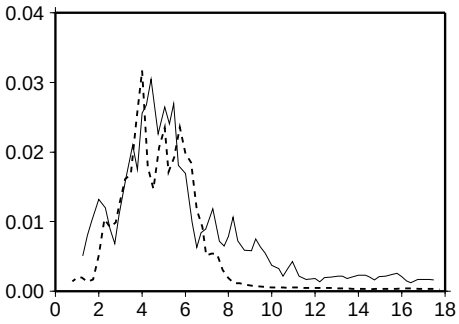

Figure 7.12: *The spectrum of the principal components plotted in Fig. 7.11 (solid line), with the spectrum of the 5 per year MSSA mode from the north (dotted line).*

The first couple of MSSA modes (mode 1 and 2) shows the eddy propagation in the central part of the channel (7.13). Also, south of Madagascar this mode shows enhanced variability. This may relate to the synchronization already observed in chapter 4: anomalies from the east Madagascar region were found to propagate westward into the upstream Agulhas region synchronously with the eddies propagating southward from the central Mozambique Channel. The second couple of MSSA modes with frequencies around four per year (mode 5/6) shows how this synchronization may be achieved (Fig. 7.14). In this mode, we see the four per year variability that is dominant in the southern band across the southern Indian Ocean (see Fig. 5.1 and chapter 6) reaching Madagascar. Also large, meridionally elongated anomalies propagate westward from the entire western coast of the island (Fig. 7.14, left panel). The forcing from the east, by Rossby waves from the southern band of variability, and most likely also from the northern band of variability (see Chapters 5 and 6), seems to generate these

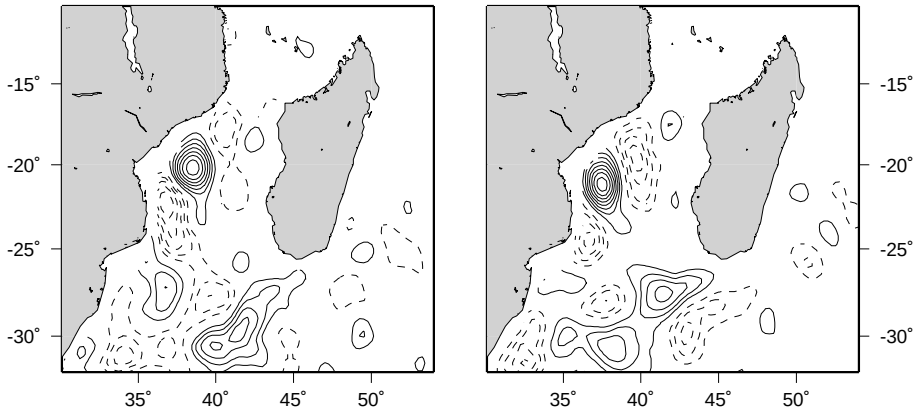

Figure 7.13: *Two EOF's (together representing over 80% of the variance of the MSSA reconstructed component) of the first MSSA mode with a frequency around 4 per year. Most of the eddy propagation signal through the central Mozambique Channel (see Fig. 7.11) is contained in this mode.*

elongated anomalies inside the Mozambique Channel.

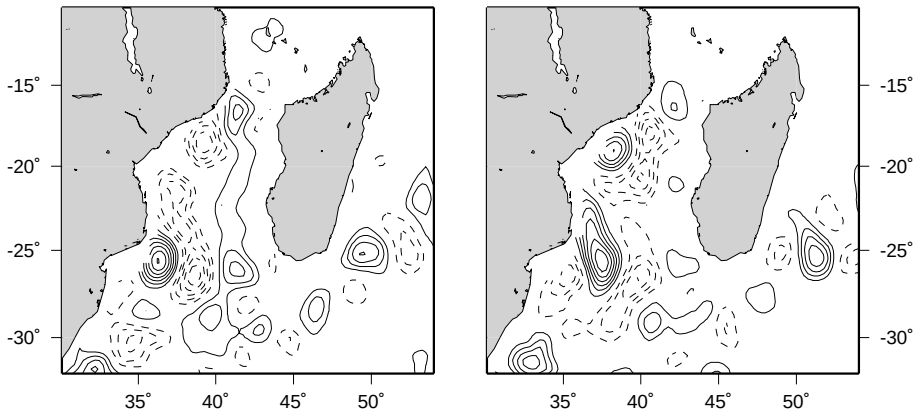

Figure 7.14: *Like Fig. 7.13, but now for the second MSSA mode with frequencies around four per year (mode 5/6). Here the incoming waves from the east (near 25°S) can be observed. The southern part of the propagation of the Mozambique eddies, south of roughly 22°S, is captured by this mode. Also, meridionally elongated features show up in the Mozambique Channel propagating westward from the coast of Madagascar.*

Such elongated anomalies are also observed in the original data: Fig. 7.15 shows a sequence of SSH anomalies in the Mozambique Channel region for February and March 1996. A meridionally elongated anomaly (with anomalous SSH values of over 10 cm) has left the coast of Madagascar in February. A month later (right panel) it has merged with the eddy at (39°E,20°S) resulting in a strengthening of the eddy in the central Mozambique Channel. This might (partly) explain the rather weak correlation between the occurrence of anomalies

in the central Mozambique Channel, and that of the anomalies in the north. It also may be an example of the process of reduction of the number of anomalies and the associated synchronization of the signals propagating from the north and east (chapter 4): two anomalies identified in February 1996 merge into one larger one a month later.

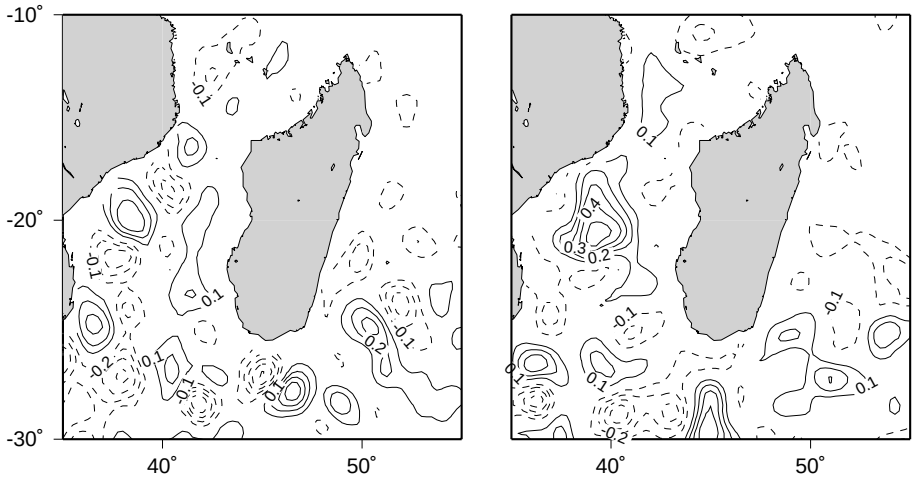

Figure 7.15: *Anomalous SSH elevations for February and March 1996 (contours are 0.1 m apart, the 0 m contour is left out). In February, a meridionally elongated anticyclonic feature is initiated from the west coast of Madagascar. A month later, the eddy already present in the channel, and the elongated anomaly, have merged into a stronger Mozambique eddy.*

7.4 Discussion

The interaction between Rossby waves coming in from the eastern Indian Ocean, the island of Madagascar, and local current characteristics has been described using statistical analyses of the SSH variability around Madagascar. The 40-60 days period signal observed in the extension of the South Equatorial current northwest of the island, seems not to propagate fully through the Mozambique Channel. However, about 5 anomalies per year do enter the Channel from the north. Once within the Mozambique Channel, their frequency is further reduced, while the eddies become more energetic. In general, four eddies per year leave the Mozambique Channel southward into the Agulhas region.

The frequency reduction to four per year seems to be established by merging of several anomalies into larger and stronger eddies within the Mozambique Channel. This merging is related to incoming Rossby waves from the east: the interaction of the Rossby waves and the island leads to elongated anticyclonic anomalies, which interact with anomalies that propagate southward through the narrows. Further study of observations, combined with theoretical analysis and supported by numerical simulations is necessary to unravel the complex interactions between Rossby waves and eddies in this complicated region around Madagascar and the Mozambique Channel.

Bibliography

Allen, M. R., and A. W. Robertson, 1996, Distinguishing modulated oscillations from coloured noise in multivariate datasets, *Climate Dynamics*, *12*, 775–784.

Arhan, M., H. Mercier, and J. R. E. Lutjeharms, 1999, The disparate evolution of three Agulhas rings in the South Atlantic Ocean, *J. Geophys. Res.*, *104*, 20,987–21,005.

Arief, D., and S. P. Murray, 1996, Low-frequency fluctuations in the Indonesian throughflow through Lombok Strait, *J. Geophys. Res.*, *101*, 12,455–12,464.

Beal, L. M., and H. L. Bryden, 1997, Observations of an Agulhas undercurrent, *Deep Sea Res., Part A*, *44*, 1715–1724.

Beaufort, L., Y. Lancelot, P. Camberlin, O. Cayre, E. Vincent, F. Bassinot, and L. Labeyrie, 1997, Insolation cycles as a major control of equatorial Indian Ocean primary production, *Science*, *278*, 1451–1454.

Beismann, J. O., R. H. Käse, and J. R. E. Lutjeharms, 1999, On the influence of submarine ridges on translation and stability of Agulhas rings, *J. Geophys. Res.*, *104*, 7897–7906.

Berger, W. H., and G. Wefer, 1996, Expeditions to the past: paleoceanographic studies in the south Atlantic, in *The South Atlantic: present and past circulation*, edited by G. W. et al., pp. 363–410. Springer.

Biastoch, A., and W. Krauss, 1999, The role of mesoscale eddies in the source regions of the Agulhas Current, *J. Phys. Oceanogr.*, *29*, 2303–2317.

Birol, F., and R. Morrow, 2001, Sources of the baroclinic waves in the southeast Indian Ocean, *J. Geophys. Res.*, *103*, 9145–9160.

Bleck, R., and D. B. Boudra, 1981, Initial testing of a numerical ocean circulation model using a hybrid (quasi-isopycnic vertical coordinate, *J. Phys. Oceanogr.*, *11*, 755–770.

Bleck, R., and L. T. Smith, 1990, A wind-driven isopynic coordinate model of the north and equatorial Atlantic Ocean. 1. model development and supporting experiments, *J. Geophys. Res.*, pp. 3273–3285.

Boudra, B. D., and E. P. Chassignet, 1988, Dynamics of Agulhas retroflection and ring formation in a numerical model. Part I: the vorticity balance, *J. Phys. Oceanogr.*, *18*, 280–303.

Boudra, D. B., and W. P. M. de Ruijter, 1986, The wind-driven circulation of the Atlantic - Iindian ocean - II. experiments using a multi-layer numerical model, *Deep Sea Res., Part A*, *33*, 447–482.

Bray, N. A., J. C. Chong, S. E. Wijffels, M. Fieux, S. Hautala, G. Meyers, and W. M. L. Morawitz, 1997, Characteristics of the Indo-Pacific throughflow in the eastern Indian Ocean, *Geoph. Res. Letters*, *24*, 2569–2572.

Broecker, W. S., 1991, The great ocean conveyor, *Oceanography*, *4*, 79–89.

Byrne, D. A., A. L. Gordon, and W. F. Haxby, 1995, Agulhas eddies: A synoptic view using Geosat ERM data, *J. Phys. Oceanogr.*, *25*, 902–917.

Cane, M. A., 1979, The response of an equatorial ocean to simple wind stress patterns: II. numerical results, *J. Mar. Res.*, *37*, 253–299.

Cane, M. A., and D. Moore, 1981, A note on low frequency equatorial basin modes, *J. Phys. Oceanogr.*, *11*, 1578–1584.

Cayre, O., L. Beaufort, and E. Vincent, 1999, Paleoproductivity in the equatorial Indian Ocean for the last 260,000 yr: a transfer function based on planctonic foraminifera, *Quaternary Sc. Rev.*, *18*, 839–857.

Chelton, D. B., 1988, WOCE/NSA altimeter algorithm workshop, Technical report 2, US WOCE.

Chelton, D. B., and M. G. Schlax, 1996, Global observations of oceanic Rossby waves, *Science*, *272*, 234–237.

Chelton, D. B., R. A. deSzoeke, M. G. Schlax, K. ElNaggar, and N. Siwertz, 1998, Geographical variability of the first baroclinic Rossby radius of deformation, *J. Phys. Oceanogr.*, *28*, 433–460.

Chong, J. C., J. Sprintall, S. Hautala, W. L. Morawitz, N. A. Bray, and W. Pandoe, 2000, Shallow thoughflow variability in the outflow straits of Indonesia, *Geoph. Res. Letters*, *27*, 125–128.

Clarke, A. J., and X. Liu, 1993, Observation and dynamics of semiannual and annual sea levels near the eastern equatorial Indian Ocean boundary, *J. Phys. Oceanogr.*, *23*, 386–399.

Clement, A. C., and A. L. Gordon, 1995, The absolute velocity field of Agulhas eddies and the Benguela Current, *J. Geophys. Res.*, *100*, 22,591–22,601.

De Ruijter, W. P. M., 1982, Asymptotic analysis of the Agulhas and Brasil Current systems, *J. Phys. Oceanogr.*, *12*, 361–373.

De Ruijter, W. P. M., and D. B. Boudra, 1985, The wind-driven circulation in the South-Atlantic-Indian Ocean ,I: Numerical experiments in a one-layer model, *Deep Sea Res., Part A*, *32*, 557–574.

De Ruijter, W. P. M., P. J. van Leeuwen, and J. R. E. Lutjeharms, 1999, Generation and evolution of Natal pulses: solitary meanders in the Agulhas Current, *J. Phys. Oceanogr.*, *29*, 3043–3055.

De Ruijter, W. P. M., A. Biastoch, S. S. Drijfhout, J. R. E. Lutjeharms, R. P. Matano, T. Pichevin, P. J. van Leeuwen, and W. Weijer, 1999, Indian-Atlantic interocean exchange: Dynamics, estimation and impact, *J. Geophys. Res.*, *104*, 20,885–20,910.

De Ruijter, W. P. M., J. R. E. Lutjeharms, and H. Ridderinkhof, 2000, Observations of the Mozambique Current in ACSEX, the Agulhas Current Sources Experiment, *Intern. WOCE Newsletter, 38*, 32–34.

De Ruijter, W. P. M., H. Ridderinkhof, J. R. E. Lutjeharms, M. W. Schouten, and C. Veth, 2002, Observations of the flow in the Mozambique Channel, In press, *Geoph. Res. Letters*.

Dewar, W. K., 1987, Ventilating warm rings: Theory and energetics, *J. Phys. Oceanogr.*, *17*, 2219–2231.

Dijkstra, H. A., and W. P. M. de Ruijter, 2001a, Barotropic instabilities of the Agulhas Current system and their relation to ring formation, *J. Mar. Res.*, *59*, 517–533.

Dijkstra, H. A., and W. P. M. de Ruijter, 2001b, On the physics of the Agulhas: steady retroflection regimes, *J. Phys. Oceanogr.*, *31*, 2971–2985.

Donguy, J. R., and B. Piton, 1991, The Mozambiue Channel revisited, *Oceanol. Acta*, *14*, 549–558.

Drijfhout, S. S., L. de Steur, C. A. Katsman, P. C. F. van der Vaart, P. J. van Leeuwen, and C. Veth, 2002, Modeling the initial decay processes of Agulhas rings in an isopycnic ocean model, *Deep Sea Res., Part A*, submitted.

Duncombe Rae, C. M., S. L. Garzoli, and A. L. Gordon, 1996, The eddy field of the southeast Atlantic Ocean: A statistical census from the Benguela Sources and Transports project, *J. Geophys. Res.*, *101*, 11,949–11,964.

Egbert, G. D., and R. D. Ray, 2000, Significant dissipation of tidal energy in the deep ocean inferred from satellite altimeter data, *Nature*, *405*, 775–778.

Feron, C. V., W. P. M. de Ruijter, and D. Oskam, 1992, Ring shedding in the Agulhas system, *J. Geophys. Res.*, *97*, 9467–9477.

Feron, R. C. V., W. P. M. de Ruijter, and P. J. van Leeuwen, 1998, A new method to determine the mean sea surface dynamic topography from satellite altimeter observations, *J. Geophys. Res.*, *103*, 1343–1362.

Fu, L. L., 1981, The general circulation and meridional heat transport of the subtropical South Atlantic determined by inverse methods, *J. Phys. Oceanogr.*, *11*, 1171–1193.

Garzoli, S. L., and A. L. Gordon, 1996, Origins and variability of the Benguela Current, *J. Geophys. Res.*, *101*, 897–906.

Garzoli, S. L., A. L. Gordon, D. P. V. Kamenkovich, and C. M. Duncombe Rae, 1996, Variability and sources of the southeastern Atlantic circulation, *J. Mar. Res.*, *54*, 1039–1071.

Garzoli, S. L., G. J. Goñi, A. J. Mariano, and D. B. Olson, 1997, Monitoring the upper southeastern Atlantic transport using altimeter data, *J. Mar. Res.*, *55*, 453–481.

Garzoli, S. L., P. L. Richardson, C. M. Duncombe Rae, D. M. Fratantoni, G. J. Goñi, and A. J. Roubicek, 1999, Thre Agulhas rings observed during the Benguela Current Experiment, *J. Geophys. Res.*, *104*, 20,971–20,985.

Gill, A. E., 1982, *Atmosphere-Ocean Dynamics*. Academic press.

Goñi, G. J., S. L. Garzoli, A. J. Roubicek, D. B. Olson, and O. B. Brown, 1997, Agulhas ring dynamics from TOPEX/Poseidon satellite altimeter data, *J. Mar. Res.*, *55*, 861–883.

Gordon, A. L., 1985, Indian-Atlantic transfer of thermocline water at the Agulhas retroflection, *Science*, *228*, 1030–1034.

Gordon, A. L., 1986, Interocean exchange of thermocline water, *J. Geophys. Res.*, *91*, 5037–5046.

Gordon, A. L., et al., 1992, Thermocline and intermediate water communication between the South Atlantic and Indian oceans, *J. Geophys. Res.*, *97*, 7223–7240.

Gordon, A. L., and W. F. Haxby, 1990, Agulhas eddies invade the south Atlantic: Evidence from Geosat altimeter and shipboard CTD-survey, *J. Geophys. Res.*, *95*, 3117–3125.

Gordon, A. L., J. R. E. Lutjeharms, and M. L. Gründlingh, 1987, Stratification and circulation at the Agulhas retroflection, *Deep Sea Res., Part A*, *34*, 565–599.

Gründlingh, M. L., 1987, Cyclogenesis in the Mozambique Ridge Current, *Deep Sea Res., Part A*, *34*, 89–103.

Gründlingh, M. L., 1995, Tracking eddies in the southeast Atlantic and southwest Indian Oceans with TOPEX/Poseidon, *J. Geophys. Res.*, *100*, 24,977 – 24,986.

Han, W., J. P. McCreary Jr., D. L. T. Anderson, and A. J. Mariano, 1999, Dynamics of eastern surface jets in the equatorial Indian Ocean, *J. Phys. Oceanogr.*, *29*, 2191–2209.

Hansen, D. V., and P. M. Poulain, 1996, Quality control and interpolations of WOCE-TOGA drifter data, *J. Atmos. Oceanic Technol.*, *13*, 900–909.

Harris, T. F. W., 1972, Sources of the Agulhas Current in the spring of 1964, *Deep Sea Res., Part A*, *19*, 633–650.

Harris, T. F. W., R. Legeckis, and D. van Foreest, 1978, Satellite infra-red images in the Agulhas Current system, *Deep Sea Res., Part A*, *25*, 543–548.

Kalnay et al., E., 1996, The ncep/ncar 40-year reanalysis project, *Bull. Amer. Meteor. Soc.*, *77*, 437–471.

Kamenkovich, V. M., Y. P. Leonov, D. A. Nechae, D. A. Byrne, and A. L. Gordon, 1996, On the influence of bottom topography on the Agulhas eddy, *J. Phys. Oceanogr.*, *26*, 892–912.

Killworth, P. D., D. B. Chelton, and R. A. de Szoeke, 1997, The speed of observed and theoretical long extratropical planetary waves, *J. Phys. Oceanogr.*, *27*, 1946–1966.

Kindle, J. C., and J. D. Thompson, 1989, The 26- and 50-day oscillations in the western Indian Ocean: model results, *J. Geophys. Res.*, *94*, 4721–4736.

Le Blanc, J. L., and J. P. Boulanger, 2001, Propagation and reflection of long equatorial waves in the Indian Ocean from TOPEX/Poseidon data during the 1993-1998 period, *Climate Dynamics*, *17*, 547–557.

Le Traon, P. Y., and J. F. Minster, 1993, Sea level variability and semiannual Rossby waves in the South Atlantic, *J. Geophys. Res.*, *98*, 12.315 – 12.326.

Le Traon, P. Y., F. Nadal, and N. Ducet, 1998, An improved mapping method of multi-satellite data, *J. Atm. Ocean. Techn.*, *25*, 522–534.

Lemoine, F. G., 1998, The development of the joint NASA GSFC and the national imagery and mapping agency (NIMA) geopotential model EGM96, NASA/TP-1998-206861. Nasa, Goddard Space Flight Center, Greenbelt, Maryland 20771.

Lorenz, E. N., 1956, Empirical orthogonal functions and statistical weather prediction, Sci. Rep. 1, Mass. Ist. of Technol., Camebridge.

Lutjeharms, J. R. E., 1988, Remote sensing corroboration of retroflection of the East Madagascar Current, *Deep Sea Res., Part A*, *35*, 2045–2050.

Lutjeharms, J. R. E., 1996, The exchange of water between the south Indian and south Atlantic Oceans, in *The South Atlantic: Present and Past Circulation*, edited by G. Wefer, et al., pp. 125–162. Springer Verlag, New York.

Lutjeharms, J. R. E., and H. R. Roberts, 1988, The Natal pulse: an extreme transient on the Agulhas Current, *J. Geophys. Res.*, *93*, 631–645.

Lutjeharms, J. R. E., and R. C. van Ballegooyen, 1988, Anomalous upstream retroflection in the Agulhas Current, *Science*, *240*, 1770–1772.

Lutjeharms, J. R. E., and R. C. Van Ballegooyen, 1988, The retroflection of the Agulhas Current, *J. Phys. Oceanogr.*, *18*, 1570–1583.

Lutjeharms, J. R. E., N. Bang, and C. P. Duncan, 1981, Characteristics of the currents east and south of Madagascar, *Deep Sea Res., Part A*, *28*, 879–899.

Lutjeharms, J. R. E., W. P. M. de Ruijter, and R. G. Peterson, 1992, Interbasin exchange at the Agulhas retroflection; the development of some oceanographic concepts, *Deep Sea Res., Part A*, *39*, 1791–1807.

Lutjeharms, J. R. E., P. M. Wedepohl, and J. M. Meeuwis, 2000, On the surface drift of the East Madagascar and Mozambique Currents, *South African J. Sc.*, *96*, 141–147.

Luyten, J. R., M. Fieux, and J. Gonella, 1980, Equatorial currents in the western Indian Ocean, *Science*, *209*, 600–603.

Madden, R. A., and P. R. Julian, 1994, Observations of the 40-50 day tropical oscillation - A review, *Mon. Weat. Rev.*, *122*.

Marcantonio, F., R. F. Anderson, S. Higgins, M. Q. Fleisher, M. Stute, and P. Schlosser, 2001, Abrubt intensification of the SW Indian monsoon during the last deglaciation: constraints from Th, Pa, and He isotopes, *Earth and Plan. Sc. Letters*, *184*, 505–514.

Matano, R., 1996, A numerical study of the Agulhas retroflection: the role of bottom topography, *J. Phys. Oceanogr.*, *26*, 2267–2279.

Matano, R., C. G. Simionato, W. P. M. De Ruijter, P. J. van Leeuwen, P. T. Strub, D. B. Chelton, and M. G. Schlax, 1998, Seasonal variability in the Agulhas retroflection region, *J. Geophys. Res.*, *25*, 4361–4364.

Matano, R., C. G. Simionato, and P. T. Strub, 1999, Modelling the wind-driven variability of the South Indian Ocean., *J. Phys. Oceanogr.*, *29*, 217–230.

Matano, R. P., E. J. Beier, P. T. Strub, and R. Tokmakian, 2001, Large-scale forcing of Agulhas variability: the seasonal cycle, *J. Phys. Oceanogr.*, In press.

Morrow, R., and F. Birol, 1998, Variability in the southeast Indian Ocean from altimetry: forcing mechanisms for the Leeuwin Current, *J. Geophys. Res.*, *103*, 18,529–18,544.

Olson, D. B., and R. H. Evans, 1986, Rings of the Agulhas Current, *Deep Sea Res., Part A*, *33*, 27–42.

Olson, D. B. R., R. Fine, and A. L. Gordon, 1992, Convective modification of water masses in the Agulhas, *Deep Sea Res., Part A*, *39*, 163–181.

Ou, H. W., and W. P. M. de Ruijter, 1986, Separation of an inertial boundary current from a curved coastline, *J. Phys. Oceanogr.*, *16*, 280–289.

Pedlosky, J., 1987, *Geophysical Fluid Dynamics*. Springer Verlag, New York.

Pedlosky, J., 2000, The transmission of Rossby waves through basin barriers, *J. Phys. Oceanogr.*, *30*, 495–511.

Pedlosky, J., and M. Spall, 1999, Rossby normal modes in basins with barriers, *J. Phys. Oceanogr.*, *29*, 2332–2349.

Peixoto, J. P., and A. H. Oort, 1992, *Physics of Climate*. AIP Press, New York.

Périgaud, C., and P. Delecluse, 1992, Annual sea level variations in the southern tropical Indian Ocean from Geosat and shallow-water simulations, *J. Geophys. Res.*, *97*, 20,169–20,178.

Phillips, N. A., 1954, Energy transformations and meridional circulations associated with simple baroclinic waves in a two-level, quasi geostrophic model, *Tellus*, *6*, 273–286.

Pichevin, T., D. Nof, and J. R. E. Lutjeharms, 1999, Why are there Agulhas rings?, *J. Phys. Oceanogr.*, *29*, 39–54.

Piola, A. R. P., H. A. Figueroa, and A. A. Bianchi, 1987, Some aspects of the surface circulation south of 20S revealed by first GARP global experiment drifters, *J. Geophys. Res.*, *92*, 5101–5114.

Plaut, G., and R. Vautard, 1994, Spells of low-frequency oscillations and weather regimes in the Northern Hemisphere, *J. of the Atm. Sc.*, *51*, 210–236.

Preiseindorfer, R. W., 1981, Principal component analysis and applications, Workshop on principal component analysis, Am. Meteor. Soc., Monterey CA.

Qiu, B., M. Mao, and Y. Kashino, 1999, Intraseasonal variability in the Indo-Pacific throughflow and the regions surrounding the Indonesian seas, *J. Phys. Oceanogr.*, *29*, 1599–1618.

Quadfasl, D. R., and J. C. Swallow, 1986, Evidence for 50-day period planetary waves in the South Equatorial current of the Indian Ocean, *Deep Sea Res., Part A*, *33*, 1307–1312.

Rennell, J., 1832, *An investigation of the currents of the Atlantic Ocean and of those which prevail between the Indian Ocean and the Atlantic*. Published for Lady Rodd by J. G. L. F. Rivington, St Pauls' Church Yard, London.

Richardson, P. L., and A. Tychensky, 1998, Meddy trajectories in the Canary Basin measured during the SEMAPHORE experiment, 1993-1995, *J. Geophys. Res.*, *103*, 25,029–25,045.

Ridderinkhof, H., and W. P. M. de Ruijter, 2002, Current measurements in the Mozambique Channel, in preparation.

Ridderinkhof, H., J. R. E. Lutjeharms, and W. P. M. de Ruijter, 2001, A research cruise to investigate the Mozambique Current, *S. Afr. J. Sci.*

Rintoul, S. R., 1991, South Atlantic interbasin exchange, *J. Geophys. Res.*, *96*, 2675–2692.

Saetre, R., and J. Da Silva, 1984, The circulation of the Mozambique Channel, *Deep Sea Res., Part A*, *31*, 585–508.

Saji, H. H., B. N. Goswami, P. N. Vinayachandran, and T. Yamagata, 1999, A dipole mode in the tropical Indian Ocean, *Nature*, *401*, 360–363.

Schlitzer, R., 1996, Mass and heat transports in the South Atlantic derived from historical hydrographic data, in *The South Atlantic: Present and Past Circulation*, edited by G. Wefer, et al., pp. 125–162. Springer Verlag, New York.

Schmeits, M. J., and H. A. Dijkstra, 2000, On the physics of the 9-month variability in the Gulf Stream region: Combining data and dynamical systems analyses, *J. Phys. Oceanogr.*, *30*, 1967–1987.

Schmidtz, W. R., 1995, On the interbasin-thermohaline circulation, *Rev. Geophysics*, *33*, 151–173.

Schott, F., M. Fieux, J. Kindle, J. Swallow, and R. Zantopp, 1988, The boundary currents east of Madagascar 2. direct measurements and model comparisons, *J. Geophys. Res.*, *93*, 4963–4974.

Schouten, M. W., W. P. M. de Ruijter, P. J. van Leeuwen, and J. R. E. Lutjeharms, 2000, Translation, decay and splitting of Agulhas rings in the south-east Atlantic ocean, *J. Geophys. Res.*, *105*, 21,913–21,925.

Schouten, M. W., W. P. M. De Ruijter, P. J. Van Leeuwen, and H. Dijkstra, 2002a, A teleconnection between the equatorial and southern Indian Ocean, *Geoph. Res. Letters*, in press.

Schouten, M. W., W. P. M. De Ruijter, and P. J. Van Leeuwen, 2002b, Upstream control of the Agulhas ring shedding, *J. Geophys. Res.*, In press.

Schrama, E. J. O., 1989, The role of orbit errors in the processing of satellite altimeter data, Ph.D. thesis, Delft University of Technology.

Schrama, E. J. O., 1996, Satelite altimetry, ocean dynamics and the marine geoid, in: Lecture notes International Summerschool Como: 'The Boudary Value Problems in Modeling the Gravity Field'.

Semtner, A. J., and R. M. Chervin, 1992, Ocean general circulation from a global eddy-resolving model, *J. Geophys. Res.*, *97*, 5493–5550.

Shapiro, G. I., S. L. Meschanov, and M. V. Emelianov, 1995, Mediterrenean lens Irving after its collision with seamounts, *Oceanologica Acta*, *18*, 309–318.

Speich, S., B. Blanke, and G. Madec, 2001, Warm and cold water routes of an O.G.C.M. conveyor belt, *Geoph. Res. Letters*, *28*(2), 311–314.

Sprintall, J., A. L. Gordon, R. Murtugudde, and R. Dwi Susanto, 2000, A semiannual Indian Ocean forced Kelvin wave observed in the Indonesian seas in May 1997, *J. Geophys. Res.*, *105*, 17,217–17,230.

Stammer, D., 1997, Global characteristics of ocean variability estimated from regional TOPEX/Poseidon altimeter measurements, *J. Phys. Oceanogr.*, *27*, 1743–1769.

Stramma, L., and J. R. E. Lutjeharms, 1997, The flow of the subtropical gyre of the South Indian Ocean, *J. Geophys. Res.*, *102*, 5513–5530.

Subrahmanyam, B., and I. S. Robinson, 2000, Sea surface height variability in the Indian Ocean from TOPEX/Poseidonaltimetry and model simulations, *Marine Geodesy*, *23*, 167–195.

Sverdrup, H. U., 1947, Wind-driven currents in a baroclinic ocean, *Proc. Natl. Acad. Sci. Wash.*, *33*, 318–326.

Swallow, J., M. Fieux, and F. Schott, 1988, The boundary currents east of Madagascar 1. geostrophic currents and transports, *J. Geophys. Res.*, *93*, 4951–4962.

van Aken, H., A. van Veldhoven, C. Veth, W. P. M. de Ruijter, P. J. van Leeuwen, S. S. Drijfhout, C. Whittle, and M. Roualt, 2002, Observations of a young Agulhas ring, Astrid, during MARE, the Mixing of Agulhas Rings Experiment, submitted, *Deep Sea Res., Part A*.

van Ballegooyen, R. C., M. L. Gründlingh, and J. R. E. Lutjeharms, 1994, Eddy fluxes of heat and salt from the southwest Indian Ocean into the southeast Atlantic Ocean: a case study, *J. Geophys. Res.*, *99*, 14,053–14,070.

Van Campo, E., J. C. Duplessy, W. L. Prell, N. Barratt, and R. Sabatier, 1987, Comparison of terrestrial and marine temperature estimates for the past 125 kyr off southeast Africa: a test for GCM simulations of paleoclimate, *Nature*, *348*, 209–212.

van der Vaart, P. C. F., and W. P. M. de Ruijter, 2001, Stability of western boundary currents with an application to pulslike behavior of the Agulhas Current, *J. Phys. Oceanogr.*, *31*, 2625–2644.

van Leeuwen, P. J., 1999, The time-mean circulation in the Agulhas region determined with the ensemble smoother, *J. Geophys. Res.*, *104*, 1393–1404.

Van Leeuwen, P. J., W. P. M. de Ruijter, and J. R. E. Lutjeharms, 2000, Natal pulses and the formation of Agulhas rings, *J. Geophys. Res.*, *105*, 6425–6436.

Verschuren, D., K. R. Laird, and B. F. Cumming, 2000, Rainfall and drought in equatorial East Africa during the past 1,100 years, *Nature*, *403*, 410–414.

Visbeck, M., and F. Schott, 1992, Analysis of seasonal current variations in the western equatorial Indian Ocean: direct measurements and GFDL model comparison, *J. Phys. Oceanogr.*, *22*, 1112–1128.

Wakker, K. F., R. C. A. Zandbergen, M. C. Naeije, and B. A. C. Ambrosius, 1990, Geosat altimeter data analysis for the oceans around South Africa, *J. Geophys. Res.*, *95*, 2991–3006.

Wang, L., C. J. Koblinsky, and S. Howden, 2001, Annual rossby wave in the southern Indian Ocean: Why does it ”appear” to break down in the middle ocean?, *J. Phys. Oceanogr.*, *31*, 54–74.

Webster, P. J., A. M. Moore, J. P. Loschnigg, and R. R. Leben, 1999, Coupled ocean-atmosphere dynamics in the Indian Ocean during 1997-98, *Nature*, *401*, 356–360.

Weijer, W., 2000, Impact of interocean exchange on the Atlantic overturning circulation, Ph.D. thesis, Utrecht University.

Weijer, W., W. P. M. de Ruijter, H. A. Dijkstra, and P. J. van Leeuwen, 1999, Impact of interbasin exchange on the Atlantic overturning circulation, *J. Phys. Oceanogr.*, *29*, 2266–2284.

Weijer, W., W. P. M. de Ruijter, and H. A. Dijkstra, 2001, Stability of the Atlantic overturning circulation: competition between Bering Strait freshwater flux and Agulhas heat and salt sources., *J. Phys. Oceanogr.*, *31*, 2385–2402.

Weijer, W., W. P. M. de Ruijter, A. Sterl, and S. S. Drijfhout, 2002, Response of the Atlantic overturning to South Atlantic sources of buoyancy, In press, *Global and Planetary Change*.

Zonneveld, K. A. F., G. Ganssen, S. Troelstra, G. J. M. Versteegh, and H. Visscher, 1997, Mechanisms forcing abrupt fluctuations of the Indian Ocean summer monsoon during the last deglaciation, *Quaternary Sc. Rev.*, *16*, 187–201.

Samenvatting

In ons huidige klimaat speelt de oceaan een belangrijke rol. Ongeveer de helft van de energie die op de aarde wordt getransporteerd van het equatoriaal gebied richting de polen, komt voor rekening van de oceanen. De andere helft gaat via de atmosfeer. Het oceaantransport komt weer voor het grootste deel tot stand via de westelijke grens-stromingen: de draaiing van de aarde zorgt voor een zonale assymetrie van de windgedreven circulatiepatronen die de grootschalige oppervlaktestromingen domineren: De poolwaardse stroming vindt plaats in een sterke stroming langs de westkust, terwijl de rest van het bekken langzaam en verspreid transport richting evenaar kent.

De belangrijkste westelijke grensstromingen zijn de Golfstroom in de Noord-Atlantische Oceaan, de Kuroshio in de noordelijke Stille Oceaan, en de en de Aghulas, Brazilie stroom, een Oost Australië Stroom op het zuidelijk halfrond. Echter, een wezenlijk verschil tussen de Golfstroom en de andere westelijke grensstromingen zit in het feit dat de Golfstroom een aanmerkelijk grotere hoeveelheid warmte richting de pool transporteert dan op grond van het windgedreven stromingspatroon in de Noord-Atlantische Oceaan zou mogen worden verwacht. Deze extra component is van groot belang voor het gematigde klimaat in Noord Europa.

Het extra noordwaarts warmtetransport in de Golfstroom komt doordat deze naast een windgedreven deel ook warm water transporteert in het kader van de thermohaline circulatie. Deze component bestaat uit water dat niet wordt gecompenseerd door een zuidwaartse stroming aan het oppervlak, maar deel uitmaakt van een vertikale circulatie. Het water zinkt door afkoeling in het subpolaire gebied van de Atlantische Oceaan, alvorens zich op diepte zuidwaarts te verspreiden. Deze watermassa, het Noord Atlantisch Diep Water, wordt in alle oceanen op een diepte van enkele kilometers teruggevonden, en komt langzaam en zeer verspreid terug naar het oppervlak, waar de circulatie wordt gesloten door oppervlaktewateren die de Atlantische Oceaan instromen.

Een belangrijke schakel in dit transport de Atlantiscche Oceaan in, bevindt zicht en zuiden van Afrika, waar de Agulhas stroming met enige regelmaat grote ringen van warm en zout water uit de Indische Oceaan loslaat, die vervolgens zelfstandig de Atlantische Oceaan in migreren. De ringen hebben een doorsnede van enkele honderden kilometers, en reiken tot enkele kilometers diep. Het belang van deze schakel in de thermohaline circulatie is tweeledig: aan de ene kant staat de directe toevoer van warmte en zout de Zuid Atlantische Oceaan in, aan de andere kant is er ook een subtieler, maar minstens zo belangrijk effect van stabilisering. De huidige configuratie van de thermohaline circulatie wordt bestendigd door de instroom

van warmte en zout bij Zuid Afrika. Dit maakt de Atlantische Oceaan minder gevoelig voor destabiliserende effecten zoals het afsmelten van de ijskappen in het arctisch gebied. Paleoklimatologische observaties wijzen erop dat tijdens de laatste ijstijd de instroom van Indische Oceaan-water tijdelijk heeft stilgelegen, en dat het einde van deze ijstijd samenvalt met hernieuwde opening van het 'Agulhas-lek'.

In deze dissertatie staan twee vragen centraal. De eerste is "in hoeverre kunnen we de uitwisseling tussen Indische en Atlantische Oceaan bij Zuid Afrika kwantficeren met behulp van satelliet-radarhoogtemetingen van het zee-oppervlak", en wordt behandeld in hoofdstuk drie. De tweede centrale vraag betreft de vorming van Agulhas ringen, en de factoren, met name in de bovenstroomse gebieden in de Indische Oceaan, die daarbij een rol spelen. In hoofdstuk vier wordt deze forcering vanuit het bovenstroomse gebied nader onderzocht, hetgeen leidt tot de hypothese dat de vorming van Agulhas ringen het eindpunt is van een lange keten die zijn oorsprong vindt ver van het Agulhasgebied zelf, het onderwerp van hoofdstuk vijf. De hoofdstukken zes en zeven vormen een uitwerking van enkele schakels in deze keten.

Het bestuderen van Agulhas ringen, en in het bijzonder het gedrag van deze ringen over langere periodes, was lange tijd zeer moeilijk. Met hydrografische metingen kon het bestaan van de ringen worden aangetoond, en door ringen op verschillende lokaties met elkaar te vergelijken kon men een beeld krijgen van het verval van de ringen, en daarmee van hun bijdrage aan de warmte- en zoutbalans van de Zuid Atlantische Oceaan. De schaarste aan metingen, gecombineerd met de zeer hoge variabiliteit van het gebied maakte dat deze schattingen niet erg betrouwbaar waren. Ook de komst van oppervlakte-temperatuur (sea surface temperature, SST) metingen vanuit satelieten (door middel van infrarood-sensoren) kon hier niet veel aan veranderen: wolken maakten gedurende forse periodes van het jaar observaties onmogelijk, en de grote energie-uitwisseling tussen atmosfeer en oceaan zorgt ervoor dat de (eerst nog zeer warme) Agulhas ringen al snel een dunne afgekoelde oppervlaktelaag krijgen die qua temperatuur overeenkomt met de omgeving. Hoewel de ringen dan nog steeds enkele kilometers diep het temperatuur-, zout en dichtheidsprofiel sterk kunnen beïnvloeden, zijn ze onzichtbaar voor infrarood-satelieten.

Sinds enkele tientallen jaren bieden altimeter-satelieten echter de mogelijkheid om de hoogte van het zeeniveau (sea surface height, SSH) tot op enkele centimeters nauwkeurig te meten. Met deze techniek zijn de Agulhas ringen, die hun dynamische structuur (en daarmee hun SSH signatuur), veel langer behouden dan hun oppervlakte-temperatuur, veel langer waarneembaar. In het eerste inhoudelijke hoofdstuk van dit proefschrift, hoofdstuk drie, wordt een studie gedaan naar het optreden en het gedrag van de Agulhas ringen gevormd tussen 1993 en 1996. Door gebruik te maken van altimetrie-gegevens kunnen de gevolgde routes, het SSH-verval, en andere aspecten van de uitwisseling tussen de Indische en Atlantische oceaan door middel van Agulhas Ringen geanalyseerd worden. De ringen, zo'n vier tot zes per jaar, kunnen tot enkele jaren na vorming gevlogd worden, soms tot nabij het Zuid Amerikaanse continent. Toch speelt het belangrijkste verval van de ringen, waarbij de SSH uitwijkingen inzakken van rond de 50 cm tot zo'n 20 cm, zich af in het oostelijk deel van de Zuid Atlantische Oceaan. Het is daar dat in de eerste maanden van hun bestaan de ringen veelvuldig interactie vertonen met elkaar, met de achtergrondstromingen, en met bodemtopgrafie. Ook splitsen regelmatig ringen op in meerdere delen, en wordt een deel van de ringen volledig weggemengd in het

gebied bij Zuidelijk Afrika. Al deze processen lijken bij te dragen tot het verval der ringen. Het deel van het water dat door de ringen meegenomen wordt de Atlantische Oceaan in, en dat terechtkomt in het oostelijk deel van het bekken, wordt geschat op tweederde. Vanaf het eerste jaar blijven de ringen opmerkelijk stabiel.

De observatie dat af en toe een half jaar helemaal geen Agulhas ringen lijken te worden afgesnoerd, leidt tot de vraag of hierbij bovenstroomse processen een rol spelen. De Agulhas zelf blijkt een opvallend regelmatig proces te kennen van langzame westwaardse propagatie van het retroflectiepunt (waar de stroming, eenmaal vrij van de kunst zich terugtbuigt naar de Indische Oceaan) gevolgd door een vrij plotselinge afsnoering van het westelijk deel van de retroflectie-lus in de vorm van een Agulhas ring. Vanaf dan bevindt de stroming zich weer in haar oostelijke positie, en begint het proces van westwaardse propagatie weer opnieuw. Dit proces doet zich zo'n vier tot vijf maal per jaar voor. Het plotseling afsnoeren waarbij de Agulhas stroming als het ware de retroflectie-lus afsnijdt, blijkt te worden geïnstigeerd door wervels uit het noorden. Grote wervels uit het Mozambique kanaal, die zoals blijkt uit de metingen gedaan tijdens de ACSEX expedities qua omvang weinig onderdoen voor Agulhas ringen, progageren vanuit het kanaal richting het Agulhas retroflectie gebied. Daar vormen deze anticyclonale ringen voor de Agulhas de verstoring die leidt tot afsnoering van een ring.

Met de Mozambique kanaal wervels zijn we echter nog niet bij het begin van de keten, want de vrij stabiele frequentie van zo'n vier wervels per jaar kan niet zomaar verklaard worden. In hoofdstuk vijf gaan we dan ook op zoek nar de oorsprong van deze frequentie. Die lijkt te liggen in het equatoriaal gebied. De wisseling van de moesson-seizoenen gaat gepaard met flinke veranderingen in het windveld. Dit windveld, met tweemaal per jaar een sterke maar zeer lokaal optredende oorstwaardse wind over het centrale deel van de equatoriale Indische Oceaan, forceert uiteindelijk, vermoedelijk via de excitatie van een equatoriale eigentrilling, versterkt door de reflectie van golven aan de Malediven Rug, de vier per jaar cyclus. Via snelle equatoriale- en kust-Kelvin golven wordt deze naar gematigde breedte getransporteerd. Via Rossby golven lopen de signalen dan in meer dan een jaar langzaam westwaats, tot aan Madagascar. Daar leidt de interactie van de Rossby golven met het eiland en de lokale stroming tot de vorming van zo'n vier Mozambique wervels per jaar, die het Mozambique kanaal in zuidwaardse richting verlaten. Deze keten is het afgelopen decennium tweemaal verstoord geweest door het optreden van grootschalige fenomenen gerelateerd aan de El Ninõ cyclus.

De Rossby golf-propagatie door de subtropische zuidelijke Indische Oceaan vormt het onderwerp van nadere studie in hoofdstuk zes. Het patroon van twee banden van variabiliteit op de vier keer per jaar-frequentie lijkt te ontstaan door modificatie van het achtergrond vorticiteitsveld door de vertikale schering in de gemiddelde stroming. In hoofdstuk zeven wordt de interactie tussen Rossby golven en de lokale stroming rond Madagascar meer gedetailleerd behandeld, en worden metingen in het Mozambique kanaal gepresenteerd. Dit betreft zowel in-situ waarnemingen, als een inventarisatie van enkele jaren altimetrie observaties van Mozambique wervels en hun karakteristieken.

Dank jullie wel!

De wetenschap is een (soms wel erg) solitair ingesteld wereldje. Toch hebben bij de totstandkoming van dit proefschrift een flink aantal mensen een rol gespeeld. Voor die rol wil ik een aantal mensen bedanken.

Allereerst bedank ik mijn promotor en dagelijks begeleider Will de Ruijter voor zijn stimulerende begeleiding, ongebreideld enthousiasme, immer positief kritische houding, en de grote vrijheid die hij bood om vier jaar lang min of meer te doen waar ik zin in had. De open communicatieve sfeer binnen de groep ocean & klimaat van het imau, en het Agulhas-clubje (met wisselende bezetting) in het bijzonder, zijn voor een groot deel zijn verdienste.

Ook copromotor Peter Jan van Leeuwen mag niet onvermeld blijven. Peter Jan groeide de afgelopen jaren sterk in zijn rol van begeleider, en zijn grote enthousiasme voor bijna alles was vaak hartverwarmend. Met name bij totstandkoming van de laatste hoofdstukken heeft hij een cruciale rol gespeeld.

Vervolgens wil ik degenen bedanken die de wetenschap op het imau tot een minder eenzaam bedrijf maakten. Ernst van der Avoird en Maurice Schmeits als vaste compagnons op het imau, Laura de Steur als fijne kamer- en bootgenoot. En natuurlijk ook de rest van de mensen op het imau (en soms van daarbuiten) die het promoveren tot een aangename tijdsbesteding maakten.

En dan de uitstapjes. Allereerst Herman Ridderinkhof, die mij tot tweemaal toe het genoegen liet smaken van de ware oceanografie: het zeegaande werk. De tochten, die onder zijn bezielende leiding steeds bleven verrassen, behoren tot de absolute hoogtepunten van mijn promotietijd. Ook wil ik de bemanning van de Pelagia niet onvermeld laten, die hier in niet geringe mate aan bijdroeg. I also thank Ricardo Matano for enabling a visit to Oregon State University in December 2000.

En natuurlijk Ingeborg, waar ik telkens weer blij van wordt.

Curriculum Vitae

Op 3 juli 1975 werd ik geboren in Den Haag. Al snel verhuisde ik naar Leiden, waar ik tussen 1986 en 1993 het Stedelijk Gymnasium Leiden bezocht. Vanaf 1993 volgde ik aan de Technische Universiteit Delft de opleiding tot Geodetisch ingenieur. Het propaedeutisch examen van die opleiding kwam in 1994, het doctoraal in 1997. Met mijn afstudeerwerk begaf ik me al richting oceaan: het ging over luchtdrukcorrecties van altimetrie-metingen. Hoewel hier niet veel uitkwam, was mijn interesse voor de oceaan en de altimetrie gewekt: de promotieplaats in Utrecht kwam dan ook precies op tijd. Tussen 1998 en 2002 was ik werkzaam aan het Instituut voor Marien en Atmosferisch Onderzoek (IMAU) van de Universiteit Utrecht. Daar deed ik onderzoek naar de uitwisseling van water tussen de Indische en Atlantische Oceaan. Als resultaat verscheen dit boekwerkje, en hoop ik op 15 mei 2002 te promoveren.

Publications

Based on chapter three:

Schouten, M. W., W. P. M. de Ruijter, P. J. van Leeuwen, and J. R. E. Lutjeharms, 2000, Translation, decay and splitting of Agulhas rings in the south-east Atlantic ocean, *J. Geophys. Res., 105*, 21,913–21,925.

Based on chapter four:

Schouten, M. W., W. P. M. De Ruijter, and P. J. Van Leeuwen, 2002b, Upstream control of the Agulhas ring shedding, *J. Geophys. Res.*, in press

Based on chapter five:

Schouten, M. W., W. P. M. De Ruijter, P. J. Van Leeuwen, and H. Dijkstra, 2002a, A teleconnection between the equatorial and southern Indian Ocean, *Geoph. Res. Letters*, in press

Schouten, M. W., W. P. M. De Ruijter, P. J. Van Leeuwen and H. A. Dijkstra, 2002, An oceanic connection between Indian Ocean equatorial winds and eddy variability around Southern Africa, *submitted to Deep Sea Research, Part II*

Based on the ACSEX I cruise in 2000:

De Ruijter, W. P. M., H. Ridderinkhof, J. R. E. Lutjeharms, M. W. Schouten, and C. Veth, 2002, Observations of the flow in the Mozambique Channel, *Geoph. Res. Letters*, in press

Based on chapter seven:

Schouten, M. W., W. P. M. De Ruijter, P. J. Van Leeuwen and H. Ridderinkhof, 2002, Eddies and variability in the Mozambique Channel, *submitted to Deep Sea Research, Part II*